



The SSP greenhouse gas concentrations and their extensions to 2500

5 Malte Meinshausen^{1,2,3}, Zebedee Nicholls^{1,2}, Jared Lewis¹, Matthew J. Gidden^{4,5},
Elisabeth Vogel^{1,2}, Mandy Freund^{1,6}, Urs Beyerle⁷, Claudia Gessner⁷, Alexander
Nauels^{1,5}, Nico Bauer³, Josep G. Canadell⁸, John S. Daniel⁹, Andrew John^{1,10}, Paul
Krummel¹¹, Gunnar Luderer³, Nicolai Meinshausen¹², Stephen A. Montzka¹³, Peter
Rayner^{2,1}, Stefan Reimann¹⁴, Steven J. Smith¹⁵, Marten van den Berg¹⁶, Guus J.M.
Velders^{17,18}, Martin Vollmer¹⁴, Hsaing Jui (Ray) Wang¹⁹

10 ¹ Climate & Energy College, The University of Melbourne, Parkville, Victoria, Australia

² School of Earth Sciences, The University of Melbourne, Parkville, Victoria, Australia

³ Potsdam Institute for Climate Impact Research (PIK), Potsdam, Germany

⁴ IIASA Institute for Applied Systems Analysis, Laxenburg, Austria

⁵ Climate Analytics, Berlin, Germany

15 ⁶ Marine and Atmospheric Research, CSIRO, Hobart, Tasmania, Australia

⁷ Institute for Atmospheric and Climate Science, Swiss Federal Institute of Technology, Zurich (ETH Zurich), Switzerland

⁸ Global Carbon Project, CSIRO Oceans and Atmosphere, Canberra, ACT, Australia

⁹ NOAA, Earth System Research Laboratory, Chemical Sciences Division, Boulder, Colorado, USA

20 ¹⁰ Department of Infrastructure Engineering, The University of Melbourne, Parkville, Victoria, Australia

¹¹ CSIRO Oceans and Atmosphere, Aspendale, Victoria, Australia

¹² Seminar for Statistics, Swiss Federal Institute of Technology (ETH Zurich), Zurich, Switzerland.

¹³ NOAA, Earth System Research Laboratory, Global Monitoring Division, Boulder, Colorado, USA

25 ¹⁴ Empa, Laboratory for Air Pollution/Environmental Technology, Swiss Federal Laboratories for
Materials Science and Technology, Dübendorf, Switzerland

¹⁵ Joint Global Change Research Institute, Pacific Northwest National Laboratory, College Park, MD,
USA

Potsdam, Germany

¹⁶ PBL Netherlands Environmental Assessment Agency, the Netherlands

30 ¹⁷ National Institute for Public Health and the Environment (RIVM), Bilthoven, Netherlands

¹⁸ Institute for Marine and Atmospheric Research Utrecht (IMAU), Utrecht University, Utrecht, The
Netherlands

¹⁹ School of Earth and Atmospheric Sciences, Georgia Institute of Technology, Atlanta, GA 30332-0340,
USA

35

Correspondence to: M. Meinshausen (malte.meinshausen@unimelb.edu.au)



Abstract. Anthropogenic increases of atmospheric greenhouse gas concentrations are the main driver of current and future climate change. The Integrated Assessment community quantified anthropogenic emissions for the Shared Socioeconomic Pathways (SSP) scenarios, each of which represents a different future socio-economic projection and political environment. Here, we provide the greenhouse gas concentration for these SSP scenarios – using the reduced complexity climate-carbon cycle model MAGICC7.0. We extend historical, observationally-based concentration data with SSP concentration projections from 2015 to 2500 for 43 greenhouse gases with monthly and latitudinal resolution. CO₂ concentrations by 2100 range from 393 to 1135 ppm for the lowest (SSP1-1.9) and highest (SSP5-8.5) emission scenarios respectively. We also provide the concentration extensions beyond 2100 based on assumptions in the trajectories of fossil fuels and land use change emissions, net negative emissions, and the fraction of non-CO₂ emissions. By 2150, CO₂ concentrations in the lowest emission scenario are approximately 350 ppm and approximately plateau at that level until 2500, whereas the highest fossil-fuel driven scenario projects CO₂ concentrations of 1737 ppm and reaches concentrations beyond 2000ppm by 2250. We estimate that the share of CO₂ in the total radiative forcing contribution of all considered 43 long-lived greenhouse gases increases from today 66% to roughly 68% to 85% by the time of maximum forcing in the 21st century. For this estimation, we updated simple radiative forcing parameterisations that reflect the Oslo Line by Line model results. In comparison to the RCPs, the five main SSPs (SSP1-1.9, SSP1-2.6, SSP2-4.5, SSP3-7.0 and SSP5-8.5) are more evenly spaced in terms of their expected global-mean temperatures, extend to lower 2100 temperatures and sea level rise than the RCP set. Performing 2 pairs of 6-member historical ensembles with CESM1.2.2, we estimate the effect on surface air temperatures of applying latitudinally and seasonally resolved GHG concentrations. We find that the ensemble differences in the MAM season provide a regional warming in higher northern latitudes of up to 0.4K over the historical period, latitudinally averaged of about 0.1K, which we estimate to be comparable to the upper bound (~5% level) of natural variability. In comparison to the comparatively straight line of the last 2000 years, the greenhouse gas concentrations since the onset of the industrial period and this studies' projections over the next 100 to 500 years unequivocally depict a 'hockey-stick' upwards shape – it is a collective choice whether the hothouse pathway is pursued or whether we manage climate damages to the SSP1-1.9 equivalent of around 1.5°C warming.

65



1 Introduction

The climate modelling community periodically undertakes large model intercomparison exercises with the latest and most sophisticated set of climate models, to gain a better understanding of the response of the climate system to a range of potential emission or concentration scenarios (Taylor et al., 2012; Meehl et al., 2007). The general circulation models (GCMs) that feature elements such as dynamic vegetation, coupled carbon cycles (Lawrence et al., 2016; Jones et al., 2016) and more sophisticated atmospheric chemistry are referred to as Earth System Models (ESMs). Most of these ESMs participating in the Sixth Model Intercomparison Phase (CMIP-6) (Eyring et al., 2016) could be driven by CO₂ emissions. However, many of the ESMs are driven by exogenous greenhouse gas concentrations instead of emissions for many of the scenarios (a) to allow for an easier separation between carbon cycle feedbacks and climate responses, (b) to allow for the inclusion of GCMs in the intercomparison exercises, and (c) to take into account non-CO₂ long-lived GHG gases, for which the ESM do not include gas-cycles yet.

This study provides and describes the standardised set of greenhouse gas concentration futures for CO₂, CH₄, N₂O and 40 other greenhouse gases. For the historical period, this GHG concentration data for CMIP6 was provided by the companion paper Meinshausen et al. (2017). This study provides the GHG concentration data until 2100 on the basis of the emission scenarios derived from socio-economically explicit Integrated Assessment Models' (IAMs) under the SSP framework (Gidden et al., 2019). We also provide an extension of the concentration data until 2500 on the basis of simplified assumptions.

These concentrations datasets are part of the protocols for several Coupled Model Intercomparison Project phase 6 (CMIP6) experiments, most notably ScenarioMIP (O'Neill et al., 2016) and AerChemMIP (Collins et al., 2017), that require concentration-driven runs (see search.es-doc.org for a full description). While greenhouse gases are arguably the most important influence of humankind on future climate in terms of radiative forcing, there is a wide range of other forcings, including anthropogenic aerosols (Hoesly et al., 2018), land-use patterns, aerosol optical properties (Stevens et al., 2017), as well as natural forcings like solar (Matthes et al., 2017) and volcanic effects (Toohey et al., 2016). These forcings are described in the companion papers and compiled in the input4mip interface to be used for the historical and future ESM experiments (Durack and Taylor, 2019), available on <https://esgf-node.llnl.gov/projects/input4mips/>.



Our future greenhouse gas concentration datasets from 2015 onwards are provided for a total of nine SSP
95 scenarios. These nine scenarios comprise five high-priority scenarios for the Sixth Assessment report by
the IPCC report, which is the group of four “Tier 1” scenarios highlighted in ScenarioMIP (O'Neill et al.,
2016) in addition to the SSP1-1.9 scenario that reflects most closely a 1.5°C target under the Paris
Agreement. Specifically, these “high priority” scenarios for IPCC AR6 are (1) the SSP1-2.6 “2°C-
scenario” of the “sustainability” SSP1 socio-economic family, whose nameplate 2100 radiative forcing
100 level is 2.6 W/m². This SSP1-2.6 scenario approximately corresponds to the previous’ scenario generation
Representative Concentration Pathway (RCP) 2.6. Secondly, the (2) SSP2-4.5 of the “middle of the road”
socio-economic family SSP2 with a nominal 4.5W/m² radiative forcing level by 2100 - approximately
corresponding to the RCP-4.5 scenario. Thirdly, (3), the SSP3-7.0 scenario is a medium-high reference
scenario within the “regional rivalry” socio-economic family, while (4), the SSP5-8.5 marks the upper
105 edge of the SSP scenario spectrum with a high reference scenario in a high fossil-fuel development world
throughout the 21st century. The additional high priority scenario that IPCC AR6 considers is SSP1-1.9
to better reflect the research regarding the Paris Agreement’s 1.5°C target. It should be noted that the
radiative forcing labels, such as “2.6” in the SSP1-2.6 scenario, are indicative “nameplates” only,
approximating total radiative forcing levels by the end of the 21st century. Those labels are merely
110 indicative, given that actual radiative forcing uncertainties (and differences across ESMs that implement
the same concentrations and aerosol abundances) are substantial.

In addition to these five high-priority scenarios, we provide concentrations for four additional SSP
scenarios, namely the three remaining “Tier 2” ScenarioMIP experiments, featuring a low reference
scenario SSP4-6.0 within the socio-economic context of the an “inequality” dominated world, as well as
115 its moderate mitigation scenario SSP4-3.4. Similarly, there is the geophysically interesting emissions
“overshoot” scenario, SSP5-3.4-OS, as it initially follows the high emission SSP5-8.5 scenario until 2030
before exhibiting the steepest annual reduction rates of all SSP scenarios and the most net negative
emissions by 2100. Lastly, we also consider the SSP3-7.0-LowNTCF variant of the SSP3-7.0 scenario
with reduced near-term climate forcer (NTCF) emissions. Given that the SSP3-7.0 scenario is the one
120 with the highest methane and air pollution precursor emissions, the SSP3-7.0-LowNTCF variant
investigates an alternative pathway for the AerChemMIP intercomparison project (Collins et al., 2017)
that exhibits very low methane, aerosol and tropospheric ozone precursor emissions - approximately in



line with the lowest other SSP scenarios for those species like SSP1-1.9 and SSP1-2.6. Note that the
NTCF nomenclature is equivalent to the term Short-Lived Climate Forcer, SLCF, which is now more
125 commonly used by the research community and IPCC context.

The presented historical global-mean and hemispheric-mean surface mole fractions in this study transition
smoothly from the end of the historical dataset (Meinshausen et al., 2017), 2014, into the start of the
projections, 2015. Also, the latitudinal gradient and seasonality, and their temporal evolution, are
consistent with the historical dataset - which in all cases are tied directly to past measurements. We used
130 a reduced complexity carbon-cycle model, MAGICC (Meinshausen et al., 2011c; Meinshausen et al.,
2011a), to produce global-mean future greenhouse gas concentration time series for each of the considered
SSPs. The same model, albeit an earlier version, was also previously used to provide the RCP greenhouse
gas concentrations projections (Meinshausen et al., 2011b). The MAGICC version used for this study
(version 7.0) is calibrated to closely represent C4MIP carbon cycle responses, includes a permafrost
135 module (Schneider von Deimling et al., 2012) and updated radiative forcing and non-CO₂ gas cycle
parameterisations (in particular for CH₄ and N₂O) that represent recent literature findings (Prather et al.,
2012; Holmes et al., 2013). The calibrated carbon cycle of MAGICC has previously been shown to reflect
well the CMIP5 ESM response range (Friedlingstein et al., 2014). Given the nearly two-year time
difference between the completion of historical and future greenhouse gas concentrations, we also
140 updated the historical observational datasets to reflect observations until early 2018 for CO₂, CH₄ and
N₂O, as well as most other gases considered here.

This study first describes the methods with separate parts for the updated observational data until 2018
(Section 2.1), the emission input data from the IAM scenarios and the input preparation steps undertaken
(2.2), the extensions of the emissions and concentrations beyond 2100 (2.3) the MAGICC model setup
145 (2.4), and the projections of latitudinal gradients (2.5) and seasonality (2.6). We also provide a new
simplified formula to reflect the Oslo Line By Line model (OLBL) radiative forcing results (Etminan et
al., 2016) in order to provide the radiative forcing aggregation of the output (2.7) and discuss additional
methodological steps (2.8). We then show the results and compare these to other recent observational
datasets (Section 3 “Results”). A discussion section follows (Section 4 “Discussion”), which includes a
150 closer look at the two most dominant GHG forcings CO₂ and CH₄ and their correlation (4.1), a discussion
on the most recent GHG concentration developments (4.2) and the comparison with RCPs concentrations



(4.4) as well as temperatures and sea level rise projections (4.5). We describe the limitations of the dataset (5), which includes issues like the integration of observational and modelled future data, missing uncertainty estimates, potential biases in future seasonality and latitudinal gradients, and a lack of reference scenarios for Montreal-controlled substances. Section 6 concludes.

2 Methods

As for the historical concentrations, we provide 43 greenhouse gases future concentration projections, namely CO₂, CH₄, N₂O, 17 ozone depleting substances, namely CFC-11, CFC-12, CFC-113, CFC-114, CFC-115, HCFC-22, HCFC-141b, HCFC-142b, CH₃CCl₃, CCl₄, CH₃Cl, CH₂Cl₂, CHCl₃, CH₃Br, Halon-1211, Halon-1301, Halon-2402, and 23 other fluorinated compounds, namely 11 HFCs (HFC-134a, HFC-23, HFC-32, HFC-125, HFC-143a, HFC-152a, HFC-227ea, HFC-236fa, HFC-245fa, HFC-365mfc, HFC-43-10mcc), NF₃, SF₆, SO₂F₂, and 9 PFCs (CF₄, C₂F₆, C₃F₈, C₄F₁₀, C₅F₁₂, C₆F₁₄, C₇F₁₆, C₈F₁₈, and C₄F₈). Our projections refer to atmospheric dry air mole fractions as does the historical data presented in Meinshausen et al. (2017), even though the projections are sometimes loosely referred to as ‘concentrations’. For CO₂, the usual unit is parts per million (ppm), for CH₄ and N₂O, the usual unit is parts per billion (ppb) and other gases are usually denoted in parts per trillion (ppt).

2.1 Updated observational data

The historical concentrations (until the end of 2014) were derived from various observational datasets of greenhouse gas concentrations, or literature studies in the case of some of greenhouse gases with lower mixing ratios. The observational data was binned by latitudinal and longitudinal boxes, averaged for monthly values and complemented by interpolations. The historical timeseries for every greenhouse gas were separated into three elements as part of the spatio-temporal binning: i) latitudinal gradient, ii) seasonality pattern and iii) global mean. This separation then permitted the use of longer observational timeseries, such as the high latitudinal CH₄ firm data – implicitly correcting for the high latitude differences to the global mean that one would expect. Interpolations, regressed latitudinal gradients and seasonality patterns were employed to derive the historical dataset, but no gas cycle models.



180 With additional observational data being available for 2015, 2016 and 2017, the previously used
observational datasources from the AGAGE and NOAA networks (Dlugokencky, 2015a, b; Prinn et al.,
2018), including multiple NOAA/ESRL/GMD flask measurements, were updated and used to determine
the initial years of the future concentration timeseries. The result of this is that – depending on the gases
- the same concentrations are used across all nine SSPs in the initial years (Table 1). As outlined below,
we employed MAGICC7.0 and its calibrated gas cycles to produce concentration time series from SSP
emissions beyond the observationally based period.

2.2 Emission data and their harmonisation

185 For the emission driven MAGICC7 runs that produce the future global-mean greenhouse gas timeseries,
we use the SSP emission data for CO₂, CH₄ and N₂O, HFCs, PFCs and SF₆ which is available from the
SSP database at IIASA (<https://tntcat.iiasa.ac.at/SspDb>). This emission data has already been subject to
several categorisation and harmonisation steps to obtain regionally consistent (in case of CO₂ and CH₄)
and sectorally resolved data (Gidden et al., 2019). We complemented those harmonisation steps to
190 consider the following species in the five RCP regions (OECD90, REF (Economies in Transition), LAM
(Latin America), MAF (Middle East and Northern Africa) and ASIA): CO₂, CH₄ and N₂O in addition to
black carbon (BC), carbon monoxide (CO), ammonium (NH₃), non-CH₄ volatile organic compounds
(NMVOC), nitrates (NO_x), organic carbon (CO) and sulphate aerosol (SO_x). For those 10 species, we
also distinguished between fossil & industrial sources and land-use related sources.

195 Regional landuse CO₂ emissions are not provided in the SSP database (Gidden et al., 2019), so we
downscaled to the RCP regions based on historical regional emission shares in the year 2015. Given
landuse CO₂ emissions can be negative in some SSP scenarios, a simple scaling approach in the regional
harmonisation would yield unrealistic results (i.e. regions with low or negative current net landuse
emissions, like the OECD, would end up with positive emissions and the other world regions would be
200 strongly negative in the future. Instead, we applied a normalisation that assumes a negative 1.5 GtC base
level against which historical regional emission shares are continued into the future, scaled with global
emissions.

Mathematically, the constant regional scaling factor is hence applied to the offset emission level, so that
the future regional emissions $E_r(y)$ in year y are:



205
$$E_r(y) = E_g(2015) \times s_{2015} + (E_g(y) - E_g(2015)) \times r$$

where

$$r = \frac{E_r(2015) + 1.5}{\sum_{r=1}^n (E_r(2015) + 1.5)}$$

210 With r being the regional share of emissions relative to that 1.5GtC offset level, s being the regional share of emissions in 2015 relative to zero, i.e. $s_{2015} = E_r(2015)/E_g(2015)$, $E_r(y)$ being the regional emissions in year y and $E_g(y)$ being the global emissions, i.e. the sum of the n regional emissions. Specifically, the factors s_{2015} and r for were the following for the regions Asia, Latin America, Middle East and Africa, OECD-90 and Economies in Transition: 0.483, 0.282, 0.189, 0.043, 0.003, for s_{2015} and 0.232 0.209, 0.199, 0.182, 0.178 for r , respectively. This choice has little effect because the regional split up of CO₂ emissions only marginally and indirectly affects the latitudinal concentrations in our chosen method. A very small difference arises for different regional landuse CO₂ emission assumptions because 215 MAGICC7 scales albedo effects with landuse CO₂ emissions and these albedo effects impact temperatures and in turn the carbon cycle again.

220 Landuse related CH₄ and fossil & industrial CO₂ and CH₄ emissions were already harmonised with historical emissions and also regionally available (Gidden et al., 2019; Gidden et al., 2018). N₂O emissions were only available as global total from the SSP database based on PRIMAP (Gütschow et al., 2016), which is why we assume constant regional and sectoral emission shares. This assumption does not have a bearing on final global concentrations.

225 For the emissions of fluorinated gases, that are listed in the Kyoto Protocol and considered here (PFCs, HFCs and SF₆), namely C₂F₆, CF₄, HFC-125, HFC-134a, HFC-143a, HFC-227ea, HFC-23, HFC-245fa, HFC-43-10mee, and SF₆, MAGICC7 takes the global and aggregated SSP emissions of the gas baskets as inputs, as provided by the IAM modellers using constant emission shares based on a future gas-specific scenario by Guus Velders (Velders et al., 2015) and described in Gidden et al. (2019). The basket of PFCs, HFCs and SF₆ is reported in the SSP database at IIASA (<https://tntcat.iiasa.ac.at/SspDb/>). Some few data points were corrected in consultation with the respective IAM modelling teams, namely the 230 SSP1-1.9 emission level in 2100 for CF₄ and C₂F₆, for which we assumed the rate of decline prolonged



from the 2080 to 2090 to the 2090 to 2100 period. HFC-32 emissions were complemented from a Kigali-Agreement consistent scenario, which has also been derived from the scenarios by Velders et al. (2015). Those scenarios were published until 2050 and we use in addition an extension up to 2100 by proportional downscaling of the GWP-weighted HFC basket – using SSP GDP and population data with an assumption
235 of constant GDP and population after 2100.

The ozone depleting substances controlled under the Montreal Protocol, namely CFC-11, CFC-12, CFC-113, CFC-114, CFC-115, HCFC-22, HCFC-141b, HCFC-142b, CH₃Br, CH₃Cl, CH₃CCl₃, CCl₄, Halon-1202, Halon-1211, Halon-1301, Halon-2402 are here assumed to follow the WMO 2014 scenario (WMO, 2014) from 1951 to 2099, as presented in detail in Velders and Daniel (2014a). For times before 1951 and
240 after 2099, the previous WMO A1 Baseline emission scenario from year 2006 (WMO, 2006) is assumed which is near-zero and close to the respective WMO 2014 values in 1951 and 2099.

Harmonized emissions of aerosol and ozone precursor species are also available for the SSP scenarios (Hoesly et al., 2018), but not discussed in this paper. These non-GHG emissions are used here as part of the complete scenario specification needed to produce future temperature and GHG concentration
245 pathways.

2.3 Extension of emissions and concentrations beyond 2100

In 2011, the RCPs were extended beyond 2100 to provide the basis for longer-term scenario studies (Meinshausen et al., 2011b), then called ‘Extended Concentration Pathways’ (ECPs). Studying this
250 longer-term behaviour of the climate system is of interest for quantities that exhibit a strong long-term commitment or non-linear behaviour (e.g. sea-level rise, ice sheet dynamics). The RCP concentration extensions were – for some gases and scenarios – based on pragmatic extensions of emissions, like an RCP8.5 CO₂ emission stabilisation from 2100 to 2150 with a subsequent ramp-down until 2250. For other RCPs, concentrations were held constant and the inverse CO₂ emissions exhibited a near-exponential
255 decline.

Here, we present the extensions beyond 2100 of the ScenarioMIP and AirChemMIP SSPs (although we do not use a new acronym like ECPs at the time of the RCPs). The final choices differ, in some respects,



from the initial sketch of these extensions that was offered in the ScenarioMIP overview paper (O'Neill et al., 2016). As described below, the collaborative exercise by the IAM modellers and MAGICC team
260 updated the original SSP extension design. In summary, the extension principles are:

- 1) From 2100 onwards, net negative fossil CO₂ emissions are brought back to zero during the 22nd century, while positive fossil CO₂ emissions are ramped down to zero by 2250.
- 2) Land use CO₂ emissions are brought back to zero by 2150.
- 3) Non-CO₂ fossil greenhouse gas emissions are ramped down to zero by 2250.
- 265 4) Land use-related non-CO₂ emissions are held constant at 2100 levels.

In the initial ScenarioMIP design (O'Neill et al., 2016), fossil CO₂ emissions for SSP5-3.4-OS and SSP1-2.6 are negative at 2100 levels until 2140 and gradually increase to zero until 2190 and 2185, respectively (Figure 2, panel a). For all scenarios with net negative fossil fuel extensions, we implemented extensions assuming constant emissions until 2140 (as suggested), but reaching zero emissions in 2190. The only
270 exception is the SSP5-3.4-OS scenario, which was ramped back to zero by a slightly earlier date (2170) so that fossil and landuse emissions (in combination with MAGICC7.0's default setting – see section 2.4) met the design criteria of an approximate merge with SSP1-2.6 concentrations in the longer-term, i.e. after 2150.

In the initial ScenarioMIP extension sketch for SSP5-8.5, total CO₂ emissions were envisaged to be “less
275 than 10 GtC/yr” by 2250 (Figure 2, panel c). Having considered multiple options, we opted for a straight ramp down of fossil CO₂ emissions to zero by 2250 due to its simplicity. Landuse CO₂ emissions for SSP1-2.6 in the initial ScenarioMIP design were held constant at 2100 levels indefinitely. SSP5-3.4-OS levels were designed to reach the same net negative landuse CO₂ levels by 2120 (Figure 2, panel b). However, the extensions presented here assume that all landuse CO₂ emissions linearly phase-out between
280 2100 and 2150, as continuing negative landuse CO₂ emissions are inconsistent with fixed 2100 landuse and land cover patterns. In the original scenario design suggestion by O'Neill et. al, all non-CO₂ greenhouse gas emissions were kept constant at 2100 levels. However, the final extensions presented here assume differentiated extension rules by sector. Specifically, we assumed a linear phase-out of all fossil and industrial non-CO₂ emissions by 2250 (incl. aerosols etc) (see e.g. Figure 2, panel c). Similarly,
285 synthetic industrial gases were assumed to be phased out by 2250 instead of assuming constant emissions



(panel g, h). For landuse-related non-CO₂ emissions, the assumption has been maintained that 2100 emission levels are held constant. That assumption seemed approximately consistent with constant landuse and land cover patterns as food production activities would continue to produce certain levels of N₂O and CH₄ emissions (panel d). In comparison to a uniform approach of holding all emissions constant at 2100 levels, the chosen differentiation to phase out fossil and industrial related emissions over time while holding land-use related emissions constant seemed more consistent with plausible futures.

2.4 Projecting global-mean concentrations with the MAGICC climate model

For projecting the SSP greenhouse gas concentrations, we updated several gas cycles and also used MAGICC's permafrost module, which was not switched on when projecting the RCP concentrations. The sections below describe these updates.

2.4.1 Methane cycle

The methane (CH₄) cycle in MAGICC projects CH₄ concentrations based on anthropogenic CH₄ emissions as an input. Internally, MAGICC derives natural CH₄ emissions by closing the CH₄ budget over a user-defined historical period (here assumed 1994 to 2004, previously 1966 to 1976). The atmospheric CH₄ lifetime as modelled in MAGICC changes over time both because of projected changes in tropospheric OH concentrations and an increased stratospheric Brewer-Dobson circulation under increased climate change (Meinshausen et al., 2011a). On top of this, increased CH₄ emissions are modelled to affect (alongside several other reactive gas emissions like CO, NMVOC and NO_x) tropospheric OH concentrations (Meinshausen et al., 2011a; Ehhalt et al., 2001). Thus, there is a feedback loop where increased CH₄ emissions lead to decreased OH-related CH₄ sinks and in turn longer CH₄ lifetimes and longer lifetimes of other GHGs, such as HCFCs and HFCs. The increased Brewer-Dobson circulation, on the other hand, leads to stronger CH₄ removals, lowering the overall lifetime. As a net effect, CH₄ lifetimes tend to be shorter in the lower emission scenarios and longer in the higher emission scenarios, such as RCP8.5.



In this study, we calibrate nine of MAGICC's CH₄ cycle parameters (see its description and parameter denotations in Appendix A2.1 of Meinshausen et al. (2011c)) to the modelled CH₄ projections by Holmes et al. (2013). They included, like MAGICC, the temperature sensitivity of CH₄'s OH-related lifetime, thereby updating results of Prather et al. (2012). These newly calibrated parameters are (a) the initial CH₄ lifetime $\tau'_{\text{CH}_4, \text{tropos}}$ (9.95 yrs, updated from 9.6 yrs), (b) the temperature-sensitivity of CH₄'s OH-related lifetime S_{rCH_4} (0.07 K⁻¹, updated from 0.058 K⁻¹), (c) a scaling factor on the sensitivity of CH₄'s lifetime to OH-changes $S_{\text{scale}}^{\text{OH}}$ (0.725, formerly 1), which is newly introduced and applies to all S_x^{OH} factors shown in equation A30 in Meinshausen (2011c), (d) the unscaled sensitivity of OH to CH₄ concentration changes $S_{\text{CH}_4}^{\text{OH}}$ (-0.5377, updated from the unscaled -0.32), noting that this update largely offsets the effect of the newly introduced scaling factor $S_{\text{scale}}^{\text{OH}}$, (e) the other sensitivities of tropospheric OH to changes in NO_x, CO, and VOC, namely $S_{\text{NO}_x}^{\text{OH}}$, $S_{\text{CO}}^{\text{OH}}$, $S_{\text{VOC}}^{\text{OH}}$ (updated to 9.3376e-3, -1.13e-4, and -3.142e-4 from 4.2e-3, -1.05e-4, and -3.15e-4, respectively). Also, we updated the partial soil related lifetime of CH₄ (150 years rather than 160 years), following to Prather et al. (2012).

The net effect of the newly calibrated MAGICC is that Holmes et al. (2013) CH₄ projections are closely matched across the range of RCPs (Supplementary Figure 1, left column). Both OH-related and total CH₄ lifetimes exhibit similar changes over time as in Holmes et al. (Supplementary Figure 1 **Error! Reference source not found.**, middle columns), with the slight upward offset explained by our historical budgeting approach deducting somewhat lower natural CH₄ emissions (which MAGICC assumes constant over time) (Supplementary Figure 1, right column).

2.4.2 Nitrous oxide projections

Prather et al. (2012) suggested that the RCP projections for N₂O concentrations performed with MAGICC6 were somewhat too low for the lower RCP2.6 scenario and slightly too high for the higher RCP8.5 scenario (although within their uncertainty ranges). Here, we use their model to back out natural emission assumptions and lifetimes to allow a multi-variable calibration of MAGICC7 to the median of the RCP N₂O concentration range suggested and these other variables by Prather et al. (2012) (Supplementary Figure 2).



To set up this calibration, we complement RCP emission pathways by historical N₂O emissions from PRIMAP-hist (Gütschow et al., 2016). We also used observed N₂O concentrations until 2014 (Meinshausen et al., 2017) to complement the future Prather et al. concentrations. The natural N₂O emission levels are calibrated (as part of the overall calibration that optimised lifetimes, budgeting periods and lifetime sensitivities) with a budgeting approach over the 10 years prior to 1991, resulting in a slightly lower assumed natural N₂O emission level of 8.013 MtN-N₂O compared to Prather et al (9.1 MtN-N₂O) and AR5 (11.0 MtN-N₂O). Nonetheless, the total natural and anthropogenic emissions are similar for present-day conditions, because Prather et al. assumes lower anthropogenic emissions (6.5 MtN-N₂O) compared to the RCP pathways, which assume in average 7.9 MtN-N₂O. Apart from the budgeting period, MAGICC7's N₂O gas cycle has three further N₂O parameters, which we calibrate to the Prather et al. results. Those are (a) the initial N₂O lifetime $\tau_{N_2O}^0$ (updated from 123 years to 139 years), the sensitivity coefficient $S_{\tau_{N_2O}}$ which scales the N₂O lifetime with the factor $\left(\frac{C_{N_2O}^t}{C_{N_2O}^0}\right)^{S_{\tau_{N_2O}}}$, where $C_{N_2O}^t$ is the current atmospheric burden at time t, and $C_{N_2O}^0$ the pre-industrial burden ($S_{\tau_{N_2O}}$ updated from -0.05 to -0.04). Lastly, we calibrated the sensitivity of the stratospheric lifetime, with which N₂O's partial stratospheric lifetime is adjusted in response to a change in the Brewer-Dobson circulation (0.04 percent change of partial lifetime per percent change of meridional flux).

2.4.3 Additional gas cycles

We extended the number of fluorinated gases to cover the full range of 43 greenhouse gases in MAGICC (i.e. including HFCs) from 12 to 23 and the number of ozone depleting substances from 16 to 18. Specifically, the newly modelled fluorinated species are perfluorocarbons C₃F₈, C₄F₁₀, C₅F₁₂, C₇F₁₆, C₈F₁₈, CC₄F₈, hydrofluorocarbons HFC-152a, HFC-236fa, HFC-365mfc, as well as NF₃, and SO₂F₂. The newly modelled ozone depleting substances are methylene chloride CH₂Cl₂, with a very short lifetime of 0.4 years, and methyl chloride CH₃Cl, with a lifetime of around one year (for lifetimes, see Table 8.A.1 of IPCC AR5 WG1 Chapter 8 (Myhre et al., 2014)). We scale the partial stratospheric lifetime (HFC-152a, 39 years; HFC-236fa, 1800 years; HFC-365mfc, 125 years; NF₃, 740 years; and SO₂F₂ with 630 years – taken from Table 1-3 in WMO (2014)) with a change of the Brewer Dobson circulation strength. For every 1% increase in the Brewer-Dobson circulation, the partial stratospheric lifetimes are reduced by 0.3%. The Brewer-Dobson circulation is assumed to increase 15% per degree of warming beyond 1980



365 levels. For the partial lifetimes related to the tropospheric OH sink, we assume a scaling with the OH
abundance (which is largely driven by CH₄, VOCs, CO and NO_x – see above).

2.4.4 Permafrost feedbacks

Earth system feedbacks from permafrost melting and its associated CO₂ and CH₄ releases were
underrepresented in CMIP5 climate models, leading – inter alia – to an ad-hoc adjustment of remaining
370 carbon budgets by 27 GtC (100 GtCO₂) in the IPCC Special Report on 1.5°C warming. Also, they were
not part of the concentration projections for the RCP scenarios. Here, we now include a representation of
permafrost feedbacks based on the MAGICC permafrost (Schneider von Deimling et al., 2012), leading
to additional cumulative CO₂ emissions of 25 to 88 GtC by 2100, 42 to 378 GtC by 2200 and 51 to 542
GtC by 2300 for the lowest (SSP1-1.9) and highest (SSP5-8.5) scenario, respectively (**Table 2**). Thus, our
375 permafrost module is in line with the IPCC Special Report on 1.5°C warming assumptions for the lowest
scenarios (25 GtC versus 27 GtC). While we do not entertain the probabilistic version in this study, our
default settings are comparable to the median values reported in Schneider von Deimling (2012). In the
highest scenarios (SSP5-8.5), these permafrost related Earth System Feedbacks cause CO₂ concentrations
that are up to 200 ppm higher by 2200 (**Figure 3a**). A later study included a more complex offline model
380 with deep carbon deposits, a vertical soil resolution and abrupt thaw processes like thermokarst lake
formations. Generally, the results are comparable, although our settings might underestimate 21st century
contributions and overestimate long-term cumulative emissions in comparison to Schneider von Deimling
(2015).

In addition to elevated CO₂ concentrations, the permafrost module also estimates future CH₄ emissions
385 related to permafrost thawing, i.e. annual emissions of up to 75 MtCH₄/yr in the highest SSP5-8.5 scenario
by 2200. Cumulatively, 0.34 GtC to 1.07 GtC of carbon are projected to be released as 451 MtCH₄ to
1431 MtCH₄ over the course of the 21st century across the 9 considered SSP scenarios (Table 2), with
even more coming in the 22nd century. The extra emissions lead to 10-240 ppb higher CH₄ concentrations
in 2200 (**Figure 3b**). Most of the carbon decomposition is assumed to happen as aerobic decomposition
390 in the mineral soils, stretching from the more southerly zonal permafrost bands to the higher latitudes
from now to 2200 (**Figure 3 e to h**).



2.5 Projecting latitudinal gradients

Compared to the previous input datasets for CMIP intercomparisons, which consisted of global-mean values only, latitudinal gradients (and seasonality) are new elements. For the historical period, these latitudinal gradients and seasonally changing surface air concentrations can be estimated from the large set of in situ and flask sampling sites with monthly sampling resolution. Further back in time, when there was insufficient latitudinal coverage, the latitudinal gradient was decomposed into two empirical orthogonal functions (EOFs, the principal components). The multiplier or score (also known as the principal component time series) for the first EOF was regressed against global anthropogenic emissions. Except for CO₂, the score for the second EOF was kept constant. For CO₂, we assumed a simplified approach by both assuming a zero intercept for the regression of global emissions versus the first EOF and a phase-out back in time of the second EOF score. These lead to the simplified and uncertain assumption that the pre-industrial CO₂ gradient was zero (Figure 9b in Meinshausen et al. (2017)). For a more detailed description of the interpolation and assimilation algorithms for the historical data, see Meinshausen et al. (2017).

For the future, there are obviously no observations from which the changes in the latitudinal gradients can be derived. We hence apply the regression procedure from the historical dataset into the future i.e. we project the score of the first EOF of the latitudinal gradient of each greenhouse gas with its global emissions. That makes the simplifying assumption that, in the future, the sources (and sinks) of these gases remain approximately constant in terms of their latitudinal location (not in terms of their magnitude). For CO₂ in the very low emission scenarios, like SSP1-1.9 with net negative CO₂ emissions, that leads to a plausible reversal of the latitudinal gradient if the northern hemisphere is the main location for the natural and anthropogenically induced net CO₂ sink.

For CH₄, which exhibits also large natural sources, predominantly in the northern hemisphere, anthropogenic emissions resulted in a derived latitudinal gradient up to 80 ppb above the global average in the northern midlatitudes while Southern hemispheric concentrations gently slope towards a minimum of 60 ppb below the global average at the pole at the end of the historical datasets (Figure 11b in Meinshausen et al., 2017). As for CO₂, we use anthropogenic CH₄ emissions to extrapolate the first EOF



score into the future. Given that CH₄ emissions do not converge to zero in any scenario, let alone become
420 negative, the strong North-South gradient is maintained in all scenarios.

2.6 Projecting seasonality

Seasonality of concentrations is by far most strongly pronounced for CO₂, given the large seasonal sink
(photosynthesis) and source (heterotrophic respiration) pattern of the northern hemispheric terrestrial
biomass. Projecting future seasonality changes depends on a correct understanding of the past seasonality
425 changes and how those seasonality changes are related to changes in ecosystem productivity (Forkel et
al., 2016; Graven et al., 2013; Welp et al., 2016), increased cropland productivity (Gray et al., 2014) and
other factors. Here, we use the net ecosystem productivity (NPP) as a proxy for future seasonality changes
and regress the historically derived seasonality change EOF score with modelled future net ecosystem
exchange by MAGICC7. NPP in MAGICC7 is projected to strongly increase in the highest SSP5-8.5
430 scenario, while following a maximum-then-decline pattern in the lower SSP1-1.9 scenario. At the end of
the historical period, the total seasonality is derived to have a minimum concentration deviation of -10.1
ppm in Northern mid-latitude August. Given these projected NPP changes in the high SSP5-8.5 scenario,
the projected total seasonality increases to approximately twice that by 2100, a projection that comes with
a high degree of uncertainty.

435 For all other gases for which we identified a significant seasonal cycle in the historical observational data,
we assume that the relative seasonality (i.e. the magnitude of monthly anomalies relative to the annual
mean) stays constant, i.e. that the absolute seasonality concentration changes scale with global-mean
concentrations.

2.7 Simplified formula to reflect radiative forcing from CO₂, CH₄ and N₂O

440 In order to present CO₂, CH₄ and N₂O in our compilation of 43 greenhouse gases and their relative
importance for future effective radiative forcings (ERFs), we use simplified radiative forcing formula (for
radiative forcing after stratospheric temperature adjustments) that represent the Oslo line-by-line model
results – which now takes into account the short-wave absorption of CH₄, among other aspects (Etminan
et al., 2016). While Etminan et al. provided simplified formulas for their Oslo line-by-line model results,
445 we here adjust those simplified formulas, resulting in a virtual elimination of the model fit errors by



Etminan of up to 3.6% for CO₂ (see Table 1 in Etminan et al. (2016) and our **Figure 4d** and **Table 3** below). Aside from slight model mis-fits, the original Etminan simplified formula for CO₂ has a validity range of only up to 2000 ppm CO₂ concentrations. Their simplified formula is an adaptation of the classical approach to approximate radiative forcing by $\alpha * \ln\left(\frac{C}{C_0}\right)$, where α is a scaling coefficient, C the

450 CO₂ concentration at time t and C_0 the concentration at the reference state, normally the pre-industrial reference value. Etminan et al. introduce the overlap of the absorption spectra between CO₂ and N₂O and also modulate the logarithmic approximation by quadratic and linear terms. When using their suggested coefficients (a_1 , b_1 and c_1 in their Table 1), the factor α in front of the $\ln\left(\frac{C}{C_0}\right)$ part reaches a maximum at $C_0 - \frac{b_1}{2a_1}$, i.e. at around 1777 ppm, when assuming C_0 as the pre-industrial concentration (277.15 ppm).

455 For CO₂ concentrations beyond 1777 ppm, the alpha value decreases, leading to an unrealistic flattening off above 2000 ppm (and eventual decline well above 3000 ppm). The highest projected SSP concentration (SSP5-8.5) reaches beyond the nominated validity range of 2000 ppm. Hence, we adapt the CO₂ radiative forcing formula to assume a constant α , once α reaches its maximal value (which is around 1808 ppm with our optimised parameter settings – see **Table 3**).

460 In summary, building on the work of Etminan, our optimised modifications of the simplified radiative forcing expressions for CO₂, CH₄ and N₂O as presented in **Table 3** have the two advantages of (a) representing the 48 Oslo line-by-line model results within rounding errors and also (b) extending its likely validity range in line with previous forcing approximations (and pending examinations by line-by-line models) to higher CO₂ concentrations. However, there is one disadvantage of our simplified formula.

465 While our formula starts from fixed C_0 , N_0 , and M_0 values at pre-industrial levels, the formulas presented in Etminan cater for the option to set C_0 , N_0 and M_0 at any value within the validity range. Hence, our formula would have to be applied twice to calculate the difference in terms of radiative forcing between a C_1 , N_1 , M_1 and a C_2 , N_2 , M_2 concentration state, if both are different from pre-industrial levels C_0 , N_0 and M_0 .

470 We also take into account new findings regarding rapid adjustments (Smith et al., 2018). In the multi-model analysis by Smith et al. (2018), CO₂ is suggested to have a slightly (~5%) higher effective radiative forcing than its instantaneous radiative forcing after stratospheric temperature adjustments alone, an



adjustment also used here. While the tropospheric rapid adjustments in the case of CO₂ is substantial, it is largely offset by the corresponding water vapour adjustment and the cloud-related rapid adjustments (Figure 3 in Smith et al., 2018). Following Smith et al. (2018), we assume that rapid adjustments largely cancel out for CH₄.

2.8 Data-flow, mean-preserving higher resolutions, and merging with historical files.

In this study's projections, the data is provided in 15° latitudinal bands with monthly resolution. These are constructed from the global-mean time series generated by MAGICC7, with the modulation towards latitudinal annual means by the time-changing latitudinal gradients (section 2.5). These latitudinal annual means are then turned into monthly data values using the latitudinally and monthly resolved seasonality fields.

There are two additional post-processing steps involved. For one, the mean-preserving interpolation routines from Section 2.1.9 of Meinshausen et al. (2017) are used to generate a monthly surface air mole fraction field at a finer 0.5° latitudinal resolution. The other step is merging the projections with the historical concentrations. To ensure a smooth transition from the previously derived historical concentration fields to the ones derived in this study, we use the latitudinally resolved differences in the month of December 2014 between the historical fields derived in Meinshausen et al. (2017) and the raw data produced here. We then add those December 2014 differences to the 2015 future datasets, phasing them out linearly over 12 months.

3 Results

This study's projected greenhouse gas concentrations provide the 'official' greenhouse gas concentrations for the SSP scenarios. They help enable the CMIP6 exercises and span a wide range of possible futures. Below, the results are presented for the various gases. The complete data repository of all projected mole fractions in various data formats, with interactive plots and factsheets is available at <http://greenhousegases.science.unimelb.edu.au>. The subset of the data recommended for the nine SSPs that are part of the ScenarioMIP and AerChemMIP experiments in netcdf format is also available on <https://esgf-node.llnl.gov/search/input4mips/>.



3.1 Carbon Dioxide

500 The projected CO₂ concentrations range from 393 to 1135 ppm in 2100, with the low scenario SSP1-1.9 decreasing to 350 ppm by 2150. Given the assumption of zero CO₂ emissions in the lower scenarios beyond that, the lower end of the projected CO₂ concentrations is not projected to decrease much further. On the upper end, under the SSP5-8.5 scenario global-average concentrations are projected to increase up to 2200 ppm by 2250 (**Table 4** and **Table 5**). The latitudinal gradient implies a difference of annual-
505 average northern midlatitudes to South pole concentrations of about 7 ppm. For the future, the applied projection methods result in a zero latitudinal gradient by ~2060 in the lowest SSP1-1.9 scenario (**Figure 5b**) because CO₂ emissions revert from positive to net negative. Under the highest SSP5-8.5 scenario, the northern midlatitude to South Pole difference expands to more than 23 ppm by 2100 (not shown in plot, but viewable in online data repository at greenhousegases.science.unimelb.edu.au).

510 3.2 Methane

Global-mean CH₄ surface air mole fractions across the SSP scenarios are projected to range from 999.7 ppb to 3372 ppb by 2100, with maximal northern hemispheric averages being ~60 ppb higher than the global average (**Table 4**). The largest difference between average Northern and Southern hemispheric concentrations (up to 120 ppb by 2100, **Table 5**) is in the highest CH₄ emissions scenario (SSP3-7.0) and whilst the smallest difference (~70 ppb) is seen in the scenarios with the lowest global CH₄ emissions
515 (SSP1-1.9, SSP1-2.6 and SSP3-4.0S). While SSP5-8.5 is projected to be the scenario with the highest radiative forcing, because of high CO₂ emissions, SSP5-8.5 is not the highest CH₄ emissions scenario, with both SSP3-7.0 and SSP4-6.0 suggesting higher total CH₄ emission by 2100 (and in our extensions beyond 2100) (**Figure 2f**).

520 3.3 Nitrous Oxide

N₂O concentrations are not projected to decrease at any point before 2200, regardless of the SSP scenario we consider. Even under the lowest emissions scenarios, SSP1-1.9 and SSP1-2.6, current global-average concentrations are projected to increase from 328.5 ppb in 2015 to 361 ppb by 2100 (**Table 5**). Under the highest N₂O scenarios (SSP3-7.0 and SSP3-7.0-lowNTCF), concentrations are projected to increase to
525 422 ppb by 2100 and over 500 ppb by 2500. Both seasonality and the latitudinal gradient is rather subdued



for N₂O, as it is both a long-lived greenhouse gas and does not exhibit strong seasonal variability in either sources or sinks.

3.4 Ozone Depleting Substances and other chlorinated substances

As all ozone depleting substances' emissions are assumed to follow a single emission scenario as a result of the Montreal Protocol (Velders and Daniel, 2014b), the SSP concentration scenarios exhibit no substantial variation across their projected concentrations. For example, by 2100, CFC-11 and CFC-12 concentrations are assumed to vary from 51.4 to 56.2 ppt, and from 114.3 ppt to 133.5 ppt, respectively (**Table 4**). These differences across the concentration scenarios are hence not a result of different emission assumptions but solely due to factors that influence the substances' lifetimes. The stratospheric partial lifetime of these substances is affected by a change in the meridional Brewer-Dobson circulation, assumed to strengthen with increasing climate forcing. The tropospheric OH-related partial lifetime is scaled by changing OH concentrations. Those OH concentrations are in turn mainly affected by CH₄ abundances and emissions of other reactive gases (CO, NMVOC, NO_x). Overall, the concentrations and radiative forcing contributions of all ozone depleting substances are assumed to strongly reduce until 2100 and beyond, following the phase-out schedules under the Montreal Protocol (**Figure 10**). See section 4.2 for a discussion of the unexpectedly slow declines of CFC-11 (Montzka et al., 2018) and other species, though.

3.5 Other fluorinated greenhouse gases

The fluorinated gas' emissions with a virtually zero ozone depleting potential - HFCs, PFCs, SF₆ and NF₃ - vary across the SSP scenarios. Most SSP scenarios assume strong decreases for several of these substances (e.g. NF₃ and SF₆), while SSP5-8.5 assumes strong increases for most of the 21st century (**Figure 2h,i**). Until recently, these fluorinated gases were not controlled under the Montreal Protocol. With the 2016 Kigali Amendment, however, a select number of HFCs have been included in the Montreal Protocol and GWP-weighted emissions of these particular HFCs will have to be phased-down globally in coming decades. When aggregating all this non-ozone depleting fluorinated gases into HFC-134a equivalent concentrations, the SSP scenarios project a wide range of 2100 values, ranging from 278 ppt to more than ten-fold that value, i.e. 2985 ppt (last row in **Table 4**). While the HFC projections are derived



from the IAM modelling team assumptions regarding the SSPs, several of the resulting HFC projections would exceed the phase-out emission levels agreed to in the Kigali Agreement.

555 3.6 Radiative forcing since 1750

In this section, we aggregate all 43 greenhouse gases' radiative forcing effect using the updated radiative forcing formula for CO₂, CH₄, and N₂O and standard radiative efficiencies from IPCC AR5 (section 2.7). Across the nine SSP scenarios, it is apparent that CO₂ makes the largest contribution to future warming (blue parts in **Figure 7**), constituting between 68% and 85% of GHG radiative forcing by 2100, and 68% to 92% of radiative forcing by the time of maximum GHG-induced radiative forcing (**Table 6**). In the scenario with the greatest radiative forcing, SSP5-8.5, radiative forcing in 2100 is projected to be approximately 8 W/m² and 9.7 W/m² for CO₂ or all GHGs, respectively (right-axis bars in **Figure 7i**). This greenhouse gas induced radiative forcing is projected to increase to nearly 13 W/m² by 2250 under SSP5-8.5. On the lower side, the SSP1-1.9 scenario exhibits a CO₂ radiative forcing of around 1 W/m² in 2150 and beyond, with total greenhouse gas induced forcing stabilising around 1.5 W/m² – equivalent to CO₂ concentrations of approximately 370 ppm (right axis in panel a of **Figure 7**).

4 Discussion

In this section, we discuss the SSP greenhouse gas concentration projections in relation to the last 2000 years of observations and cumulative carbon emissions, which are an important metric for mitigation efforts. We also provide a comparison to previous RCP pathways.

4.1 CO₂ and CH₄ concentrations

After CO₂, the greenhouse gas with the second largest radiative forcing contribution in the 21st century is CH₄ (**Figure 7**). To a large extent, greenhouse gas induced future warming is hence influenced by the concentrations of CO₂ and CH₄. Two examples in which methane and CO₂ forcings and their relative strength are important. i: Firstly, discussions about the benefit of the mitigation of short-lived forcers often accounts for CH₄ as a short-lived forcer, which usually contributes most of the climate benefits of any short-lived forcer mitigation strategy (Rogelj et al., 2015; Rogelj et al., 2014). Hence, when the



climate benefits of reducing short-lived forcers are compared to those of reducing CO₂ emissions, the actual comparison is mostly between CH₄ and CO₂. Secondly, deriving the remaining carbon budget from Earth System Model runs from single or a few scenario runs is contingent on those scenarios showing a representative level of CH₄ versus CO₂ concentrations. Here, we consider mid-21st century CH₄ and CO₂ concentrations across the range of SSP scenarios. We place them in the context of the RCP scenarios as well as 475 scenarios of the IPCC Special Report on 1.5°C emissions database (<https://data.ene.iiasa.ac.at/iamc-1.5c-explorer/>) (Figure 9). We focus on mid-century concentrations as they are close to the expected point of peak warming in the scenarios that are in line with the Paris Agreement temperature targets of 1.5°C and well below 2.0°C. The comparison shows that SSP1-1.9 and SSP1-2.6 result in relatively similar CH₄ concentrations by 2050, albeit their CO₂ concentrations differ by approximately 7% (437 ppm versus 469 ppm, respectively, Table 5). The other scenario with low CH₄ concentrations in 2050, i.e. SSP3-7.0-lowNTCF, falls outside the scenario space considered here, namely the SR.15 database (<https://data.ene.iiasa.ac.at/iamc-1.5c-explorer/>, see Figure 9 below). This is by design, as this scenario is the result of adapting a high emission scenario (SSP3-7.0) so that it features very low short-lived climate forcer emissions (Collins et al., 2017). See also Appendix C in Gidden et al. (2019) for a detailed comparison of SSP3-7.0 and SSP3-7.0-lowNTCF emissions. The comparison of mid-century CO₂ and CH₄ concentrations also reveals that the main reason for higher implied warming of SSP4-3.4 in comparison to SSP1-2.6 are elevated CH₄ concentrations. Thus, to a limited extent, the SSP4-3.4 and SSP1-2.6 scenarios represent a similar pair of scenarios to the SSP3-7.0 and SSP3-7.0-lowNTCF scenarios, but for a lower level of cumulative CO₂ emissions.

4.2 Most recent concentration observations

While updating the historical observations for our future concentrations, several recent trends are noteworthy. We discuss these in this section, covering CH₄, ozone depleting substances as CFC-11, CFC-12, CFC-113 as well as HFC-23 and SF₆.

Regarding CH₄, atmospheric observations show a plateauing of CH₄ concentrations from 1999 to 2005 as followed by an increased growth rate from 2007 (Nisbet et al., 2016). Available literature suggests that changes in natural and anthropogenic sources and OH-related sinks are involved (Rigby et al., 2017), for example reduced biomass burning emissions (Worden et al., 2017) or reduced thermogenic fossil-fuel



related emissions (Schaefer et al., 2016) to explain the plateau of concentrations until 2006, but large uncertainties remain, particularly related to natural wetland and inland water sources (Saunio et al., 2016). Schaefer et al. (2016) suggest that the renewed onset of increasing CH₄ concentrations could be related to increased emissions from the agricultural sector.

610 Our CH₄ concentration time series, both the historical ones and the future projections from 2015 onwards, capture this observed increase in the trend **Figure 6b**) – although there is uncertainty as to whether the underlying processes and emission sources are correct. Nevertheless, our employed simple model MAGICC7 also captures this temporary plateau of CH₄ concentrations when run in an emission-driven model, possibly not the earlier parts though (left column in Supplementary Figure 1). Note that the
615 transition in 2017 from observationally-driven concentrations to our model-driven concentration timeseries exhibits a slight offset in concentrations (section 5.3), as MAGICC7 inferred a slightly stronger increase in CH₄ concentrations over 2016 based on the IAM’s emissions, than observed (**Figure 6**).

For nitrous oxide, there appears to be a small downward adjustment in the growth rate around 2014, with atmospheric growth in years 2016 and 2017 being slightly lower than in 2014 (**Figure 6c**), although
620 observed 2018 growth rates picked up again and the slight offset seems to be well within the noise of recent growth rate variations. For a close comparison of recent observations and our concentration timeseries, see the CH₄- and nitrous oxide-related factsheets at <http://greenhousegases.science.unimelb.edu.au>.

Recent observations regarding substances whose production is largely phased out under the Montreal
625 Protocol are also notable (Montzka et al., 2018; Rigby et al., 2019). CFC-11 measurements show some elevated northern hemisphere values from 2013 onward and the global average concentrations are 5-10 ppt above published projections from 2012 to 2017, which consider compliance with projected Montreal Protocol controls, even though the global concentration continues to decline (Velders and Daniel, 2014b) (see panel h in online CFC-11 factsheets at <http://greenhousegases.unimelb.edu.au>). Our projections
630 reflect the elevated atmospheric concentrations until 2016, but then continue on the assumption of compliance with the Protocol and those additional emission sources to be halted. By analyzing measurement data from sites around the world, it was also concluded that the additional CFC-11 emissions – roughly a 25% increase since 2012– originate in part from the eastern Asian region (Rigby



et al., 2019; Montzka et al., 2018), and an updated study has identified that about half of the global
635 increase can be attributed to 2 provinces in eastern China (Rigby et al., 2019). Although less pronounced,
CFC-12 and CFC-113 concentrations have also not declined as expected since 2013, although for neither
of these gases emissions are thought to have actually increased in recent years, as is the case for CFC-11
(**Figure 10b**). Even stronger is the diversion of projected and recently observed concentrations for CFC-
114, when comparing against the recent Velders and Daniel projections (2014b). For a discussion of
640 recent concentrations of CFC-13, and inferred emissions of CFC-13 (which also seem to increase due to
Asian sources) and the two isomers of CFC-114 as well as CFC-115, see Vollmer et al. (2018).

Chloroform (CHCl_3) exhibited a concentration decline since 2000 but is increasing again in the global
atmosphere (see Chloroform Factsheet available in the online data repository at
<http://greenhousegases.science.unimelb.edu.au>). Fang et al. (2019) point to a recent strong growth of
645 chloroform emissions in China. Similarly, the similarly short-lived methylene chloride (CH_2Cl_2) had
almost stagnant atmospheric concentrations around the year 2000, but high growth has been observed in
subsequent years, almost doubling atmospheric global-average concentrations from around 20 ppt to 40
ppt by 2017 (Hossaini et al., 2015). See also Chapter 1 of the 2018 Ozone Assessment Report (Engel et
al., 2018).

650 Emissions of HFC-23 originate almost completely as a by-product of the production of HCFC-22. Under
the Kyoto Protocol, abated emissions of HFC-23 are eligible to be credited in project based offset
mechanisms – leading to a bulk of offset credits under the Clean Development Mechanism and also two
former Joint Implementation projects in Russia (Schneider, 2011). It has been shown that so-called
'perverse incentives' likely resulted in additional production – in order to broaden the magnitude of
655 claimable abatement credits (Schneider and Kollmuss, 2015). Given that the monetary value of those
offsets credits far exceeded the abatement costs, the Kigali Amendment to the Montreal Protocol in
October 2016 lead to a new regulatory approach for HFC emissions (Velders et al., 2015). Nevertheless,
rather high individual station measurements (classified as "pollution" events) lead to high monthly
average concentrations at the Gosan South Korean station. Together with accelerating growth trends for
660 HFC-23 since 2015, this could point to a continued large increase of emissions (see panel h in HFC-23
related factsheets on <http://greenhousegases.science.unimelb.edu.au>). Similarly, SF_6 concentrations
continue to increase at unprecedented rates. They will remain high for a long time (without other



anthropogenic interventions) due to SF₆'s very long lifetime. The commonly assumed lifetime so far (also assumed in this study) has been 3200 years (Myhre et al., 2013), although recent findings about a loss
665 mechanism in the polar vortex suggest a lower new best estimate of 850 years (Ray et al., 2017).

4.3 The long-term projections in the context of last 2000 years

As the historical compilation of greenhouse gas concentrations based on firm and ice core records indicated, multiple literature studies indicate relatively flat concentration of CO₂, CH₄ and N₂O over the past 2000 years. Historical fluctuations over the last 2000 years of a few ppm or ppb, e.g. around 1650
670 for CO₂, a miniscule in comparison to recently observed concentration changes since the onset of industrialisation and projected future changes (**Figure 8**). For example, CO₂ concentrations could reach to levels beyond 1500 ppm in the SSP3-7.0 and SSP5-8.5 scenarios and even reach beyond 2000ppm by 2200 under SSP5-8.5. Those CO₂ concentrations in excess of 1500ppm have likely not been present on Earth for more than 40 million years ((Fig. 4 in Royer, 2006) – i.e. before the current Antarctic and
675 Northern hemisphere ice sheets formed. Reflecting the shorter lifetime, concentrations of methane can reduce pronouncedly over the 21st century. For CO₂, for which lower scenarios foresee the option of net negative emissions, concentrations also recede over the long term to around 350ppm in case of the SSP1-1.9 scenario. Reflecting the longer lifetime and base level of agricultural emissions, N₂O concentrations are not foreseen to drop below current levels in any of the investigated SSP scenarios over the coming
680 500 years (**Figure 8**).

4.4 Comparing SSP and RCP concentrations

For every generation of climate scenarios, whether these are the IS92, SRES, RCP or now the SSP scenarios, it is pertinent to clarify the differences and similarities of the new scenario set to the previous one(s). In particular due to the unavoidable delay in the analysis and use of the climate projections in the
685 impact communities, clarifying the comparability to previous scenarios is paramount. Here, we compare both the greenhouse gas concentrations and an indication of global climate effects (section 4.5).

Four RCP scenarios are now replaced in the SSP generation of scenarios with five “high priority” scenarios (4 ScenarioMIP “Tier1” cases plus SSP1-1.9) in addition to 4 additional scenarios that investigate additional forcing levels (see panels a,c in **Figure 11**). Aside from this difference in the sheer



690 number of scenarios, compared to the RCPs, the actual concentration levels differ substantially for most
corresponding SSP scenarios. For example, the SSP5-8.5 scenario features substantially higher CO₂
concentrations by 2100 and beyond than the RCP8.5 scenario (panels a,b in **Figure 11**). Somewhat
compensating though, the CH₄ concentrations by 2100 are substantially lower under the SSP5-8.5
695 scenario compared to the RCP8.5 scenarios (**Figure 11c**), and that difference is even more pronounced
by 2300 due to the different extension principles followed for RCP extensions (Meinshausen et al., 2011b)
and those for SSPs (section 2.3). Specifically, the SSP5-8.5 fossil and industrial CH₄ emissions are
assumed to be phased out by 2250 with land use-related CH₄ emissions kept constant at 2100 under the
SSP5-8.5 extension. That contrasts with the RCP8.5 extension, in which a long term CH₄ concentration
700 stabilisation at very high levels of 3500 ppb was implemented. Similarly, for N₂O, the new SSP5-8.5
scenario implies lower concentrations by 2100 and beyond compared to the RCP8.5 (**Figure 11e,f**). Under
the SSP family, the SSP3-7.0 becomes the scenario with the highest emissions and concentrations for
both CH₄ and N₂O.

On the lower side of the scenarios, the most marked differences are that the new SSP1-2.6 has higher CO₂
concentrations, compared to the previous RCP2.6 and SSP1-1.9 has the lowest CO₂ concentrations
705 (**Figure 9** and **Figure 11a**). CH₄ concentrations are very similar across these three scenarios by the middle
of the century, whereas by the end of the 21st century, the new SSP1-1.9 and SSP1-2.6 scenarios show
reduced levels of only 1000 ppb, substantially below today's CH₄ concentration levels. For N₂O, the story
is the other way around: SSP1-1.9 and SSP1-2.6 follow almost identical concentration trajectories while
the previous RCP2.6 scenario is lower.

710 **4.5 Comparing SSP and RCP temperature and sea level rise implications**

A key interest to the user communities of the new SSP scenarios is their comparability with previous RCP
scenarios, not only in terms of concentrations (section 4.4) but also more aggregated in terms of their
overall global mean temperature and sea level rise implications. While a comprehensive assessment will
require the corresponding analysis of CMIP5 and forthcoming CMIP6 ESM results, we here provide an
715 initial assessment using a consistent modelling setup for both RCP and SSP scenarios. Specifically, we
run MAGICC7.0 in a probabilistic setting that captures a skewed-normal climate sensitivity likely range
from 2°C to 5°C with a best estimate of 3°C – with corresponding parameters being drawn consistently



from the historical constraining study described in Meinshausen et al.(2009). The methodological setup of using an adapted climate sensitivity range is also used in Rogelj et al. (2012), when comparing SRES and RCP scenarios. In addition, we updated the CO₂, CH₄ and N₂O forcing parameterisations in MAGICC7.0 as described above (section 2.7). Here, we also use the probabilistic MAGICC sea level model introduced by Nauels et al. (2017) and include our permafrost module (section 2.4.4). Note that a fully calibrated version of MAGICC7 (version 7.x) will be available after the analysis of the CMIP6 ESM data. In addition, we normalised the SSP global-mean surface air temperature (GMSAT) and global-mean sea level rise data to the AR5 reference period 1986-2005 to facilitate a comparison with published key RCP data by IPCC AR5 (Table SPM.2 of the IPCC WGI AR5 SPM).

When comparing the results of these temperature and sea level rise projections with those of IPCC AR5, it is noteworthy that our default MAGICC7.0 setting yields similar results for low scenarios RCP2.6 as IPCC AR5 did. However, at the high end, our illustrative probabilistic setting yields much warmer projections of up to nearly 6.0°C by 2100 for median projections under the RCP8.5 scenarios - compared to median projections around 5.0°C (CHECK) for RCP8.5 relative to pre-industrial levels provided by IPCC AR5 (**Figure 12 a**). The main reason is the higher than previously assumed upper climate sensitivity range (5°C), included permafrost feedbacks as well as substantially higher methane forcing (section 2.7). Using the previous probabilistic setup for MAGICC6, our results are closely comparable to those reported by IPCC AR5 (TO DO - SHOW THAT IN FIGURE). A comparison with forthcoming CMIP6 ensemble results will show whether the new default settings are too warm compared to the Earth System Model ensemble.

When considering relative differences across SSP and RCP scenarios, we note that SSP5-8.5 is closely comparable to RCP8.5, although somewhat cooler. That might be due to lower methane concentrations in SSP5-8.5 compared to RCP8.5 (**Figure 9**) and also higher sulfur and BC aerosol emissions (Figure 5 in Gidden et al., 2019). The SSP2-4.5 scenario is relatively closely comparable to the RCP4.5 scenario. While the former RCP6.0 scenario has been relatively close to RCP4.5, even undercutting RCP4.5 emissions for much of the early 21st century, the new SSP3-7.0 is more evenly spaced in between SSP2-4.5 and SSP5-8.5. The RCP4.5 and RCP6.0 similarity and overcrossing brought both communication challenges and opportunities. The opportunity is that it can be easier communicated and “shown” that a higher or lower early-century emission level is not 1:1 correlated with a higher or lower emission level



for the rest of the century. In fact, the second highest 2020 CO₂ emissions after RCP8.5 were associated with the RCP2.6 scenario that implied the lowest temperature change by the end of the century. In the five high-priority SSP scenarios, the ranking is much more evenly spaced. That has the communication opportunity for simplicity and clarity about which scenario is higher or lower than another one, which had been a challenge when comparing RCP4.5 and RCP6.0. The opportunity of showing cross-overs and that early concentration levels not necessarily dictate late-century concentration levels is mostly indicated by the SSP5-3.4-OS scenario, which initially follows the highest SSP5-8.5 scenario before embarking on very low and strongly negative emissions. The strong peak & decline shape is interesting from a geophysical point of view. This strong increase and decrease shape even of temperatures (**Figure 12a**) featured by SSP5-3.4-OS has not been part of the RCP scenario family and hence could provide new insights about the asymmetric nature of carbon cycle and heat uptake/release patterns during a strong drawdown phase of CO₂ versus the historical steady increase.

For sea level rise, the comparison of MAGICC7.0 results between SSPs and RCPs and between the latter and the IPCC AR5 RCP results is closely reflecting our results for temperature projections. While AR6 RCP2.6 range remains close to the AR5 equivalent range for RCP2.6, the AR6 RCP8.5 2081-2100 median is about 0.1 m higher than for the AR5 RCP8.5, with the upper bound of the 90% model range close to 1.1 m instead of around 0.8 m for the AR5 equivalent. In this context, it is important to note that the AR5 consistent sea level model setup presented in Nauels et al. (2017) is applied, without accounting for any additional potentially nonlinear contributions, in particular from the Antarctic ice sheet, that have been discussed since IPCC AR5 (DeConto and Pollard, 2016; Edwards et al., 2019; Golledge et al., 2019). Hence, the GMSLR differences shown here are the result of the updated MAGICC model as well as the different GHG concentrations underlying the new SSP pathways and the resulting differences in warming of the atmosphere and ocean.

4.6 Estimating the effect of latitudinally and seasonally resolved GHG concentrations on surface air temperatures in ESMs

A much-improved assimilation process results from considering seasonally and latitudinally resolved GHG concentration – as individual station monthly mean measurements can easily be “bias” corrected to account for their latitudinal and seasonal variations to inform the global mean. In addition, however, the



775 latitudinally and seasonally resolved GHG concentration data we provide also offers an opportunity to
drive Earth System models with more accurate forcings, so that a comparison of the ESM historical runs
with observational data can be performed – excluding ESM biases that might result from GHG
concentrations that are applied with a globally uniform GHG concentration levels or spatial fields that are
sometimes rather dissimilar from observations (Figures S46 and S47 in Supplementary of Meinshausen
780 et al., 2017). In order to test the approximate magnitude of applying either globally uniform (“yearmean-
global”) or latitudinally and seasonally resolved GHG concentrations (“lat-mon”), we performed 6
historical ensemble members of the CESM1.2.2 model (Hurrell et al., 2013) under each setup. To increase
the signal to noise ratio, we then took the averages over the 155 years of model simulations from 1850 to
2005 across the 6 ensembles, resulting in 930 years of model data under each experiment. Given the
785 seasonality of the data, we average the DJF and MAM monthly means in the “lat-mon” experiment and
subtract the the reference scenario’s “yearmean-global” respective average. In the DJF and MAM
northern hemispheric winter season, one would expect a slight positive warming signal in the higher
northern latitudes – given the latitudinal gradient of methane concentrations and the seasonally higher
CO₂ concentrations. Indeed, we observe a regional warming signal of up to 0.4K over Northern American
790 and Eurasian land masses, which is – in the DJF season – however latitudinally overcompensated by a
strong cooling signal in the North Atlantic (**Figure 13 a**). In the MAM season, the slight cooling signal
in the North Atlantic does not fully offset the warming over the land-masses (**Figure 13b**), resulting in a
latitudinally averaged warming signal of approximately 0.1K in the high polar north above 65 degree
North (**Figure 13d**). Given the high natural variability in the higher latitudes, we consider the significance
795 of this warming signal by comparing our warming signal to corresponding differences of arbitrarily
chosen control run segments. From an approximately 4500 year long control run for CESM1.2.2 at pre-
industrial conditions, we randomly chose hundred pairs of 930-year long segments to compute the
variability of the differences. It turns out that our warming signals are within the min-max range of those
100 sample pairs regarding the latitudinally averaged warming differences, indicating that the expected
800 warming signal due to applying latitudinally and seasonally resolved GHG concentration data is not
beyond the variability range. For the MAM region, there are only a few (approximately 3-5) of the paired
differences that result in a higher warming signal though, suggesting that the GHG warming signal might
be comparable in magnitude to the variability to be expected at a 5% confidence level. In the DJF region,
a strong North Atlantic cooling is reducing the latitudinally aggregated warming signal. Whether that



805 North Atlantic cooling is a result of natural variability in our modestly sized 6-member ensembles or whether it is a dynamical response to generally higher latitude forcing (and possible reduced overturning in the North Atlantic thermohaline circulation branch) cannot be detected from our initial ESM runs.

5 Limitations

In this section, we provide a number of key limitations that come with the SSP concentration datasets.
810 Some of these limitations arise from the underlying emission scenario data (section 5.1 and 5.2), some due to imperfect matches between recent observational and model results (section 5.3), some are intrinsic model limitations (section 5.4 and 5.5). Likely the largest limitation is that - by design - this study provides default concentration timeseries for the future but does not represent the uncertainty range of future greenhouse gas concentrations for each scenario (section 5.6).

815 5.1 Limited emission variations across scenarios for gases other than CO₂, CH₄ and N₂O.

The main focus of Integrated Assessment Models rests on projecting sectorally resolved energy, transport, industry, waste, agricultural and landuse emissions for CO₂, CH₄ and N₂O as well as air pollutant emissions. The other industrial greenhouse gases in the basket of gases of the Kyoto Protocol, namely hydrofluorocarbons (HFCs), perfluorocarbons (PFCs), SF₆ and NF₃ are often modelled as a group or in
820 subgroups. Subsequent downscaling mechanisms can then yield individual gas timeseries, although they often lack specific process dynamics, i.e. follow the same growth and decline trajectory independent of their actual end-use applications. This is certainly a limitation of many of the forward-looking PFC projections.

In terms of the ozone-depleting substances (ODS), a feature, or limitation, is that the presented SSP
825 scenarios do not capture baseline or reference scenarios or in fact any emission-driven scenario variation at all. This is because the future ODS emissions are strongly constrained by the Montreal Protocol phase-out schedules. The real-world uncertainty in ODS emissions comes from non-compliance to the Protocol and from uncertainties in emission factors from banks and bank magnitudes. In our study, in which we assume identical emissions in all of our different scenarios, future variations in concentrations are hence
830 purely climate-driven, i.e. illustrate the effect that circulation or atmospheric chemistry changes across



the scenarios can have on the ODS lifetimes. It might be worth considering whether, for future assessments, the climate community's scenarios and the ozone community's scenarios could not be commonly designed. For example, some of the scenarios could include ODS emission futures that reflect lower or even non-compliance with the Montreal Protocol to allow studies on the "world avoided" 835 (Morgenstern et al., 2008; Velders et al., 2007). An integration of scenarios used for the Ozone Assessments and the climate assessments may be desirable.

Finally, another limitations is that a few minor long-lived greenhouse gases are not included in this compilation of 43 gases, such as CFC-13 or the isomer CFC-114a (Vollmer et al., 2018).

5.2 Individual scenario features and overall scenario spectrum

840 Despite all the multi-year design efforts by large research international communities, there are some inevitable limitations of the overall group of scenarios. In particular, the final set of scenarios might be more appropriate for the earth system research community than for those interested in exploring policy relevant outcomes. For example, one of the scenarios that features new characteristic is the SSP5-3.4-OS scenario. That scenario assumes the greatest net negative emissions after an initial high emissions growth 845 rate. Its high-peak-then-strong-decline feature tests the biophysical models and will be pivotal to examine the asymmetry of the ramp-up and ramp-down characteristics of the carbon cycle, ocean heat uptake and multiple other Earth System properties. Yet, for policy purposes, that is substantially outside the target space of the Paris Agreement, aiming to keep temperatures to below 2°C warming.

A possible shortcoming for the climate science and impact community is that the new SSP generation of 850 scenarios does not provide a very closely matching overlap with the RCP scenarios, as multiple scenario features are substantially different (see e.g. CO₂ and CH₄ concentrations in **Figure 9**). Thus, from a climate science perspective, maintaining a single multi-gas scenario unaltered from the previous generation of scenarios could have provided a useful reference point with which to quantify the change in our climate system knowledge for future projections. Given the amount of human and material 855 resources used for the CMIP6 runs, it is however a question of balance between historical comparability and the capability to link to earlier studies and putting resources into the most relevant, up-to-date, scenarios. However, there is also a desire to use the best available forcing data to simulate the historical



860 period. Because the actual historical evolution of concentrations and SLCF emissions has been different in detail from previous scenarios, and historical emission and concentration estimates are updated over time (e.g. Hoesly et al., 2018), the community has thus far decided to use the most up to date data for each subsequent CMIP exercise.

5.3 Transition issues from observational to modelled concentrations.

865 MAGICC has been calibrated to allow a smooth continuation from historical time series to future projections. For some gases, this transition is possibly suboptimal. For example, atmospheric measurements since 2013 produced some rather high chloroform (CHCl_3) concentrations in the northern hemisphere, which lead to a stronger latitudinal gradient assumption in the assimilation framework for those recent years. The future projections are not reflecting a continuation of this high implied emission spike and hence revert to a lower latitudinal gradient and slightly smaller global-mean chloroform concentrations (see panel f in the Chloroform factsheet available on
870 <http://greenhousegases.science.unimelb.edu.au>). A similar transition issue is also present for HFC-23, HFC-245fa, HFC-43-10mee, CH_2Cl_2 , Halon-1301 and even more pronounced for HFC-32, whose actual global emissions seem to increase much stronger than assumed in the 2020s in our Kigali-aligned emission scenario by Velders et al. (2015).

5.4 Main limitations due to sequential scenario generation process

875 The sequential and concentration-driven nature of the main ESM CMIP6 experiments poses the challenge that future projections of greenhouse gas concentrations are required before the ESM results can be evaluated. In other words, the best estimate of future CO_2 concentrations, given a certain emission pathway, will certainly differ at the end of the CMIP6 analysis cycle from the setting with which the MAGICC7 climate model was driven with for this study. This sequential problem could only be avoided
880 with an altered experimental design, performing most future ESM experiments in an emission-driven, but computationally more demanding, design. An advantage of the concentration driven runs is that climate feedbacks and carbon cycle feedbacks can more easily be separated.

In addition to the inconsistencies introduced by the sequential and concentration-driven nature of future climate scenario experiments, there are clearly limitations of MAGICC and its chosen default parameter



885 settings for this study. A full evaluation of the extent to which the chosen parameters yield a concentration
response that is representative of the higher complexity atmospheric chemistry model projections that are
part of CMIP6 will be of key interest for future studies.

5.5 Variable natural emissions.

890 Except for the interactive carbon cycle, this study assumes constant natural emissions levels for
substances like CH₄, N₂O, CH₃Br, CH₃Cl and others. This is clearly a limitation, as under climate change
and human management of the land and ocean, the magnitude of these natural emissions (indirectly
influenced by human activities) will change over time. Future research could build knowledge of the time-
varying natural emission sources into the projection model used.

5.6 No uncertainty estimates

895 A major limitation of our study is the lack of uncertainty estimates. Given the primary purpose of this
study of providing a single reference concentration projection as input dataset for the CMIP6 experiments,
uncertainty ranges around the projections are not necessary. However, in multiple other potential
applications of this dataset, properly derived uncertainty information could have opened up new use cases.
For example, simple inversion studies could attempt to derive seasonally varying sink and source patterns
900 from our observationally based historical monthly and latitudinally resolved concentration patterns.
Without the appropriate uncertainty information, any inversion approach will have to make ad-hoc
assumptions.

6 Conclusion

905 The projected human-induced increase of atmospheric greenhouse gas abundances over the 21st century
swamps all observed variations for the last 2000 years (**Figure 8**). The new SSP scenarios span an even
broader range of CO₂ concentration futures, with the higher end (SSP5-8.5) yielding higher concentrations
than the previous RCP8.5 scenario and the lower end SSP1-1.9 scenario resulting in CO₂ emissions down
to 350 ppm in the longer term (2150). Also, in a more technical aspect, the SSP concentrations are
breaking new ground. For the first time, the greenhouse gas projections are available for 43 greenhouse



910 gases, with latitudinal and seasonal variations captured. For example, by 2050, Northern hemispheric concentrations in the SSP3-7.0 scenario are 1.2% and 4.3% higher than Southern hemispheric averages for CO₂ and CH₄, respectively - with corresponding non-negligible implications for radiative forcing (Table 5).

915 Given the substantial efforts that go into the data collection by observational network communities, a worthwhile effort in continuation from the present study would be to build a real-time framework to provide a system that updates GHG historical and future projections, including uncertainties, for a wide range of - perhaps also updated - scenarios from the integrated assessment community. While updates of observations, gas cycle models or emission scenarios in between the major IPCC or WMO Assessments are useful for a range of scientific studies, the new GHG projections data could be frozen every several
920 years to provide a new range of benchmark scenarios for Earth System Models. Efforts to provide more frequent updates for emissions data are also underway (e.g. Hoesly et al., 2018).

More than 20 years ago, the IPCC started to put forward future concentration scenarios, the so-called IS-92 scenarios. Back then in 1992, CO₂ concentrations were at 356 ppm (Keeling et al., 1976; Keeling and Whorf, 2004). Today, in 2019, atmospheric CO₂ concentrations already rose to 411 ppm. In equilibrium
925 and assuming a central climate sensitivity of 3°C, these CO₂ concentrations of 411 ppm alone would imply a temperature change of 1.7°C above pre-industrial levels (using the simple and standard CO₂ forcing formula of $RF = 5.35 \cdot \ln(C/C_0)$ with C being the current and C₀ being the pre-industrial concentrations). While zero CO₂ emissions would yield decreasing concentrations, it becomes clear that only a future emission trajectory that effectively reduces atmospheric CO₂ concentration levels below today's levels
930 would provide a reasonable chance to keep warming at or below 1.5°C in the longer term. And even such 1.5°C of warming could come with multi-meter sea level rise by 2300 (Mengel et al., 2018) and the likely demise of coral reefs (Frieler et al., 2013). Thus, while the shown scenarios span a scientifically valid wide range of plausible futures, from a climate impact point of view - and trying to achieve the Paris Agreement targets - all except for the lowest scenarios investigated in this study will hopefully remain
935 hypothetical futures.



7 Data Availability

A supplementary data table is available with global and annual mean mole fractions. The complete dataset with latitudinally and monthly resolved data in netcdf format is available via <https://pcmdi.llnl.gov/search/input4mips/>. Additional data formats, i.e. CSV, XLS, MATLAB .mat files of the same data are also available via <http://greenhousegases.science.unimelb.edu.au>.

8 Author contributions.

Together with EV, MM designed the study. ZN and MG performed the emission data collation, downscaling and harmonisation steps. MM, EV, and MF build the MATLAB libraries for this project. MF, ZN and MM did the verification of the final data product in comparison to the historical datasets. The new MAGICC parameterisations were developed by MM, ZN, and AJ. MAGICC runs for the concentration projections and postprocessing of the data was performed by MM, ZN, EV, and MF. ZN coordinated the transfer of data to the Input4MIP project. JL, ZN and AN performed the MAGICC temperature and SLR projections. UB setup and performed the CESM1.2.2 runs with CG leading the analysis. GV contributed the future ODS and halogenated emission projections. MM produced the figures with Figure 8 being produced by JL and MM. All authors contributed to writing and commenting on the manuscript.

9 Acknowledgements

We would like to thank the broad community of scientists, lab technicians, research assistants and respective funding agencies that make the observational records of greenhouse gas concentrations possibly, specifically those of the AGAGA and NOAA networks. See Meinshausen et al., 2017 for a detailed acknowledgement. Without those observational records, our ability to project greenhouse gas into the future would not be possible. We also would like to thank the IAM modelling teams, especially the IMAGE, MESSAGE-Globiom, AIM, REMIND-MagPie and GCAM4 teams, who created chosen SSP benchmark emission scenarios underlying this study. The author team thanks for the discussions with the IAM modellers on the design of the SSP extensions, especially Keywan Riahi, Detlef van Vuuren, David



965 Klein and Shinichiro Fujimori. Lastly, the authors acknowledge the web-teams that make the use of the
datasets possible. Specifically, we would like to thank Paul Durack for handling the data integration for
the ESGF server. Also, we would warmly like to thank Melissa Makin and Usha Nattala and Uli Felzmann
from the Faculty of Science IT team at the University of Melbourne, who made it possible that the full
970 datasets, factsheets and interactive plots of this study are available in a user-accessible fashion on
greenhousegases.unimelb.edu.au. We thank Keith Shine for very helpful discussions on section 2.7. MM
thankfully acknowledges the support by the Australian Research Council Future Fellowship grant
FT130100809. This work was undertaken in collaboration with partners in the European Union's Horizon
2020 research and innovation programme CRESCENDO (grant no. 641816), of which the University of
970 Melbourne is an unfunded partner.



10 Tables

975

Table 1 - Derivation and construction of future CMIP6 mixing ratio fields for the greenhouse gas concentration series from 2015 onwards. Note that in addition to the steps shown below, a post-processing step was implemented to scale any differences in the December 2014 values between the raw future data and the previously submitted historical greenhouse gas concentration data. Those data differences in monthly latitudinal values for Dec 2014 were linearly scaled to zero until Dec 2015 in order to provide for a smooth transition between historical and future datasets (section 2.8). See section 2.1 for a description of how the observational data was updated.

Gas	Time period	Observational data source	Global and annual-mean C_{global}	Seasonality $\hat{S}_{l,m}$	Seasonality Change $\Delta S_{l,m}$	Latitudinal gradient \hat{L}
CO ₂	2015-2016	NOAA ESRL Carbon Cycle Cooperative Global Air Sampling Network, 1968-2016. Version: 2017-07-28 (updated from historical run version: 2015-08-03), monthly station averages (Dlugokencky, 2015b; NOAA ESRL GMD, 2014a, b, c, d)	Calculated based on observational data source as described in Meinshausen et al. (2017)	Mean over 1984-2013 period.	Leading EOF of residuals from observation – extended into future with projected GPP from MAGICC7.0 calibrated carbon cycle to the UVIC C4MIP model (Friedlingstein et al., 2006). (This is a change from the historical GHG methodology, when we used only observational temperature and CO ₂ concentrations)	Two leading EOFs and their scores derived from latitudinal residuals from annual mean values.
	2016 to 2500	n/a	MAGICC7.0 CO ₂ global-mean projections driven by harmonized SSP GHG emissions (Gidden et al., 2019) or extended emissions beyond 2100 (section 2.3).			The score for the first EOF is regressed against global annual fossil fuel & industry emissions from SSP scenarios. Score for the second EOF assumed constant in future.
CH ₄	2015-2016	AGAGE monthly station means, incl. pollution events ('.mop') (Cunnold et al., 2002) & NOAA	Calculated based on observational data source as described	Mean over 1985-2013 period. Applied as relative	Absolut seasonality changing given that it is applied	Two leading EOFs and their scores derived from latitudinal residuals from annual mean values. The score for the first EOF is regressed against



		ESRL monthly station data (Dlugokencky, 2015a); Version 2017-07-28;	in Meinshausen et al. (2017).	seasonality, i.e. percent deviation from global-mean.	relative to global-mean.	global annual fossil fuel & industry emissions from SSP scenarios. Score for the second EOF assumed constant in future.
	2016-2500	n/a	MAGICC7.0 CH ₄ global-mean projections driven by harmonized SSP emissions extended emissions beyond 2100 (section 2.3).			
N ₂ O	2015 to 2016	AGAGE monthly station means, incl. pollution events (Prinn et al., 1990) (Version Dec 2017) & Combined Nitrous Oxide data (monthly station averages) from the NOAA/ESRL Global Monitoring Division; Version Thu, Jan 25, 2018 1:50:47 PM	Calculated based on observational data source as described in Meinshausen et al. (2017).	Mean over 1985-2013 period. Applied as relative seasonality, i.e. percent deviation from global-mean.	Absolut seasonality changing given that it is applied relative to global-mean.	Two leadings EOFs and their scores derived from latitudinal residuals from annual mean values; The score for the first EOF is regressed against global total N ₂ O emissions to extrapolate into the future. Score for the second EOF assumed constant in future.
	2016 to 2500	n/a	MAGICC7.0 N ₂ O global-mean projections driven by harmonized SSP emissions (Gidden et al., 2019) extended emissions beyond 2100 (section 2.3).			
Other greenhouse gases	2015 to 2017	Data input sources as described in Meinshausen (2017) with several data inputs updated to newer versions of the	Calculated based on observational data source as described in Meinshausen et al. (2017).	Depending on the gas, either assumed zero or mean over recent	Either zero or absolute seasonality changing given that it is applied relative to	The leading EOF and its score derived from residuals from observations; with the score for the leading EOF regressed against global total CH ₄



		data, namely: AGAGE monthly station means, incl. pollution events (Prinn et al., 2018) (Version Dec 2017); 04-Feb-18 update of NOAA/ESRL/GMD data (Montzka et al., 2015), were appropriate.		historical period, normally 1990-2013, period. See online factsheets at greenhousegases.science.unimelb.edu.au for a gas-to-gas depiction of the seasonality.	global-mean – depending on the gas.	emissions to extrapolate into the future.
	2016/2017 to 2500	n/a	MAGICC7.0 driven by harmonized SSP emissions or WMO (2014) scenario A1 emission projections (with extensions beyond 2100).			

980



Table 2 - Cumulative CO₂ and CH₄ emissions from MAGICC's permafrost module under the considered SSPs. The permafrost module has 50 zonal bands, a mineral and peatland soil module and 50 latitudinal zonal bands. See Schneider von Deimling et al. (Schneider von Deimling et al., 2012) for a detailed description. See **Figure 3** for timeseries of induced CO₂ and CH₄ atmospheric concentration changes.

	Time horizon	SSP1-1.9	SSP1-2.6	SSP2-4.5	SSP3-7.0-LowNTCF	SSP3-7.0	SSP4-3.4	SSP4-6.0	SSP5-3.4-OS	SSP5-8.5
Cumulative CO₂ emissions (GtC)	2100	25	31	46	54	65	38	56	48	88
	2200	42	58	121	252	288	78	167	83	378
	2300	51	74	173	410	444	99	248	101	542
Cumulative CH₄ emissions (MtCH₄)	2100	451	549	789	919	1,089	670	953	835	1,431
	2200	884	1,231	2,527	5,083	5,911	1,639	3,467	1,744	7,999
	2300	1,177	1,774	4,246	10,505	11,673	2,404	6,170	2,389	15,096



990

Table 3 - Simplified expressions for radiative forcing relative to pre-industrial (1750) levels by changes of surface air mole fractions of CO₂, CH₄, N₂O – reflecting the Oslo Line-by-line model results. This table can be compared to Table 1 in Etminan et al. (2016), but note that their formulae can be directly applied to any sets of (C, Co), (M, Mo) and (N, No) within the range of fitting, unlike the case here where Co, Mo and No are pre-specified at pre-industrial levels.

Gas	Simplified Expression	Coefficients	Maximal absolute fit error % (Wm ⁻²)
CO ₂	$C_{\alpha_{max}} = C_0 - \frac{b_1}{2a_1} \approx 1808 \text{ ppm}$ $\alpha' = d_1 - \frac{b_1^2}{4a_1}, \text{ for } C > C_{\alpha_{max}}$ $\alpha' = d_1 + a_1(C - C_0)^2 + b_1(C - C_0), \text{ for } C_0 < C < C_{\alpha_{max}}$ $\alpha' = d_1, \text{ for } C < C_0$ $\alpha_{N_2O} = c_1 * \sqrt{N}$ $RF_{CO_2} = (\alpha' + \alpha_{N_2O}) * \ln\left(\frac{C}{C_0}\right)$	$a_1 = -2.4785e-07 \text{ Wm}^{-2}\text{ppm}^{-2}$ $b_1 = 0.00075906 \text{ Wm}^{-2}\text{ppm}^{-1}$ $c_1 = -0.0021492 \text{ Wm}^{-2}\text{ppb}^{-0.5}$ $d_1 = 5.2488 \text{ Wm}^{-2}$ $C_0 = 277.15 \text{ ppm}$	0.11% (0.0037 Wm ⁻²)
N ₂ O	$RF_{N_2O} = (a_2\sqrt{C} + b_2\sqrt{N} + c_2\sqrt{M} + d_2) * (\sqrt{N} - \sqrt{N_0})$	$a_2 = -0.00034197 \text{ Wm}^{-2}\text{ppm}^{-1}$ $b_2 = 0.00025455 \text{ Wm}^{-2}\text{ppb}^{-1}$ $c_2 = -0.00024357 \text{ Wm}^{-2}\text{ppb}^{-1}$ $d_2 = 0.12173 \text{ Wm}^{-2}\text{ppb}^{-0.5}$ $N_0 = 273.87 \text{ ppb}$	1.5% (0.0059 Wm ⁻²)
CH ₄	$RF_{CH_4} = (a_3\sqrt{M} + b_3\sqrt{N} + d_3) * (\sqrt{M} - \sqrt{M_0})$	$a_3 = -8.9603e-05 \text{ Wm}^{-2}\text{ppb}^{-1}$ $b_3 = -0.00012462 \text{ Wm}^{-2}\text{ppb}^{-1}$ $d_3 = 0.045194 \text{ Wm}^{-2}\text{ppb}^{-0.5}$ $M_0 = 731.41 \text{ ppb}$	0.55% (0.0032 Wm ⁻²)



993 **Table 4** - Overview of future scenario range of individual GHG concentrations. The table indicates the minimum and maximum surface air mole fractions
 994 across the 9 SSP scenarios considered in this study. For spreadsheets with annual data tables per scenario, see greenhousegases.science.unimelb.edu.au.
 995 The third column indicates the region, with global ('GL'), Northern hemispheric ('NL') and Southern hemispheric ('SH') data shown for CO₂, CH₄ and
 996 N₂O. The last three rows provide the equivalence concentrations. The CFC-11-eq concentrations summarize – in terms of radiative forcing equivalent –
 997 all greenhouse gases aside from CO₂, CH₄, N₂O and CFC-12. The CFC-12-eq concentrations summarize all the ozone depleting substances (ODS)
 998 controlled under the Montreal Protocol, while HFC-134a-eq summarizes the remaining fluorinated gases. Altogether CO₂, CH₄, N₂O, CFC-12-eq and
 999 HFC-134a-eq together represent the radiative forcing of the entirety of the 43 greenhouse gases considered here (cf. Table 5 in Meinshausen et al., 2017).

GAS	UNIT	REG	2015	2025	2050	2075	2100	2150	2200	2250	2300	2500
CO ₂	ppm	GL	399.9	426.5 - 432.4	437.6 - 562.8	419.7 - 801.7	393.5 - 1135.2	349 - 1737.3	343.4 - 2108.3	343.3 - 2206.4	342 - 2161.7	336.9 - 2010
		NH	401.7	428.2 - 434.9	437.8 - 567.2	419.5 - 808.5	392.9 - 1142.3	348.5 - 1742	343.4 - 2110.7	343.3 - 2206.4	342 - 2161.7	336.9 - 2010
		SH	398.2	424.9 - 429.9	437.5 - 558.3	419.9 - 794.9	394.1 - 1128.2	349.5 - 1732.6	343.4 - 2106	343.3 - 2206.3	342 - 2161.7	336.9 - 2010
CH ₄	ppb	GL	1841.9	1865.1 - 2049.1	1358.8 - 2503.7	1184.3 - 2934.1	999.7 - 3372.2	961.8 - 3096.2	927.6 - 2571.6	875.2 - 2107.1	864.4 - 1988.1	864 - 1938.4
		NH	1889.7	1910.3 - 2098.2	1400 - 2554.8	1224.3 - 2989.5	1038.8 - 3430.7	1000.6 - 3151.1	966.1 - 2622.8	913.1 - 2154.7	902.4 - 2035.7	901.9 - 1986
		SH	1794.1	1820 - 1999.9	1317.5 - 2452.5	1144.3 - 2878.7	960.6 - 3313.7	922.9 - 3041.3	889.1 - 2520.3	837.2 - 2059.5	826.4 - 1940.5	826 - 1890.8
N ₂ O	ppb	GL	328.2	334.9 - 336.4	343.5 - 361.9	348.5 - 391	353.9 - 422.4	361.2 - 472.5	363.4 - 498.5	362.2 - 508.7	360 - 512	356.4 - 517.5
		NH	328.5	335.1 - 336.7	343.8 - 362.2	348.8 - 391.3	354.2 - 422.7	361.5 - 472.8	363.7 - 498.8	362.5 - 509	360.3 - 512.3	356.7 - 517.8
		SH	327.9	334.6 - 336.1	343.2 - 361.6	348.2 - 390.7	353.6 - 422.1	360.9 - 472.2	363.2 - 498.3	361.9 - 508.4	359.7 - 511.8	356.1 - 517.2
SF ₆	ppt	GL	8.6	11.3 - 11.9	14.3 - 21.7	16.1 - 32.7	17.2 - 43.5	18.5 - 60.7	19.1 - 70.5	19.1 - 73.1	18.8 - 72	17.7 - 67.6
NF ₃	ppt	GL	1.4	2.3 - 2.5	3.3 - 5.8	3.8 - 9.3	4 - 12.7	4.2 - 17.4	4.1 - 19.2	3.9 - 18.5	3.6 - 16.6	2.5 - 10.9
SO ₂ F ₂	ppt	GL	2.1	2.8 - 3	2.4 - 4	1.6 - 4.4	1.1 - 4.1	0.5 - 2.9	0.2 - 1.8	0.1 - 0.8	0 - 0.2	0 - 0
CF ₄	ppt	GL	81.8	88.3 - 89.7	96.1 - 106.3	99.2 - 123.2	101.3 - 136	103.8 - 154.6	105.3 - 165.7	105.7 - 169.4	105.6 - 169.2	105.2 - 168.6
C ₂ F ₆	ppt	GL	4.5	5.1 - 5.2	5.7 - 6.9	5.8 - 8.6	5.8 - 10	5.8 - 12.2	5.8 - 13.4	5.7 - 13.8	5.7 - 13.7	5.6 - 13.5
C ₃ F ₈	ppt	GL	0.6	0.7 - 0.8	0.9 - 1.1	0.9 - 1.5	0.9 - 1.8	0.9 - 2.2	0.9 - 2.5	0.9 - 2.6	0.9 - 2.5	0.8 - 2.5
c-C ₄ F ₈	ppt	GL	1.4	1.7 - 1.8	2.1 - 2.6	2.2 - 3.5	2.3 - 4.1	2.4 - 5	2.5 - 5.5	2.5 - 5.6	2.4 - 5.5	2.3 - 5.2
C ₄ F ₁₀	ppt	GL	0.2	0.2 - 0.2	0.2 - 0.3	0.2 - 0.3	0.2 - 0.4	0.2 - 0.5	0.2 - 0.5	0.2 - 0.5	0.2 - 0.5	0.2 - 0.5



C₅F₁₂	ppt	GL	0.1	0.1 - 0.1	0.1 - 0.2	0.1 - 0.2	0.1 - 0.2	0.1 - 0.2	0.1 - 0.2	0.1 - 0.2	0.1 - 0.2	0.1 - 0.2
C₆F₁₄	ppt	GL	0.3	0.3 - 0.4	0.4 - 0.5	0.4 - 0.7	0.4 - 0.8	0.4 - 1	0.4 - 1.1	0.4 - 1.1	0.4 - 1.1	0.4 - 1
C₇F₁₆	ppt	GL	0.1	0.2 - 0.2	0.2 - 0.3	0.2 - 0.3	0.2 - 0.4	0.2 - 0.5	0.2 - 0.6	0.2 - 0.6	0.2 - 0.6	0.2 - 0.6
C₈F₁₈	ppt	GL	0.1	0.1 - 0.1	0.1 - 0.1	0.1 - 0.2	0.1 - 0.2	0.1 - 0.2	0.1 - 0.3	0.1 - 0.3	0.1 - 0.3	0.1 - 0.2
HFC-23	ppt	GL	27.9	31.5 - 32	28.7 - 29.9	25.8 - 27	22.8 - 24.1	17.2 - 19.4	12.8 - 16	9.5 - 13.1	7.1 - 10.7	2.1 - 4.8
HFC-32	ppt	GL	9.8	6.5 - 7.5	0.1 - 0.7	0 - 0.2	0 - 0	0 - 0	0 - 0	0 - 0	0 - 0	0 - 0
HFC-43-10MEE	ppt	GL	0.3	0.3 - 0.3	0.1 - 0.4	0 - 0.4	0 - 0.4	0 - 0.2	0 - 0.1	0 - 0	0 - 0	0 - 0
HFC-125	ppt	GL	17.8	52.1 - 78.6	49.8 - 371.6	31.5 - 744.8	22.7 - 988.8	14.2 - 809.2	8.5 - 458.2	3.4 - 137	0.8 - 13.7	0 - 0
HFC-134A	ppt	GL	84.8	109.6 - 143.7	36.1 - 239.4	11.4 - 358	6.6 - 423.3	4.4 - 286.9	2.5 - 145.5	0.6 - 24.6	0 - 0.2	0 - 0
HFC-143A	ppt	GL	16.7	36.7 - 50.9	39 - 234.3	29.6 - 509.6	23.7 - 745.9	16.1 - 748.4	10.4 - 500.9	5.4 - 213.3	2.2 - 53.1	0.1 - 0.4
HFC-152A	ppt	GL	7.5	4.6 - 8.2	0.2 - 6.5	0.1 - 7.6	0.1 - 6.5	0.1 - 3.8	0 - 1.8	0 - 0.1	0 - 0	0 - 0
HFC-236FA	ppt	GL	0.1	0.2 - 0.3	0.3 - 1.3	0.3 - 3.1	0.3 - 5.3	0.3 - 7.9	0.3 - 8.2	0.2 - 6.7	0.2 - 4.9	0.1 - 1.4
HFC-227EA	ppt	GL	1.1	1.8 - 2.4	1.4 - 6.4	0.8 - 9.8	0.5 - 10.9	0.2 - 8.2	0.1 - 4.7	0 - 1.5	0 - 0.2	0 - 0
HFC-245FA	ppt	GL	2.2	3.6 - 5.8	1.1 - 18.4	0.5 - 34.5	0.5 - 39.1	0.4 - 24.5	0.2 - 12.1	0 - 1.3	0 - 0	0 - 0
HFC-365MFC	ppt	GL	0.9	1.2 - 1.6	0.2 - 2.5	0.1 - 3.8	0.1 - 4.3	0 - 2.7	0 - 1.3	0 - 0.2	0 - 0	0 - 0
CCL₄	ppt	GL	82.1	67.4 - 67.4	32.4 - 32.7	13.3 - 13.8	5 - 5.5	0.6 - 0.8	0.1 - 0.1	0 - 0	0 - 0	0 - 0
CHCl₃	ppt	GL	10.4	8.8 - 9.7	5.8 - 9.5	5.5 - 9	5.5 - 8.3	5.4 - 7.4	5.4 - 6.4	5.4 - 5.5	5.4 - 5.4	5.4 - 5.4
CH₂Cl₂	ppt	GL	37.8	24.7 - 46.7	8 - 59.2	7.7 - 86.2	7.8 - 90	7.6 - 63	7.3 - 35.5	7.1 - 8	7.1 - 7.1	7.1 - 7.1
CH₃CCl₃	ppt	GL	3.2	0.4 - 0.4	0 - 0	0 - 0	0 - 0	0 - 0	0 - 0	0 - 0	0 - 0	0 - 0
CH₃Cl	ppt	GL	549.8	546.5 - 577.6	466.1 - 582.4	425.6 - 566	421.6 - 556.5	418.5 - 536.2	394 - 509.7	363.7 - 479.1	358.2 - 475.9	358.1 - 476.8
CH₃Br	ppt	GL	6.7	6.5 - 6.9	5.3 - 6.9	5 - 6.8	4.9 - 6.6	4.7 - 6.3	4.6 - 5.9	4.4 - 5.5	4.4 - 5.5	4.4 - 5.5
CFC-11	ppt	GL	231.5	204.4 - 204.4	137.8 - 138.9	86.3 - 89.4	51.4 - 56.2	17.3 - 22.4	5.5 - 8.7	1.7 - 3.4	0.5 - 1.3	0 - 0
CFC-12	ppt	GL	518	471.6 - 471.7	364.3 - 366	277.6 - 283.6	208.7 - 220.2	114.3 - 133.5	61.2 - 81.4	32.5 - 49.6	17.3 - 30.3	1.4 - 4.2



CFC-113	ppt	GL	72.1 - 72.1	64.7 - 64.7	48.7 - 48.9	36.1 - 37	26.4 - 28	13.7 - 16.2	6.9 - 9.4	3.5 - 5.5	1.7 - 3.2	0.1 - 0.4
CFC-114	ppt	GL	16.3 - 16.3	15.8 - 15.8	13.9 - 13.9	12 - 12.1	10.3 - 10.6	7.5 - 8.1	5.4 - 6.2	3.8 - 4.7	2.7 - 3.6	0.7 - 1.3
CFC-115	ppt	GL	8.5 - 8.5	8.8 - 8.8	9.1 - 9.1	9 - 9	8.6 - 8.7	7.7 - 7.9	6.9 - 7.2	6.2 - 6.6	5.5 - 6	3.5 - 4.1
HCFC-22	ppt	GL	233.7 - 233.7	237.2 - 241.1	49.9 - 59.5	4.5 - 8.8	0.3 - 1.4	0 - 0	0 - 0	0 - 0	0 - 0	0 - 0
HCFC-141B	ppt	GL	24.2 - 24.2	27.2 - 27.7	14.1 - 16.2	3.5 - 5.2	0.8 - 1.4	0.3 - 0.5	0.2 - 0.3	0 - 0	0 - 0	0 - 0
HCFC-142B	ppt	GL	22.1 - 22.1	21.2 - 21.5	8.7 - 9.8	1.9 - 3	0.4 - 0.9	0 - 0.1	0 - 0	0 - 0	0 - 0	0 - 0
HALO N-1211	ppt	GL	3.7 - 3.7	2.6 - 2.6	0.7 - 0.8	0.2 - 0.2	0 - 0	0 - 0	0 - 0	0 - 0	0 - 0	0 - 0
HALO N-1301	ppt	GL	3.3 - 3.3	3.3 - 3.3	2.8 - 2.8	2.1 - 2.1	1.5 - 1.6	0.6 - 0.8	0.3 - 0.4	0.1 - 0.2	0 - 0.1	0 - 0
HALO N-2402	ppt	GL	0.4 - 0.4	0.4 - 0.4	0.2 - 0.2	0.1 - 0.1	0 - 0	0 - 0	0 - 0	0 - 0	0 - 0	0 - 0
CFC-11-EQ	ppt	GL	818.9 - 818.9	848.9 - 908.6	528.3 - 1102.9	371 - 1599.7	305.6 - 1975	235 - 1698.5	189.8 - 1126.9	155 - 563.5	135.3 - 323.9	115.2 - 251.1
CFC-12-EQ	ppt	GL	1047.8 - 1047.9	967.1 - 969	627.8 - 637.9	433 - 444.4	320.6 - 329.5	175.3 - 197.1	99.2 - 124.3	58.4 - 82.2	38.7 - 57.5	17.7 - 24.5
HFC-134A-EQ	ppt	GL	271.1 - 271.1	388.3 - 485.4	327.5 - 1259.5	286.2 - 2274	277.9 - 2984.9	254.7 - 2638	223.2 - 1755.3	186.7 - 864	165.4 - 483.5	147 - 375.5

1000
 1001
 1002



1003 **Table 5** - Overview of CO₂, CH₄ and N₂O concentrations in the eight SSP scenarios considered in this study with global-average (‘GL’), Northern
 1004 hemispheric (‘NH’) and Southern hemispheric (‘SH’) surface air mole fractions. For annual and latitudinally resolved mole fractions and other greenhouse
 1005 gases, see supplementary material or greenhousegases.science.unimelb.edu.au.

SSP1-1.9			2015	2025	2050	2075	2100	2150	2200	2250	2300	2400	2500
CO ₂	ppm	GL	399.9	426.5	437.6	419.7	393.5	349.0	343.4	343.3	342.0	339.2	336.9
		NH	401.7	428.2	437.8	419.5	392.9	348.5	343.4	343.3	342.0	339.2	336.9
		SH	398.2	424.9	437.5	419.9	394.1	349.5	343.4	343.3	342.0	339.2	336.9
CH ₄	ppb	GL	1,842.0	1,875.2	1,427.9	1,184.3	1,036.4	969.8	928.9	881.3	1,112.0	870.9	871.4
		NH	1,889.7	1,919.9	1,468.8	1,224.3	1,075.6	1,008.6	967.2	919.2	909.6	908.8	909.3
		SH	1,794.2	1,830.6	1,387.0	1,144.3	997.2	931.1	890.5	843.4	833.8	833.0	833.5
N ₂ O	ppb	GL	328.2	335.1	343.6	349.0	354.0	361.4	363.9	362.7	360.6	358.2	357.1
		NH	328.5	335.4	343.8	349.3	354.3	361.7	364.2	363.0	360.9	358.5	357.4
		SH	327.9	334.8	343.3	348.7	353.7	361.2	363.6	362.4	360.3	357.9	356.8
SSP1-2.6			2015	2025	2050	2075	2100	2150	2200	2250	2300	2400	2500
CO ₂	ppm	GL	399.9	427.7	469.3	471.0	445.6	411.1	403.2	399.7	396.0	389.5	384.3
		NH	401.7	429.6	470.4	471.2	445.3	410.9	403.2	399.7	396.0	389.5	384.3
		SH	398.2	425.7	468.2	470.8	445.9	411.4	403.2	399.7	396.0	389.4	384.3
CH ₄	ppb	GL	1,842.0	1,865.1	1,519.4	1,248.4	1,056.4	977.4	927.6	875.2	1,112.0	863.5	864.0
		NH	1,889.7	1,910.3	1,561.5	1,288.8	1,095.9	1,016.4	966.1	913.1	902.4	901.5	901.9
		SH	1,794.2	1,820.0	1,477.3	1,208.0	1,016.9	938.4	889.1	837.2	826.4	825.6	826.0
N ₂ O	ppb	GL	328.2	334.9	343.5	348.5	353.9	361.2	363.4	362.2	360.0	357.5	356.4
		NH	328.5	335.1	343.8	348.8	354.2	361.5	363.7	362.5	360.3	357.8	356.7
		SH	327.9	334.6	343.2	348.2	353.6	360.9	363.2	361.9	359.7	357.2	356.1
SSP2-4.5			2015	2025	2050	2075	2100	2150	2200	2250	2300	2400	2500
CO ₂	ppm	GL	399.9	429.0	506.9	575.5	602.8	626.3	643.1	637.0	621.3	597.8	579.2
		NH	401.7	431.2	509.2	577.3	603.6	626.8	643.4	637.0	621.3	597.8	579.2
		SH	398.2	426.9	504.5	573.6	602.0	625.7	642.8	637.0	621.3	597.8	579.2
CH ₄	ppb	GL	1,841.9	1,960.7	2,020.2	1,815.7	1,683.2	1,479.6	1,255.4	1,038.1	1,112.0	999.2	997.3



		NH	1,889.7	2,008.0	2,066.6	1,860.7	1,727.7	1,522.4	1,296.6	1,077.6	1,040.9	1,038.7	1,036.8
		SH	1,794.2	1,913.3	1,973.9	1,770.8	1,638.6	1,436.7	1,214.2	998.6	961.8	959.7	957.8
N₂O	ppb	GL	328.2	336.0	356.2	371.5	377.3	378.3	375.9	371.4	367.0	362.0	359.8
		NH	328.5	336.3	356.5	371.8	377.6	378.6	376.2	371.7	367.2	362.3	360.1
		SH	327.9	335.7	355.9	371.2	377.0	378.0	375.6	371.1	366.7	361.7	359.5
SSP3-7.0		2015	2025	2050	2075	2100	2150	2200	2250	2300	2400	2500	
CO₂	ppm	GL	399.9	432.3	540.6	683.0	867.2	1,235.3	1,456.8	1,513.7	1,482.8	1,423.6	1,371.1
		NH	401.7	434.8	543.9	686.8	871.6	1,238.3	1,458.3	1,513.7	1,482.8	1,423.6	1,371.1
		SH	398.2	429.9	537.3	679.2	862.8	1,232.4	1,455.3	1,513.6	1,482.7	1,423.6	1,371.1
CH₄	ppb	GL	1,841.9	2,006.5	2,472.0	2,934.1	3,372.2	3,096.2	2,571.6	2,107.1	1,112.0	1,959.1	1,938.4
		NH	1,889.7	2,055.4	2,524.2	2,989.5	3,430.7	3,151.1	2,622.8	2,154.7	2,035.7	2,006.7	1,986.0
		SH	1,794.2	1,957.7	2,419.8	2,878.7	3,313.7	3,041.3	2,520.3	2,059.5	1,940.5	1,911.5	1,890.8
N₂O	ppb	GL	328.2	336.4	361.8	390.7	421.8	471.4	497.2	507.2	510.5	514.3	516.0
		NH	328.5	336.7	362.1	391.0	422.1	471.7	497.4	507.5	510.8	514.6	516.3
		SH	327.9	336.1	361.5	390.4	421.5	471.1	496.9	506.9	510.2	514.0	515.7
SSP3-7.0-LowNFC		2015	2025	2050	2075	2100	2150	2200	2250	2300	2400	2500	
CO₂	ppm	GL	399.9	432.4	538.8	677.5	858.7	1,221.5	1,447.2	1,509.7	1,482.8	1,426.1	1,374.1
		NH	401.7	434.9	542.2	681.4	863.2	1,224.6	1,448.7	1,509.7	1,482.8	1,426.1	1,374.1
		SH	398.2	429.9	535.5	673.5	854.1	1,218.5	1,445.7	1,509.7	1,482.7	1,426.1	1,374.1
CH₄	ppb	GL	1,841.9	1,940.3	1,358.8	1,202.5	1,219.9	1,203.5	1,164.6	1,129.1	1,112.0	1,088.0	1,068.8



		NH	1,889.7	1,985.6	1,400.0	1,244.0	1,262.1	1,245.3	1,205.9	1,170.1	1,152.9	1,129.0	1,109.8
		SH	1,794.2	1,895.0	1,317.5	1,161.0	1,177.8	1,161.8	1,123.2	1,088.2	1,071.0	1,047.1	1,027.9
N₂O	ppb	GL	328.2	336.4	361.9	391.0	422.4	472.5	498.5	508.7	512.0	515.8	517.5
		NH	328.5	336.7	362.2	391.3	422.7	472.8	498.8	509.0	512.3	516.1	517.8
		SH	327.9	336.1	361.6	390.7	422.1	472.2	498.3	508.4	511.8	515.5	517.2
SSP4-3.4		2015	2025	2050	2075	2100	2150	2200	2250	2300	2400	2500	
CO₂	ppm	GL	399.9	427.3	472.9	490.2	473.4	408.8	396.2	395.2	392.4	387.5	383.4
		NH	401.7	429.3	474.0	490.3	472.5	408.0	396.2	395.2	392.4	387.5	383.4
		SH	398.2	425.3	471.8	490.1	474.3	409.5	396.2	395.2	392.4	387.5	383.4
CH₄	ppb	GL	1,841.9	2,030.9	2,223.4	2,370.0	2,336.3	2,177.6	2,023.8	1,842.7	1,112.0	1,786.8	1,786.2
		NH	1,889.7	2,078.9	2,271.3	2,417.9	2,383.2	2,223.4	2,068.6	1,886.6	1,832.2	1,830.7	1,830.1
		SH	1,794.1	1,983.0	2,175.4	2,322.2	2,289.5	2,131.7	1,978.9	1,798.8	1,744.5	1,743.0	1,742.3
N₂O	ppb	GL	328.2	335.7	353.9	373.7	394.7	425.2	441.1	446.8	448.2	449.9	450.7
		NH	328.5	336.0	354.2	374.0	395.0	425.5	441.3	447.1	448.5	450.2	451.0
		SH	327.9	335.4	353.6	373.4	394.4	424.9	440.8	446.5	447.9	449.6	450.4
SSP4-6.0		2015	2025	2050	2075	2100	2150	2200	2250	2300	2400	2500	
CO₂	ppm	GL	399.9	428.3	515.6	606.9	668.4	741.0	783.9	786.2	768.7	739.1	714.0
		NH	401.7	430.5	518.2	609.2	669.7	741.8	784.3	786.2	768.7	739.1	714.0
		SH	398.2	426.0	513.0	604.7	667.1	740.1	783.4	786.2	768.7	739.1	714.0
CH₄	ppb	GL	1,841.9	2,049.1	2,503.7	2,688.5	2,645.5	2,382.6	2,111.4	1,864.6	1,112.0	1,791.0	1,785.6
		NH	1,889.7	2,098.2	2,554.8	2,739.6	2,695.8	2,431.2	2,158.3	1,909.8	1,844.7	1,836.3	1,830.9
		SH	1,794.1	1,999.9	2,452.5	2,637.3	2,595.3	2,334.1	2,064.4	1,819.3	1,754.1	1,745.7	1,740.4
N₂O	ppb	GL	328.2	335.9	359.7	383.4	404.7	435.8	451.2	456.1	456.8	457.7	458.1
		NH	328.5	336.2	360.0	383.7	405.0	436.1	451.4	456.4	457.1	457.9	458.4
		SH	327.9	335.6	359.4	383.2	404.4	435.5	450.9	455.8	456.5	457.4	457.8
SSP5-3.4-OS		2015	2025	2050	2075	2100	2150	2200	2250	2300	2400	2500	
CO₂	ppm	GL	399.9	432.2	549.3	554.5	496.6	409.4	404.7	401.8	398.5	392.4	387.5



		NH	401.7	434.7	551.9	553.8	495.6	408.7	404.7	401.8	398.5	392.4	387.5
		SH	398.2	429.7	546.7	555.1	497.7	410.1	404.7	401.8	398.5	392.4	387.5
CH₄	ppb	GL	1,841.9	1,964.3	2,125.1	1,205.4	999.7	961.8	941.9	916.8	1,112.0	910.5	910.6
		NH	1,889.7	2,012.6	2,168.8	1,245.2	1,038.8	1,000.6	980.5	955.2	950.1	948.9	948.9
		SH	1,794.2	1,916.0	2,081.4	1,165.5	960.6	922.9	903.3	878.5	873.4	872.2	872.2
N₂O	ppb	GL	328.2	336.3	356.3	371.1	383.8	398.4	404.7	405.1	403.6	401.9	401.1
		NH	328.5	336.6	356.6	371.4	384.1	398.7	405.0	405.4	403.9	402.1	401.4
		SH	327.9	336.0	356.1	370.8	383.6	398.1	404.4	404.8	403.3	401.6	400.8
SSP5-8.5		2015	2025	2050	2075	2100	2150	2200	2250	2300	2400	2500	
CO₂	ppm	GL	399.9	431.8	562.8	801.7	1,135.2	1,737.3	2,108.3	2,206.4	2,161.7	2,080.5	2,010.0
		NH	401.7	434.3	567.2	808.5	1,142.3	1,742.0	2,110.7	2,206.4	2,161.7	2,080.5	2,010.0
		SH	398.2	429.4	558.3	794.9	1,128.2	1,732.6	2,106.0	2,206.3	2,161.7	2,080.5	2,010.0
CH₄	ppb	GL	1,841.9	1,954.5	2,446.5	2,672.3	2,415.3	1,906.9	1,515.6	1,157.3	1,112.0	1,038.5	1,019.0
		NH	1,889.7	2,002.6	2,499.2	2,724.9	2,465.2	1,953.8	1,559.4	1,198.1	1,109.0	1,079.3	1,059.8
		SH	1,794.2	1,906.4	2,393.7	2,619.6	2,365.5	1,860.1	1,471.8	1,116.5	1,027.4	997.7	978.2
N₂O	ppb	GL	328.2	336.3	358.2	377.1	391.8	407.8	413.6	413.0	410.5	407.8	406.6
		NH	328.5	336.6	358.5	377.4	392.1	408.1	413.9	413.3	410.8	408.1	406.9
		SH	327.9	336.0	357.9	376.8	391.5	407.5	413.3	412.7	410.2	407.5	406.3



1007
 1008

1009 **Table 6** - Fraction of greenhouse gas induced forcing due to CO₂ concentrations in SSP scenarios at the point of maximal greenhouse gas
 1010 induced forcing until 2300 (upper row) or in year 2100 (lower row)

	SSP1- 1.9	SSP1- 2.6	SSP4- 3.4	SSP2- 4.5	SSP4- 6.0	SSP3- 7.0	SSP5- 8.5	SSP3-7.0- lowntcf	SSP5- 3.4-OS
Point of maximal GHG forcing over 2000 to 2300	68%	74%	70%	83%	81%	86%	92%	90%	75%
2100	76%	80%	68%	79%	76%	77%	82%	85%	82%

1011
 1012



1013 **Table 7** - SSP Global Mean Surface Air Temperature (GMSAT) and Global Mean Sea Level Rise (GMSLR) projections
 1014 for the end of the 21st century (2081-2100 average and 2100 estimate) and 2300. GMSAT is shown in Kelvin relative to
 1015 1750, GMSLR is shown in metres relative to the 1986-2005 average. Mean and 5th to 95th percentiles are provided for
 1016 both variables.
 1017

	GMT in K			GMSLR in m		
	2081-2100	2100	2300	2081-2100	2100	2300
SSP1-1.9	1.2 (0.6 to 1.8)	1.1 (0.6 to 1.8)	0.6 (0.1 to 1.3)	0.44 (0.30 to 0.62)	0.47 (0.32 to 0.65)	0.80 (0.54 to 1.19)
SSP1-2.6	1.6 (1.0 to 2.4)	1.6 (0.9 to 2.4)	1.3 (0.6 to 2.4)	0.49 (0.35 to 0.69)	0.53 (0.37 to 0.73)	1.07 (0.69 to 1.60)
SSP2-4.5	2.6 (1.7 to 3.8)	2.8 (1.8 to 4.1)	3.8 (1.7 to 6.7)	0.59 (0.41 to 0.82)	0.66 (0.46 to 0.89)	2.02 (1.13 to 3.12)
SSP4-3.4	2.0 (1.3 to 3.1)	2.1 (1.3 to 3.2)	1.8 (0.9 to 3.3)	0.53 (0.36 to 0.75)	0.58 (0.40 to 0.81)	1.30 (0.82 to 1.98)
SSP3-7.0	3.8 (2.6 to 5.7)	4.4 (3.0 to 6.5)	9.8 (5.5 to >15 ^{**})	0.68 (0.47 to 0.95)	0.79 (0.56 to 1.07)	4.51 (2.36 to 8.51)
SSP3-LowNTCF	3.4 (2.3 to 5.1)	3.9 (2.6 to 5.8)	9.5 (5.3 to >15 ^{**})	0.64 (0.45 to 0.89)	0.74 (0.53 to 1.00)	4.22 (2.22 to 7.63)
SSP4-6.0	3.3 (2.2 to 4.9)	3.6 (2.4 to 5.3)	6.0 (2.9 to 10.8)	0.65 (0.45 to 0.90)	0.74 (0.53 to 1.00)	2.87 (1.53 to 4.72)
SSP5-3.4-OS	2.1 (1.2 to 3.1)	1.9 (1.1 to 3.0)	1.1 (0.3 to 2.3)	0.58 (0.40 to 0.81)	0.62 (0.42 to 0.87)	1.08 (0.66 to 1.68)
SSP5-8.5	5.0 (3.3 to 7.6)	5.8 (3.8 to 8.6)	10.8 (6.4 to >15 ^{**})	0.79 (0.54 to 1.13)	0.94 (0.66 to 1.29)	5.31 (2.86 to 10.31)

1018 ****** MAGICC has an internal cutoff temperature in each land-ocean and hemispheric box at 25K. Any temperatures
 1019 indications beyond 10K should be considered illustrative only given that the calibrated range of MAGICC covers only
 1020 lower temperature levels.
 1021



1022 **11 Figures Captions**

1023

1024 **Figure 1** - The SSP scenarios and their five socio-economic SSP families. Shown are illustrative temperature levels relative to pre-industrial
1025 levels with historical temperatures (front band), current (2020) temperatures (small block in middle) and the branching of the respective
1026 scenarios over the 21st century along the five different socio-economic families. The small black horizontal bars on the 2100 pillars for
1027 each SSP indicate illustrative temperature levels (obtained by the MAGICC7.0 default setting used to produce the GHG concentrations)
1028 for the range of SSP scenarios that were available from the IAM community at the time of creating the benchmark SSP scenarios. The
1029 more opaque bands over the 21st century indicate the five SSP scenarios SSP1-1.9, SSP1-2.6, SSP2-4.5, SSP3-7.0 and SSP5-8.5 that are
1030 used as priority scenarios in IPCC. The more transparent bands indicate the remaining “Tier 2” SSP scenarios, namely SSP3-7.0-LowNTCF
1031 (used in AerChemMIP), SSP4-3.4, SSP4-6.0, and SSP5-3.4-OS. Also shown is a blue indicative bar on the right side, indicating the effect
1032 of mitigation action, which reduces temperature levels in 2100 and throughout the 21st century - depending on the respective reference
1033 scenario and level of mitigation.

1034

1035 **Figure 2** - Extensions of SSP emission scenarios to derive SSP concentration scenarios for CO₂ (panels a-c), CH₄ (d to e), nitrous oxide
1036 (f), NF₃ (g) and SF₆ (panel i). Shown are the four SSP scenarios for which long-term CMIP6 model experiments are planned (bold lines
1037 with color-box labels), namely for SSP5-8.5 (red), SSP5-34-OS (orange), SSP1-2.6 (blue) and SSP1-1.9 (turquoise). Also shown are RCP
1038 extensions (Meinshausen et al., 2011b), and those of other SSP scenarios following the same design principles (see text). While the design
1039 principles for CO₂ emissions are specific, other gases from fossil and industrial sources are assumed to be phased out by 2225, and landuse-
1040 related emissions are assumed to stay constant at their 2100 values.

1041

1042 **Figure 3** - The assumed permafrost related emissions by using MAGICC’s permafrost module in its default settings for the SSP GHG
1043 concentration projections, close to the median of the probabilistic MAGICC permafrost version (Schneider von Deimling et al., 2012). In
1044 the highest scenario, SSP5-8.5, CO₂ and CH₄ concentrations by 2300 would have been about 250 ppm and 150 ppb, respectively, lower



1045 without including the permafrost module (panel a and b). The additional CO₂ from mineral soil and peatland carbon decomposition reach
1046 a maximum in the highest scenario SSP5-8.5 around 2140 of about 3 GtC emissions per year (panel c), mainly due to the aerobic mineral
1047 soil decomposition (panel e). See **Table 2** for cumulative emissions.

1048

1049 **Figure 4** - Simplified parameterisation to emulate 48 Oslo Line by line model results (bright blue open numbered circles). Shown are the
1050 IPCC TAR simplified formula for CO₂ (three options), CH₄ and N₂O forcing with their default parameter settings (grey-blue lines) in the
1051 background. The simplified formula results by Etminan (2016) are shown as orange lines. Adjusting pre-industrial concentration values to
1052 default 1750 values improves the fit of the Etminan simplified formula (red lines in panels a to c and red error terms in panel d). This
1053 study's simplified formula results are shown in green, matching the Oslo-line-by-line model results within rounding – and continuing a
1054 forcing approximation beyond 2000 ppm CO₂ in line with previously derived formulas (red dashed circle in panel a). See text.

1055

1056 **Figure 5** - CO₂ concentrations under the SSP1-1.9 scenario. The base seasonality pattern derived from historical observations with monthly
1057 and 15° latitudinal resolution (panel a) is modulated over time using the first EOF of the residuals (panel a.1), scaled with projected NPP
1058 into the future (panel a.2). The latitudinal gradient is assumed flat in pre-industrial times, with latitudinal gradients over the observational
1059 record being derived from historical observations – and here compared with CMIP5 ESM models – see Meinshausen et al. (2017) (panel
1060 b). The projection of the latitudinal gradient uses global total CO₂ emissions regressed against the score (dark blue line in panel d) of the
1061 first latitudinal EOF (dark blue line in panel c). The principal component's score of the second EOF's is assumed zero in the future
1062 (turquoise line in panel c,d). Resulting surface air mole fractions fields show a return to current CO₂ (~2019) concentrations by the end of
1063 the 21st century (panel e and f). Historical NOAA surface flask station datasets (grey dots in panels f, g, h with station indicators provided
1064 in legend of panel f) are used for these future projections beyond the end of 2014 reach of the historical dataset (grey shaded background
1065 in panels f, g, h). Various comparison datasets shown, namely the WDCGG timeseries (Tsutsumi et al., 2009), the NOAA Marine Boundary
1066 Layer (MBL) product (<https://www.esrl.noaa.gov/gmd/ccgg/mbl/>) and the NASA AQUA satellite data
1067 (ftp://acdisc.gsfc.nasa.gov/ftp/data/s4pa/Aqua_AIRS_Level3/AIRX3C2M.005/), the Petrenko timeseries (made available in the
1068 supplement to Buizert et al. (2012)). Also shown are the MAGICC global-mean projections (bright blue line “MAGICCconc”). These



1069 overview figures are available for all 43 gases and all 9 scenarios on greenhousegases.science.unimelb.edu.au as a total of 387 so-called
1070 factsheets. See also Table 12 in Meinshausen (2017) for a description of all data labels.

1071

1072 **Figure 6** - Transition between historical runs and future SSP concentrations for CO₂ (panel a), CH₄ (panel b) and N₂O (panel c) surface
1073 mole fractions. The observational in situ and flask station datapoints reach into the first years of the future SSP datasets (grey dots). Derived
1074 northern-hemispheric (orange), global (black) and Southern hemispheric averages (blue) are shown with annual averages (thick lines) and
1075 monthly averages (thin lines with seasonality variability). On the right axis side, the illustrative arrows indicate the min-max range across
1076 the scenarios for Northern hemispheric, global and Southern hemispheric annual-average concentrations by 2030 across all 9 SSP scenarios.
1077 The NOAA/AGAGE global mean dataserries are shown in green. For description of labels of other comparison data, see Table 12 in
1078 Meinshausen (2017).

1079

1080 **Figure 7** - Overview of all greenhouse gases within SSP scenarios and their relative importance in terms of radiative forcing. The radiative
1081 forcing contributions are stacked, starting with CO₂ (blue shaded area) at the bottom, followed by methane (CH₄), nitrous oxide (N₂O) and
1082 the other 40 greenhouse gases. Default radiative forcing efficiencies or parameterisations are used, with CO₂, CH₄ and N₂O being based
1083 on a parameterisation of the Oslo-line-by-line model (section 2.7). Seasonal and latitudinal variation is indicated by the three bars on the
1084 right of each panel for the global average, northern hemispheric and southern hemispheric monthly mean concentrations for the year 2100.
1085 The light-blue shaded areas on the left side of each panel from 1750 to 2014 are based on historical greenhouse gas observations, the 21st
1086 century span from 2015 to 2100 (white area) and the extension until 2300 and beyond is based on the MAGICC7.0 model. For the IPCC
1087 AR6, the five scenarios SSP1-1.9 (panel a), SSP1-2.6 (b), SSP2-4.5 (d), SSP3-7.0 (g) and SSP5-8.5 (i) are chosen as key scenarios for
1088 knowledge integration across chapters and Working Groups.

1089 **Figure 8** - Overview of SSP concentrations of CO₂, CH₄ and N₂O in the context of the historical observational dataset. For the respective
1090 main ice core and firn datasets (WAIS, Law Dome, EPICA DML etc.), please see Figure 6b in Meinshausen et al. (2017). The 21st century
1091 is shown as grey vertical band.



1092
1093 **Figure 9** – The 2050 CO₂ and CH₄ concentrations of SSPs (dark blue circles), RCP (orange circles) and scenarios of the IPCC Special
1094 Report on 1.5C warming database (grey dots). All scenarios' concentrations were derived by using the SSP or RCP or SR1.5 harmonised
1095 emission scenarios together with the same MAGICC7.0 default settings as used for the CMIP6 SSP concentration projections.

1096

1097 **Figure 10** - Atmospheric surface air mole fractions of four CFCs, namely CFC-12 (panel a), CFC-11 (panel b), CFC-113 (panel c) and
1098 CFC-114 (panel c). This study's Northern hemispheric averages (orange lines), Southern hemispheric averages (blue lines) and global
1099 averages (black lines) are shown in comparison with recent measurements of the NOAA and/or AGAGE networks (grey dots), the global
1100 averages derived by Montzka et al. (2018) and the projections by Velders and Daniel (2014b) (dashed lines with diamond markers). The
1101 latter can be seen as near-lifetime limited projections whereas observations hint to recent (since 2012) emissions increases, leading to a
1102 slower-than-projected fall in global atmospheric concentrations. For an exploration of CFC-11's decline rates, see the recent studies by
1103 Montzka et al. (2018) and Rigby et al. (2019). Note that the high "outlier" monthly mean values for CFC-11 and CFC-114 are primarily
1104 from the AGAGE Gosan station and include all data, i.e., so-called "pollution" events in which case temporary high concentration air
1105 masses pass the measurement station. The apparent disappearance of those high pollution events at the end of 2015 is due to that particular
1106 AGAGE data timeseries only having been available until then at the point of this analysis, although a recent publication (Rigby et al., 2019)
1107 shows that these enhancements continued at least through 2017.

1108

1109 **Figure 11** - Overview of SSP concentrations in comparison with RCP concentrations for CO₂, CH₄ and N₂O. The original RCP scenarios
1110 are shown in thicker black lines and various linestyles. Applying the new MAGICC7 default setting used for the SSP scenarios to the RCP
1111 emissions results in generally higher concentrations (grey lines).

1112

1113



1114 **Figure 12** - Comparison of illustrative Global Mean Surface Air Temperature (GMSAT) (panel a) and global-mean sea level rise (SLR)
1115 projections (panel b) under SSP and RCP scenarios. The global-mean temperatures are given relative to pre-industrial (1750) levels,
1116 normalized to 0.92 C over the 1995-2014 period. Time series for the time period 2000-2100 are shown for the nine SSPs relative to 1750
1117 with bold solid lines indicating the higher priority SSP scenarios and thin dashed lines indicating other so-called “Tier 2” scenarios. Shaded
1118 areas indicate the 5%-95% confidence intervals for each scenario. Bar plots illustrate the 2081-2100 average relative to 1750 for the nine
1119 SSPs (yellow shaded area with barplots), and the RCP scenarios, using the same MAGICC7.0 setup (left light grey shaded bar plot area)
1120 and a former MAGICC6 setup used at the time of IPCC AR5 (right light grey area). We also show the likely range of temperature and sea
1121 level rise averages as reported in IPCC AR5 for that period - based on multiple lines of evidence (dark grey shaded set of barplots on the
1122 right). Observational data for global-mean surface temperatures (GMST), normalized over the same 1986-2005 period, is shown for
1123 Berkeley Earth (black solid), Cowtan & Way (Cowtan and Way, 2014) (long dashed), HadCRUT4 (Morice et al., 2012; Brohan et al.,
1124 2006) (small dashes) and NASA GISS (Lenssen et al., 2019)(dash-dotted). Observational data for sea level rise is taken from NASA
1125 (Beckley et al., 2010).

1126

1127 **Figure 13** - Warming signal induced by latitudinally and seasonally resolved GHG concentrations (“lat_mon”) compared to an annually
1128 and global-mean uniform GHG concentrations (“yearmean_global”) in an Earth System Model, namely CESM1.2.2 (Hurrell et al., 2013).
1129 We averaged the full historical scenario from 1850 to 2005 across all 6 ensemble members in each setup (“lat_mon” and
1130 “yearmean_global”) and produced the averages for the December-Januar-February DJF average (panel a) and the March-April-May
1131 averages (b). The latitudinally averaged warming signals that result from using spatially and temporarily resolved GHG concentrations are
1132 shown in the lower panels (thick blue lines), here compared against comparable one hundred differenced pairs of 930-year long control
1133 run segments (thin grey lines). In the high upper North during the MAM season, approximately 97 of the 100 control run segment
1134 differences are lower.

1135



1136 **12 References**

- 1137 Beckley, B. D., Zelensky, N. P., Holmes, S. A., Lemoine, F. G., Ray, R. D., Mitchum, G. T., Desai, S. D., and Brown, S. T.:
1138 Assessment of the Jason-2 Extension to the TOPEX/Poseidon, Jason-1 Sea-Surface Height Time Series for Global Mean Sea
1139 Level Monitoring, *Marine Geodesy*, 33, 447-471, 10.1080/01490419.2010.491029, 2010.
- 1140 Brohan, P., Kennedy, J. J., Harris, I., Tett, S. F. B., and Jones, P. D.: Uncertainty estimates in regional and global observed
1141 temperature changes: A new data set from 1850, *J. Geophys. Res.-Atmos.*, 111, D12106, 10.1029/2005JD006548, 2006.
- 1142 Buizert, C., Martinerie, P., Petrenko, V. V., Severinghaus, J. P., Trudinger, C. M., Witrant, E., Rosen, J. L., Orsi, A. J.,
1143 Rubino, M., Etheridge, D. M., Steele, L. P., Hogan, C., Laube, J. C., Sturges, W. T., Levchenko, V. A., Smith, A. M., Levin,
1144 I., Conway, T. J., Dlugokencky, E. J., Lang, P. M., Kawamura, K., Jenk, T. M., White, J. W. C., Sowers, T., Schwander, J.,
1145 and Blunier, T.: Gas transport in firn: multiple-tracer characterisation and model intercomparison for NEEM, Northern
1146 Greenland, *Atmos. Chem. Phys.*, 12, 4259-4277, 10.5194/acp-12-4259-2012, 2012.
- 1147 Collins, W. J., Lamarque, J. F., Schulz, M., Boucher, O., Eyring, V., Hegglin, M. I., Maycock, A., Myhre, G., Prather, M.,
1148 Shindell, D., and Smith, S. J.: AerChemMIP: quantifying the effects of chemistry and aerosols in CMIP6, *Geosci. Model*
1149 *Dev.*, 10, 585-607, 10.5194/gmd-10-585-2017, 2017.
- 1150 Cowtan, K., and Way, R. G.: Coverage bias in the HadCRUT4 temperature series and its impact on recent temperature trends,
1151 *Quarterly Journal of the Royal Meteorological Society*, 140, 1935-1944, 2014.
- 1152 Cunnold, D., Steele, L., Fraser, P., Simmonds, P., Prinn, R., Weiss, R., Porter, L., O'Doherty, S., Langenfelds, R., and
1153 Krummel, P.: In situ measurements of atmospheric methane at GAGE/AGAGE sites during 1985–2000 and resulting source
1154 inferences, *Journal of Geophysical Research: Atmospheres*, 107, 2002.
- 1155 DeConto, R. M., and Pollard, D.: Contribution of Antarctica to past and future sea-level rise, *Nature*, 531, 591, 2016.
- 1156 Dlugokencky, E. J., P.M. Lang, A.M. Croswell, K.A. Masarie, and M.J. Croswell: Atmospheric Methane Dry Air Mole
1157 Fractions from the NOAA ESRL Carbon Cycle Cooperative Global Air Sampling Network, 1983-2014. NOAA (Ed.), 2015a.
- 1158 Dlugokencky, E. J., P.M. Lang, K.A. Masarie, A.M. Croswell, M.J. Croswell: Atmospheric Carbon Dioxide Dry Air Mole
1159 Fractions from the NOAA ESRL Carbon Cycle Cooperative Global Air Sampling Network, 1968-2014. NOAA (Ed.), 2015b.
- 1160 Durack, P. J., and Taylor, K.: CMIP6 Forcing datasets summary, <http://goo.gl/r8up31>, 46, 2019.
- 1161 Edwards, T. L., Brandon, M. A., Durand, G., Edwards, N. R., Golledge, N. R., Holden, P. B., Nias, I. J., Payne, A. J., Ritz,
1162 C., and Wernecke, A.: Revisiting Antarctic ice loss due to marine ice-cliff instability, *Nature*, 566, 58, 2019.
- 1163 Ehhalt, D., Prather, M. J., Dentener, F., Derwent, R. G., Dlugokencky, E., Holland, E., Isaksen, I. S. A., Katima, J., Kirchhoff,
1164 V., Matson, P., Midgley, P., and Wang, M.: Atmospheric Chemistry and Greenhouse Gases, in: *Climate Change 2001: The*
1165 *Scientific Basis*, edited by: Houghton, J. T., Ding, Y., Griggs, D. J., Noguer, M., van der Linden, P. J., Dai, X., Maskell, K.,
1166 and Johnson, C. A., Cambridge University Press, Cambridge, UK, 892, 2001.



- 1167 Engel, A., Rigby, M., Burkholder, J. B., Fernandez, R. P., Froidevaux, L., Hall, B. D., Hossaini, R., Saito, T., Vollmer, M.
1168 K., and Yao, B.: Update on Ozone-Depleting Substances (ODCs) and Other Gases of Interest to the Montreal Protocol,
1169 Chapter 1, in: Scientific Assessment of Ozone Depletion: 2018, World Meteorological Organization, Geneva, Switzerland,
1170 2018.
- 1171 Etminan, M., Myhre, G., Highwood, E., and Shine, K.: Radiative forcing of carbon dioxide, methane, and nitrous oxide: A
1172 significant revision of the methane radiative forcing, *Geophysical Research Letters*, 43, 2016.
- 1173 Eyring, V., Bony, S., Meehl, G. A., Senior, C. A., Stevens, B., Stouffer, R. J., and Taylor, K. E.: Overview of the Coupled
1174 Model Intercomparison Project Phase 6 (CMIP6) experimental design and organization, *Geosci. Model Dev.*, 9, 1937-1958,
1175 10.5194/gmd-9-1937-2016, 2016.
- 1176 Fang, X., Park, S., Saito, T., Tunnicliffe, R., Ganesan, A. L., Rigby, M., Li, S., Yokouchi, Y., Fraser, P. J., Harth, C. M.,
1177 Krummel, P. B., Mühle, J., O'Doherty, S., Salameh, P. K., Simmonds, P. G., Weiss, R. F., Young, D., Lunt, M. F., Manning,
1178 A. J., Gressent, A., and Prinn, R. G.: Rapid increase in ozone-depleting chloroform emissions from China, *Nature Geoscience*,
1179 12, 89-93, 10.1038/s41561-018-0278-2, 2019.
- 1180 Forkel, M., Carvalhais, N., Rödenbeck, C., Keeling, R., Heimann, M., Thonicke, K., Zaehle, S., and Reichstein, M.: Enhanced
1181 seasonal CO₂ exchange caused by amplified plant productivity in northern ecosystems, *Science*, aac4971, 2016.
- 1182 Friedlingstein, P., Cox, P., Betts, R., Bopp, L., von Bloh, W., Brovkin, V., Cadule, P., Doney, S., Eby, M., Fung, I., Bala, G.,
1183 John, J., Jones, C., Joos, F., Kato, T., Kawamiya, M., Knorr, W., Lindsay, K., Matthews, H. D., Raddatz, T., Rayner, P.,
1184 Reick, C., Roeckner, E., Schnitzler, K.-G., Schnur, R., Strassmann, K., Weaver, K., Yoshikawa, C., and Zeng, N.: Climate-
1185 Carbon Cycle Feedback Analysis: Results from the C4MIP Model Intercomparison, *Journal of Climate*, 19, 3337-3353,
1186 10.1175/JCLI3800.1, 2006.
- 1187 Friedlingstein, P., Meinshausen, M., Arora, V. K., Jones, C. D., Anav, A., Liddicoat, S. K., and Knutti, R.: Uncertainties in
1188 CMIP5 Climate Projections due to Carbon Cycle Feedbacks, *Journal of Climate*, 27, 511-526, 10.1175/jcli-d-12-00579.1,
1189 2014.
- 1190 Frieler, K., Meinshausen, M., Golly, A., Mengel, M., Lebek, K., Donner, S. D., and Hoegh-Guldberg, O.: Limiting global
1191 warming to 2 degrees C is unlikely to save most coral reefs, *Nature Climate Change*, 3, 165-170, 10.1038/nclimate1674,
1192 2013.
- 1193 Gidden, M. J., Fujimori, S., van den Berg, M., Klein, D., Smith, S. J., van Vuuren, D. P., and Riahi, K.: A methodology and
1194 implementation of automated emissions harmonization for use in Integrated Assessment Models, *Environmental Modelling
1195 & Software*, 105, 187-200, <https://doi.org/10.1016/j.envsoft.2018.04.002>, 2018.
- 1196 Gidden, M. J., Riahi, K., Smith, S. J., Fujimori, S., Luderer, G., Kriegler, E., van Vuuren, D. P., van den Berg, M., Feng, L.,
1197 Klein, D., Calvin, K., Doelman, J. C., Frank, S., Fricko, O., Harmsen, M., Hasegawa, T., Havlik, P., Hilaire, J., Hoesly, R.,
1198 Horing, J., Popp, A., Stehfest, E., and Takahashi, K.: Global emissions pathways under different socioeconomic scenarios
1199 for use in CMIP6: a dataset of harmonized emissions trajectories through the end of the century, *Geosci. Model Dev.*, 12,
1200 1443-1475, 10.5194/gmd-12-1443-2019, 2019.



- 1201 Gollede, N. R., Keller, E. D., Gomez, N., Naughten, K. A., Bernales, J., Trusel, L. D., and Edwards, T. L.: Global
1202 environmental consequences of twenty-first-century ice-sheet melt, *Nature*, 566, 65, 2019.
- 1203 Graven, H. D., Keeling, R. F., Piper, S. C., Patra, P. K., Stephens, B. B., Wofsy, S. C., Welp, L. R., Sweeney, C., Tans, P. P.,
1204 Kelley, J. J., Daube, B. C., Kort, E. A., Santoni, G. W., and Bent, J. D.: Enhanced Seasonal Exchange of CO₂ by Northern
1205 Ecosystems Since 1960, *Science*, 341, 1085-1089, 10.1126/science.1239207, 2013.
- 1206 Gray, J. M., Frohking, S., Kort, E. A., Ray, D. K., Kucharik, C. J., Ramankutty, N., and Friedl, M. A.: Direct human influence
1207 on atmospheric CO₂ seasonality from increased cropland productivity, *Nature*, 515, 398-401, 10.1038/nature13957, 2014.
- 1208 Gütschow, J., Jeffery, M. L., Gieseke, R., Gebel, R., Stevens, D., Krapp, M., and Rocha, M.: The PRIMAP-hist national
1209 historical emissions time series, *Earth Syst. Sci. Data Discuss.*, 2016, 1-44, 10.5194/essd-2016-12, 2016.
- 1210 Hoesly, R. M., Smith, S. J., Feng, L., Klimont, Z., Janssens-Maenhout, G., Pitkanen, T., Seibert, J. J., Vu, L., Andres, R. J.,
1211 Bolt, R. M., Bond, T. C., Dawidowski, L., Kholod, N., Kurokawa, J. I., Li, M., Liu, L., Lu, Z., Moura, M. C. P., O'Rourke,
1212 P. R., and Zhang, Q.: Historical (1750–2014) anthropogenic emissions of reactive gases and aerosols from the Community
1213 Emissions Data System (CEDS), *Geosci. Model Dev.*, 11, 369-408, 10.5194/gmd-11-369-2018, 2018.
- 1214 Holmes, C. D., Prather, M. J., Sovde, O. A., and Myhre, G.: Future methane, hydroxyl, and their uncertainties: key climate
1215 and emission parameters for future predictions, *Atmospheric Chemistry and Physics*, 13, 285-302, 2013.
- 1216 Hossaini, R., Chipperfield, M., Montzka, S., Rap, A., Dhomse, S., and Feng, W.: Efficiency of short-lived halogens at
1217 influencing climate through depletion of stratospheric ozone, *Nature Geoscience*, 8, 186-190, 2015.
- 1218 Hurrell, J. W., Holland, M. M., Gent, P. R., Ghan, S., Kay, J. E., Kushner, P. J., Lamarque, J.-F., Large, W. G., Lawrence,
1219 D., Lindsay, K., Lipscomb, W. H., Long, M. C., Mahowald, N., Marsh, D. R., Neale, R. B., Rasch, P., Vavrus, S., Vertenstein,
1220 M., Bader, D., Collins, W. D., Hack, J. J., Kiehl, J., and Marshall, S.: The Community Earth System Model: A Framework
1221 for Collaborative Research, *Bulletin of the American Meteorological Society*, 94, 1339-1360, 10.1175/bams-d-12-00121.1,
1222 2013.
- 1223 Jones, C. D., Arora, V., Friedlingstein, P., Bopp, L., Brovkin, V., Dunne, J., Graven, H., Hoffman, F., Ilyina, T., and John, J.
1224 G.: C4MIP–The Coupled Climate–Carbon Cycle Model Intercomparison Project: experimental protocol for CMIP6,
1225 *Geoscientific Model Development*, 9, 2853-2880, 2016.
- 1226 Keeling, C. D., Bacastow, R. B., Bainbridge, A. E., Ekdahl, C. A., Guenther, P. R., Waterman, L. S., and Chin, J. F.:
1227 Atmospheric carbon dioxide variations at Mauna Loa observatory, Hawaii, *Tellus*, 28, 538-551, 1976.
- 1228 Atmospheric CO₂ records from sites in the SIO air sampling network: <http://cdiac.esd.ornl.gov/trends/co2/sio-keel.htm>,
1229 access: May, 2004.
- 1230 Lawrence, D. M., Hurtt, G. C., Arneeth, A., Brovkin, V., Calvin, K. V., Jones, A. D., Jones, C. D., Lawrence, P. J., de Noblet-
1231 Ducoudré, N., and Pongratz, J.: The Land Use Model Intercomparison Project (LUMIP) contribution to CMIP6: rationale
1232 and experimental design, *Geoscientific Model Development*, 9, 2973-2998, 2016.



- 1233 Lenssen, N. J. L., Schmidt, G. A., Hansen, J. E., Menne, M. J., Persin, A., Ruedy, R., and Zyss, D.: Improvements in the
1234 GISTEMP Uncertainty Model, *Journal of Geophysical Research: Atmospheres*, 124, 6307-6326, 10.1029/2018jd029522,
1235 2019.
- 1236 Matthes, K., Funke, B., Anderson, M., Barnard, L., Beer, J., Charbonneau, P., Clilverd, M., Dudok de Wit, T., Haberreiter,
1237 M., and Hendry, A.: Solar forcing for CMIP6 (v3. 2), *Geoscientific Model Development*, 10, 2247-2302, 2017.
- 1238 Meehl, G. A., Covey, C., Delworth, T., Latif, M., McAvaney, B., Mitchell, J. F., Stouffer, R. J., and Taylor, K. E.: The WCRP
1239 CMIP3 multimodel dataset: A new era in climate change research, *Bulletin of the American Meteorological Society*, 88,
1240 1383-1394, 2007.
- 1241 Meinshausen, M., Meinshausen, N., Hare, W., Raper, S. C. B., Frieler, K., Knutti, R., Frame, D. J., and Allen, M. R.:
1242 Greenhouse-gas emission targets for limiting global warming to 2°C, *Nature*, 458, 1158, 2009.
- 1243 Meinshausen, M., Raper, S. C. B., and Wigley, T. M. L.: Emulating coupled atmosphere-ocean and carbon cycle models with
1244 a simpler model, *MAGICC6: Part I – Model Description and Calibration, Atmospheric Chemistry and Physics* 11, 1417-
1245 1456, 2011a.
- 1246 Meinshausen, M., Smith, S., Calvin, K., Daniel, J., Kainuma, M., Lamarque, J. F., Matsumoto, K., Montzka, S., Raper, S.,
1247 Riahi, K., Thomson, A., Velders, G., and van Vuuren, D. P.: The RCP greenhouse gas concentrations and their extensions
1248 from 1765 to 2300, *Climatic Change*, 109, 213-241, 10.1007/s10584-011-0156-z, 2011b.
- 1249 Meinshausen, M., Wigley, T. M. L., and Raper, S. C. B.: Emulating atmosphere-ocean and carbon cycle models with a
1250 simpler model, *MAGICC6: Part 2– Applications, Atmospheric Chemistry and Physics* 11, 1457-1471, 2011c.
- 1251 Meinshausen, M., Vogel, E., Nauels, A., Lorbacher, K., Meinshausen, N., Etheridge, D. M., Fraser, P. J., Montzka, S. A.,
1252 Rayner, P. J., Trudinger, C. M., Krummel, P. B., Beyerle, U., Canadell, J. G., Daniel, J. S., Enting, I. G., Law, R. M., Lunder,
1253 C. R., O'Doherty, S., Prinn, R. G., Reimann, S., Rubino, M., Velders, G. J. M., Vollmer, M. K., Wang, R. H. J., and Weiss,
1254 R.: Historical greenhouse gas concentrations for climate modelling (CMIP6), *Geosci. Model Dev.*, 10, 2057-2116,
1255 10.5194/gmd-10-2057-2017, 2017.
- 1256 Mengel, M., Nauels, A., Rogelj, J., and Schleussner, C.-F.: Committed sea-level rise under the Paris Agreement and the
1257 legacy of delayed mitigation action, *Nature communications*, 9, 601, 2018.
- 1258 Montzka, S., McFarland, M., Andersen, S., Miller, B., Fahey, D., Hall, B., Hu, L., Siso, C., and Elkins, J.: Recent trends in
1259 global emissions of hydrochlorofluorocarbons and hydrofluorocarbons: Reflecting on the 2007 adjustments to the Montreal
1260 Protocol, *The Journal of Physical Chemistry A*, 119, 4439-4449, 2015.
- 1261 Montzka, S. A., Dutton, G. S., Yu, P., Ray, E., Portmann, R. W., Daniel, J. S., Kuijpers, L., Hall, B. D., Mondeel, D., Siso,
1262 C., Nance, J. D., Rigby, M., Manning, A. J., Hu, L., Moore, F., Miller, B. R., and Elkins, J. W.: An unexpected and persistent
1263 increase in global emissions of ozone-depleting CFC-11, *Nature*, 557, 413-417, 10.1038/s41586-018-0106-2, 2018.
- 1264 Morgenstern, O., Braesicke, P., Hurwitz, M. M., O'Connor, F. M., Bushell, A. C., Johnson, C. E., and Pyle, J. A.: The World
1265 Avoided by the Montreal Protocol, *Geophysical Research Letters*, 35, 10.1029/2008gl034590, 2008.



- 1266 Morice, C. P., Kennedy, J. J., Rayner, N. A., and Jones, P. D.: Quantifying uncertainties in global and regional temperature
1267 change using an ensemble of observational estimates: The HadCRUT4 data set, *Journal of Geophysical Research:*
1268 *Atmospheres*, 117, 2012.
- 1269 Myhre, G., Shindell, D., Breon, F. M., Collins, W., Fuglestedt, J., Huang, J., Koch, D., Lamarque, J. F., Lee, D., Mendoza,
1270 B., Nakajima, T., Robock, A., Stephens, G., Takemura, T., and Zhang, H.: Anthropogenic and Natural Radiative Forcing, in:
1271 *Climate Change 2013: The Physical Science Basis. Contribution of Working Group I to the Fifth Assessment, Report of the*
1272 *Intergovernmental Panel on Climate Change*, edited by: Stocker, T. F., Qin, D., Plattner, G.-K., Tignor, M., Allen, S. K.,
1273 Boschung, J., Nauels, A., Xia, Y., Bex, V., and Midgley, P. M., Cambridge University Press, Cambridge, New York, 2013.
- 1274 Nauels, A., Meinshausen, M., Mengel, M., Lorbacher, K., and Wigley, T. M. L.: Synthesizing long-term sea level rise
1275 projections - the MAGICC sea level model v2.0, *Geoscientific Model Development*, 10, 2495-2524, 10.5194/gmd-10-2495-
1276 2017, 2017.
- 1277 Nisbet, E. G., Dlugokencky, E. J., Manning, M. R., Lowry, D., Fisher, R. E., France, J. L., Michel, S. E., Miller, J. B., White,
1278 J. W. C., Vaughn, B., Bousquet, P., Pyle, J. A., Warwick, N. J., Cain, M., Brownlow, R., Zazzeri, G., Lanoisellé, M., Manning,
1279 A. C., Gloor, E., Worthy, D. E. J., Brunke, E.-G., Labuschagne, C., Wolff, E. W., and Ganesan, A. L.: Rising atmospheric
1280 methane: 2007–2014 growth and isotopic shift, *Global Biogeochemical Cycles*, 30, 1356-1370, 10.1002/2016gb005406,
1281 2016.
- 1282 NOAA ESRL GMD: Atmospheric Carbon Dioxide Dry Air Mole Fractions from quasi-continuous measurements at South
1283 Pole. K.W. Thoning, D. R. K., and A. Crotwell (Ed.), National Oceanic and Atmospheric Administration (NOAA), Earth
1284 System Research Laboratory (ESRL), Global Monitoring Division (GMD): Boulder, Colorado, USA, 2014a.
- 1285 NOAA ESRL GMD: Atmospheric Carbon Dioxide Dry Air Mole Fractions from quasi-continuous measurements at Mauna
1286 Loa, Hawaii. K.W. Thoning, D. R. K., and A. Crotwell (Ed.), National Oceanic and Atmospheric Administration (NOAA),
1287 Earth System Research Laboratory (ESRL), Global Monitoring Division (GMD): Boulder, Colorado, USA, 2014b.
- 1288 NOAA ESRL GMD: Atmospheric Carbon Dioxide Dry Air Mole Fractions from quasi-continuous measurements at Barrow,
1289 Alaska. K.W. Thoning, D. R. K., and A. Crotwell (Ed.), National Oceanic and Atmospheric Administration (NOAA), Earth
1290 System Research Laboratory (ESRL), Global Monitoring Division (GMD): Boulder, Colorado, USA, 2014c.
- 1291 NOAA ESRL GMD: Atmospheric Carbon Dioxide Dry Air Mole Fractions from quasi-continuous measurements at
1292 American Samoa. K.W. Thoning, D. R. K., and A. Crotwell (Ed.), National Oceanic and Atmospheric Administration
1293 (NOAA), Earth System Research Laboratory (ESRL), Global Monitoring Division (GMD): Boulder, Colorado, USA, 2014d.
- 1294 O'Neill, B. C., Tebaldi, C., Vuuren, D. P. v., Eyring, V., Friedlingstein, P., Hurtt, G., Knutti, R., Kriegler, E., Lamarque, J.-
1295 F., and Lowe, J.: The scenario model intercomparison project (ScenarioMIP) for CMIP6, *Geoscientific Model Development*,
1296 9, 3461-3482, 2016.
- 1297 Prather, M. J., Holmes, C. D., and Hsu, J.: Reactive greenhouse gas scenarios: Systematic exploration of uncertainties and
1298 the role of atmospheric chemistry, *Geophysical Research Letters*, 39, 2012.



- 1299 Prinn, R., Cunnold, D., Rasmussen, R., Simmonds, P., Aleya, F., Crawford, A., Fraser, P., and Rosen, R.: Atmospheric
1300 emissions and trends of nitrous oxide deduced from 10 years of ALE-GAGE data, *Journal of Geophysical Research:*
1301 *Atmospheres*, 95, 18369-18385, 1990.
- 1302 Prinn, R. G., Weiss, R. F., Arduini, J., Arnold, T., DeWitt, H. L., Fraser, P. J., Ganesan, A. L., Gasore, J., Harth, C. M.,
1303 Hermansen, O., Kim, J., Krummel, P. B., Li, S., Loh, Z. M., Lunder, C. R., Maione, M., Manning, A. J., Miller, B. R.,
1304 Mitrevski, B., Mühle, J., O'Doherty, S., Park, S., Reimann, S., Rigby, M., Saito, T., Salameh, P. K., Schmidt, R., Simmonds,
1305 P. G., Steele, L. P., Vollmer, M. K., Wang, R. H., Yao, B., Yokouchi, Y., Young, D., and Zhou, L.: History of chemically
1306 and radiatively important atmospheric gases from the Advanced Global Atmospheric Gases Experiment (AGAGE), *Earth*
1307 *Syst. Sci. Data*, 10, 985-1018, 10.5194/essd-10-985-2018, 2018.
- 1308 Ray, E. A., Moore, F. L., Elkins, J. W., Rosenlof, K. H., Laube, J. C., Röckmann, T., Marsh, D. R., and Andrews, A. E.:
1309 Quantification of the SF₆ lifetime based on mesospheric loss measured in the stratospheric polar vortex, *Journal of*
1310 *Geophysical Research: Atmospheres*, 122, 4626-4638, 10.1002/2016JD026198, 2017.
- 1311 Rigby, M., Montzka, S. A., Prinn, R. G., White, J. W. C., Young, D., O'Doherty, S., Lunt, M. F., Ganesan, A. L., Manning,
1312 A. J., Simmonds, P. G., Salameh, P. K., Harth, C. M., Mühle, J., Weiss, R. F., Fraser, P. J., Steele, L. P., Krummel, P. B.,
1313 McCulloch, A., and Park, S.: Role of atmospheric oxidation in recent methane growth, *Proceedings of the National Academy*
1314 *of Sciences*, 114, 5373-5377, 10.1073/pnas.1616426114, 2017.
- 1315 Rigby, M., Park, S., Saito, T., Western, L. M., Redington, A. L., Fang, X., Henne, S., Manning, A. J., Prinn, R. G., Dutton,
1316 G. S., Fraser, P. J., Ganesan, A. L., Hall, B. D., Harth, C. M., Kim, J., Kim, K. R., Krummel, P. B., Lee, T., Li, S., Liang, Q.,
1317 Lunt, M. F., Montzka, S. A., Mühle, J., O'Doherty, S., Park, M. K., Reimann, S., Salameh, P. K., Simmonds, P., Tunnicliffe,
1318 R. L., Weiss, R. F., Yokouchi, Y., and Young, D.: Increase in CFC-11 emissions from eastern China based on atmospheric
1319 observations, *Nature*, 569, 546-550, 10.1038/s41586-019-1193-4, 2019.
- 1320 Rogelj, J., Meinshausen, M., and Knutti, R.: Global warming under old an new scenarios using IPCC climate sensitivity
1321 range estimates, *Nature Climate Change*, 2, 248-253, 2012.
- 1322 Rogelj, J., Schaeffer, M., Meinshausen, M., Shindell, D. T., Hare, W., Klimont, Z., Velders, G. J., Amann, M., and
1323 Schellnhuber, H. J.: Disentangling the effects of CO₂ and short-lived climate forcer mitigation, *Proceedings of the National*
1324 *Academy of Sciences*, 111, 16325-16330, 2014.
- 1325 Rogelj, J., Meinshausen, M., Schaeffer, M., Knutti, R., and Riahi, K.: Impact of short-lived non-CO₂ mitigation on carbon
1326 budgets for stabilizing global warming, *Environmental Research Letters*, 10, 2015.
- 1327 Royer, D. L.: CO₂-forced climate thresholds during the Phanerozoic, *Geochim Cosmochim Acta*, 70, 5665-5675, 2006.
- 1328 Saunio, M., Bousquet, P., Poulter, B., Peregón, A., Ciais, P., Canadell, J. G., Dlugokencky, E. J., Etiope, G., Bastviken, D.,
1329 Houweling, S., Janssens-Maenhout, G., Tubiello, F. N., Castaldi, S., Jackson, R. B., Alexe, M., Arora, V. K., Beerling, D. J.,
1330 Bergamaschi, P., Blake, D. R., Brailsford, G., Brovkin, V., Bruhwiler, L., Crevoisier, C., Crill, P., Covey, K., Curry, C.,
1331 Frankenberg, C., Gedney, N., Höglund-Isaksson, L., Ishizawa, M., Ito, A., Joos, F., Kim, H. S., Kleinen, T., Krummel, P.,
1332 Lamarque, J. F., Langenfelds, R., Locatelli, R., Machida, T., Maksyutov, S., McDonald, K. C., Marshall, J., Melton, J. R.,
1333 Morino, I., Naik, V., O'Doherty, S., Parmentier, F. J. W., Patra, P. K., Peng, C., Peng, S., Peters, G. P., Pison, I., Prigent, C.,



- 1334 Prinn, R., Ramonet, M., Riley, W. J., Saito, M., Santini, M., Schroeder, R., Simpson, I. J., Spahni, R., Steele, P., Takizawa,
1335 A., Thornton, B. F., Tian, H., Tohjima, Y., Viovy, N., Voulgarakis, A., van Weele, M., van der Werf, G. R., Weiss, R.,
1336 Wiedinmyer, C., Wilton, D. J., Wiltshire, A., Worthy, D., Wunch, D., Xu, X., Yoshida, Y., Zhang, B., Zhang, Z., and Zhu,
1337 Q.: The global methane budget 2000–2012, *Earth Syst. Sci. Data*, 8, 697–751, 10.5194/essd-8-697-2016, 2016.
- 1338 Schaefer, H., Fletcher, S. E. M., Veidt, C., Lassey, K. R., Brailsford, G. W., Bromley, T. M., Dlugokencky, E. J., Michel, S.
1339 E., Miller, J. B., Levin, I., Lowe, D. C., Martin, R. J., Vaughn, B. H., and White, J. W. C.: A 21st-century shift from fossil-
1340 fuel to biogenic methane emissions indicated by $\delta^{13}\text{C}/\text{CH}_4$, *Science*, 352, 80,
1341 10.1126/science.aad2705, 2016.
- 1342 Schneider, L., and Kollmuss, A.: Perverse effects of carbon markets on HFC-23 and SF₆ abatement projects in Russia, *Nature*
1343 *Climate Change*, 5, 1061, 10.1038/nclimate2772, 2015.
- 1344 Schneider, L. R.: Perverse incentives under the CDM: an evaluation of HFC-23 destruction projects, *Climate Policy*, 11, 851-
1345 864, 10.3763/cpol.2010.0096, 2011.
- 1346 Schneider von Deimling, T., Meinshausen, M., Levermann, A., Huber, V., Frieler, K., Lawrence, D. M., and Brovkin, V.:
1347 Estimating the near-surface permafrost-carbon feedback on global warming, *Biogeosciences*, 9, 649–665, 10.5194/bg-9-649-
1348 2012, 2012.
- 1349 Schneider von Deimling, T., Grosse, G., Strauss, J., Schirrmeyer, L., Morgenstern, A., Schaphoff, S., Meinshausen, M., and
1350 Boike, J.: Observation-based modelling of permafrost carbon fluxes with accounting for deep carbon deposits and
1351 thermokarst activity, *Biogeosciences*, 12, 3469–3488, 2015.
- 1352 Smith, C. J., Kramer, R. J., Myhre, G., Forster, P. M., Soden, B. J., Andrews, T., Boucher, O., Faluvegi, G., Fläschner, D.,
1353 Hodnebrog, Ø., Kasoar, M., Kharin, V., Kirkevåg, A., Lamarque, J.-F., Mülmenstädt, J., Olivie, D., Richardson, T., Samset,
1354 B. H., Shindell, D., Stier, P., Takemura, T., Voulgarakis, A., and Watson-Parris, D.: Understanding Rapid Adjustments to
1355 Diverse Forcing Agents, *Geophysical Research Letters*, 45, 12,023–012,031, 10.1029/2018gl079826, 2018.
- 1356 Stevens, B., Fiedler, S., Kinne, S., Peters, K., Rast, S., Müsse, J., Smith, S. J., and Mauritsen, T.: MACv2-SP: A
1357 parameterization of anthropogenic aerosol optical properties and an associated Twomey effect for use in CMIP6,
1358 *Geoscientific Model Development*, 10, 433–452, 2017.
- 1359 Taylor, K. E., Stouffer, R. J., and Meehl, G. A.: An overview of CMIP5 and the experiment design, *Bulletin of the American*
1360 *Meteorological Society*, 93, 485–498, 2012.
- 1361 Toohey, M., Stevens, B., Schmidt, H., and Timmreck, C.: Easy Volcanic Aerosol (EVA v1.0): an idealized forcing generator
1362 for climate simulations, *Geosci. Model Dev.*, 9, 4049–4070, 10.5194/gmd-9-4049-2016, 2016.
- 1363 Tsutsumi, Y., Mori, K., Hirahara, T., Ikegami, M., and Conway, T. J.: Technical report of global analysis method for major
1364 greenhouse gases by the World Data Center for greenhouse gases, WMO/TD, 2009.
- 1365 Velders, G., and Daniel, J.: Uncertainty analysis of projections of ozone-depleting substances: mixing ratios, EESC, ODPs,
1366 and GWPs, *Atmospheric Chemistry and Physics*, 14, 2757–2776, 2014a.



- 1367 Velders, G. J. M., Andersen, S. O., Daniel, J. S., Fahey, D. W., and McFarland, M.: The importance of the Montreal Protocol
1368 in protecting climate, *P Natl Acad Sci USA*, 104, 4814-4819, 2007.
- 1369 Velders, G. J. M., and Daniel, J. S.: Uncertainty analysis of projections of ozone-depleting substances: mixing ratios, EESC,
1370 ODPs, and GWPs, *Atmos. Chem. Phys.*, 14, 2757-2776, 10.5194/acp-14-2757-2014, 2014b.
- 1371 Velders, G. J. M., Fahey, D. W., Daniel, J. S., Andersen, S. O., and McFarland, M.: Future atmospheric abundances and
1372 climate forcings from scenarios of global and regional hydrofluorocarbon (HFC) emissions, *Atmospheric Environment*, 123,
1373 200-209, <https://doi.org/10.1016/j.atmosenv.2015.10.071>, 2015.
- 1374 Vollmer, M. K., Young, D., Trudinger, C. M., Mühle, J., Henne, S., Rigby, M., Park, S., Li, S., Guillevic, M., Mitrevski, B.,
1375 Harth, C. M., Miller, B. R., Reimann, S., Yao, B., Steele, L. P., Wyss, S. A., Lunder, C. R., Arduini, J., McCulloch, A., Wu,
1376 S., Rhee, T. S., Wang, R. H. J., Salameh, P. K., Hermansen, O., Hill, M., Langenfelds, R. L., Ivy, D., O'Doherty, S., Krummel,
1377 P. B., Maione, M., Etheridge, D. M., Zhou, L., Fraser, P. J., Prinn, R. G., Weiss, R. F., and Simmonds, P. G.: Atmospheric
1378 histories and emissions of chlorofluorocarbons CFC-13 (CClF₃), Σ CFC-114 (C₂Cl₂F₄), and CFC-115 (C₂ClF₅), *Atmos.*
1379 *Chem. Phys.*, 18, 979-1002, 10.5194/acp-18-979-2018, 2018.
- 1380 Welp, L. R., Patra, P. K., Rödenbeck, C., Nemani, R., Bi, J., Piper, S. C., and Keeling, R. F.: Increasing summer net CO₂
1381 uptake in high northern ecosystems inferred from atmospheric inversions and remote sensing, *Atmos. Chem. Phys.(Discuss)*,
1382 submitted, 2016.
- 1383 WMO: Scientific Assessment of Ozone Depletion: 2006, World Meteorological Organization, Geneva, Switzerland, 572,
1384 2006.
- 1385 WMO: Scientific Assessment of Ozone Depletion: 2014, World Meteorological Organization, Geneva, Switzerland, 416,
1386 2014.
- 1387 Worden, J. R., Bloom, A. A., Pandey, S., Jiang, Z., Worden, H. M., Walker, T. W., Houweling, S., and Röckmann, T.:
1388 Reduced biomass burning emissions reconcile conflicting estimates of the post-2006 atmospheric methane budget, *Nature*
1389 *Communications*, 8, 2227, 10.1038/s41467-017-02246-0, 2017.
- 1390
- 1391
- 1392



1393

1394

1395

1396

1397

1398

1399

1400

1401

1402 **13 Figures**

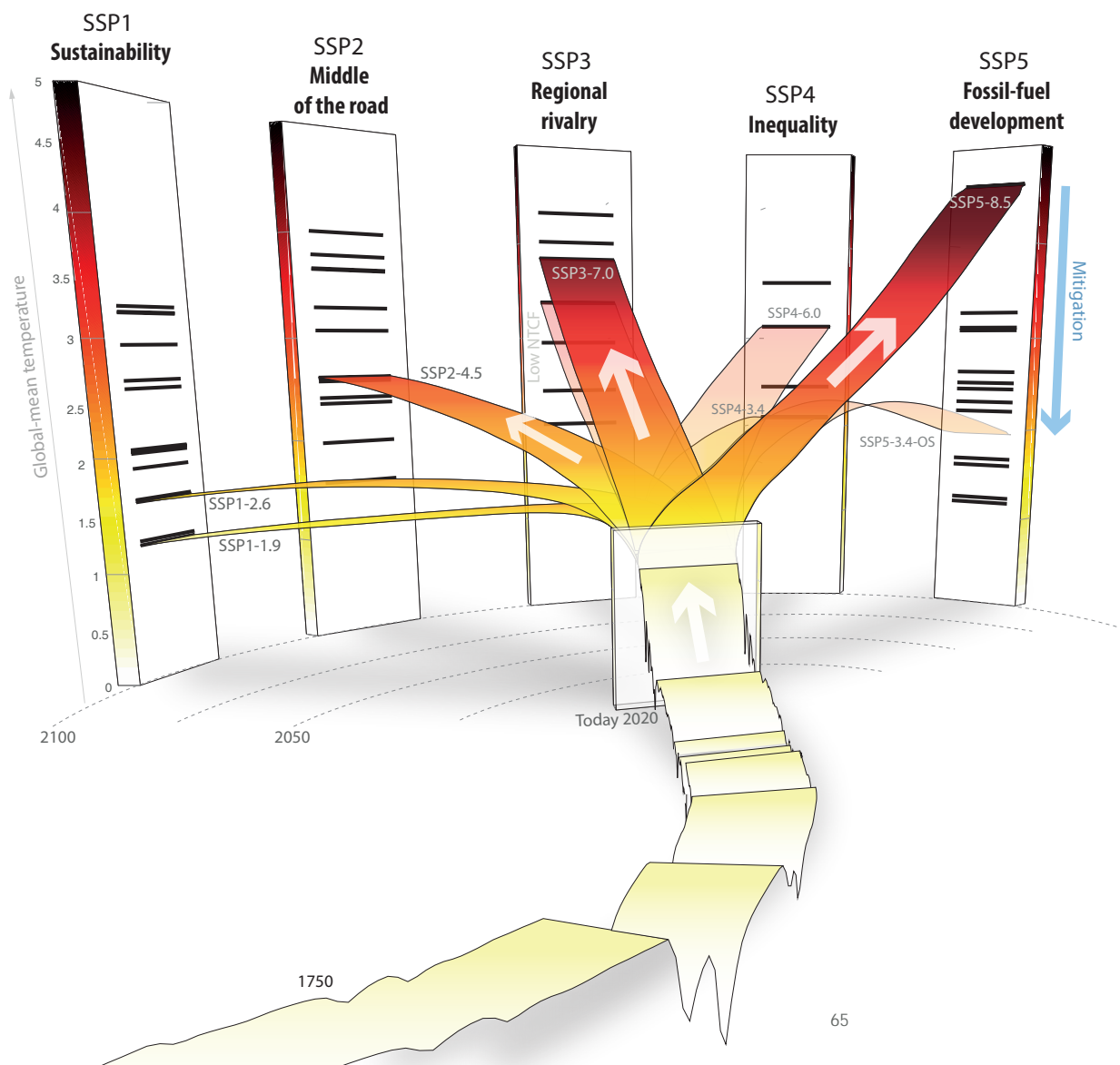


Figure 1

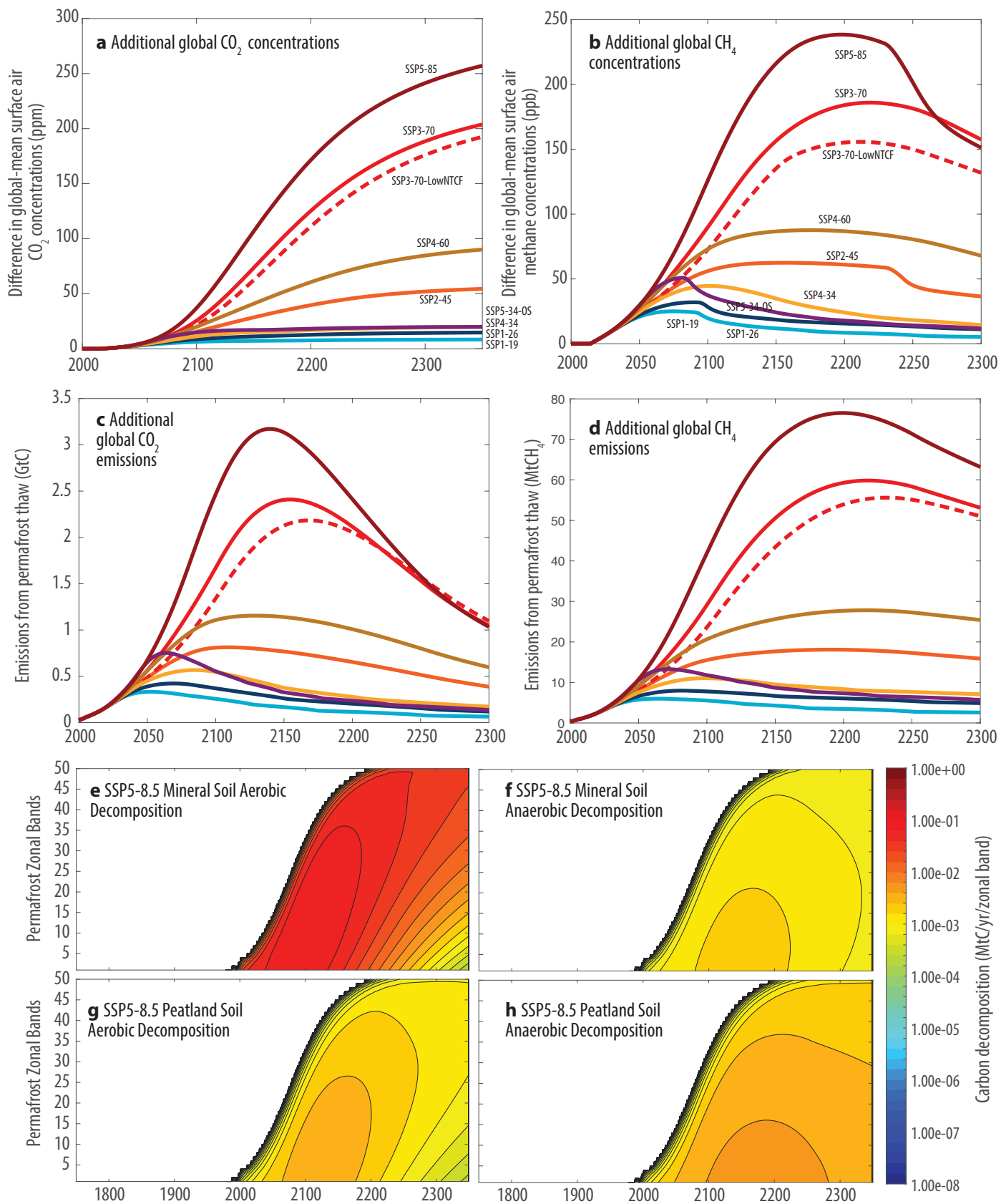


Figure 3

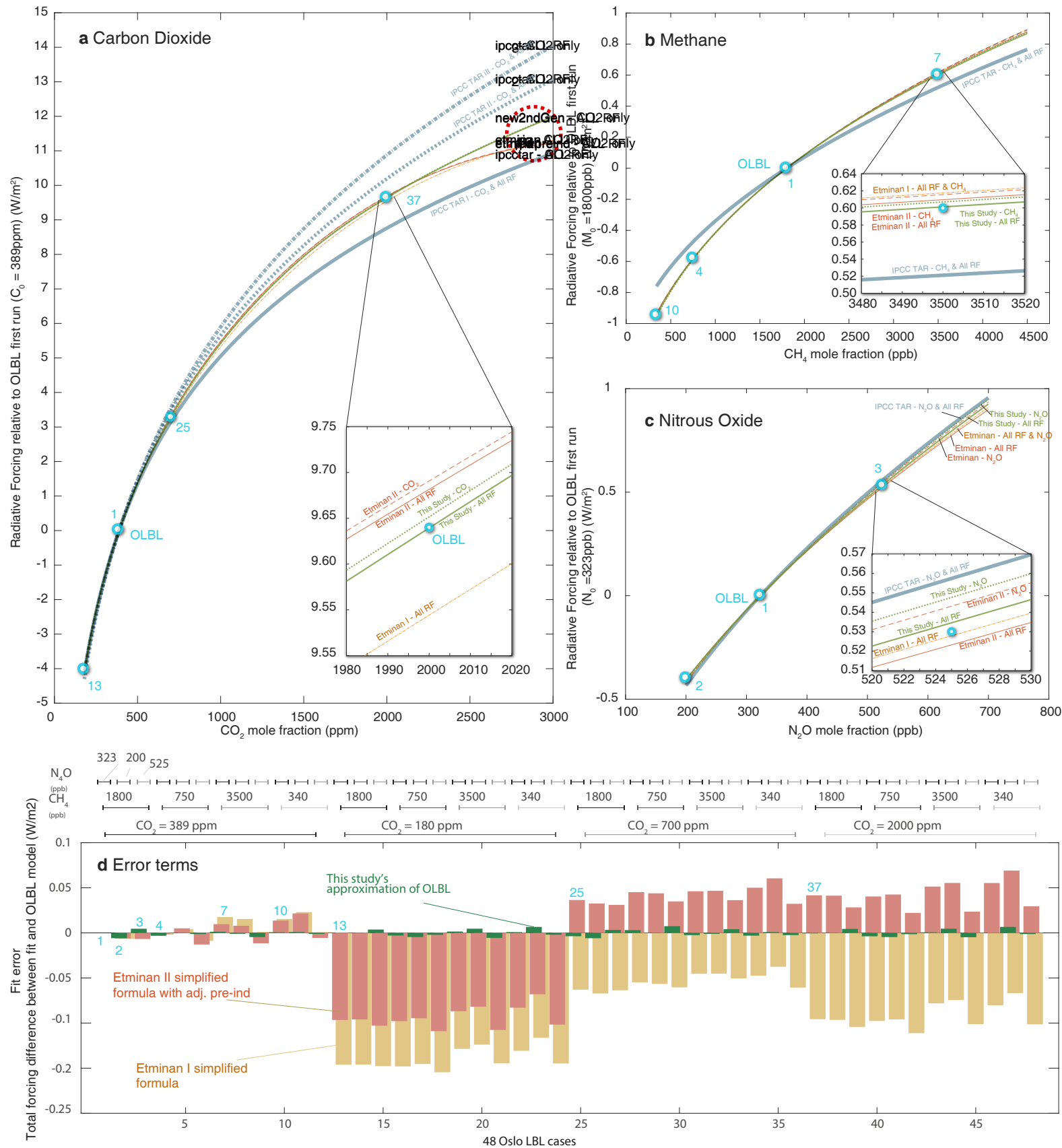


Figure 4

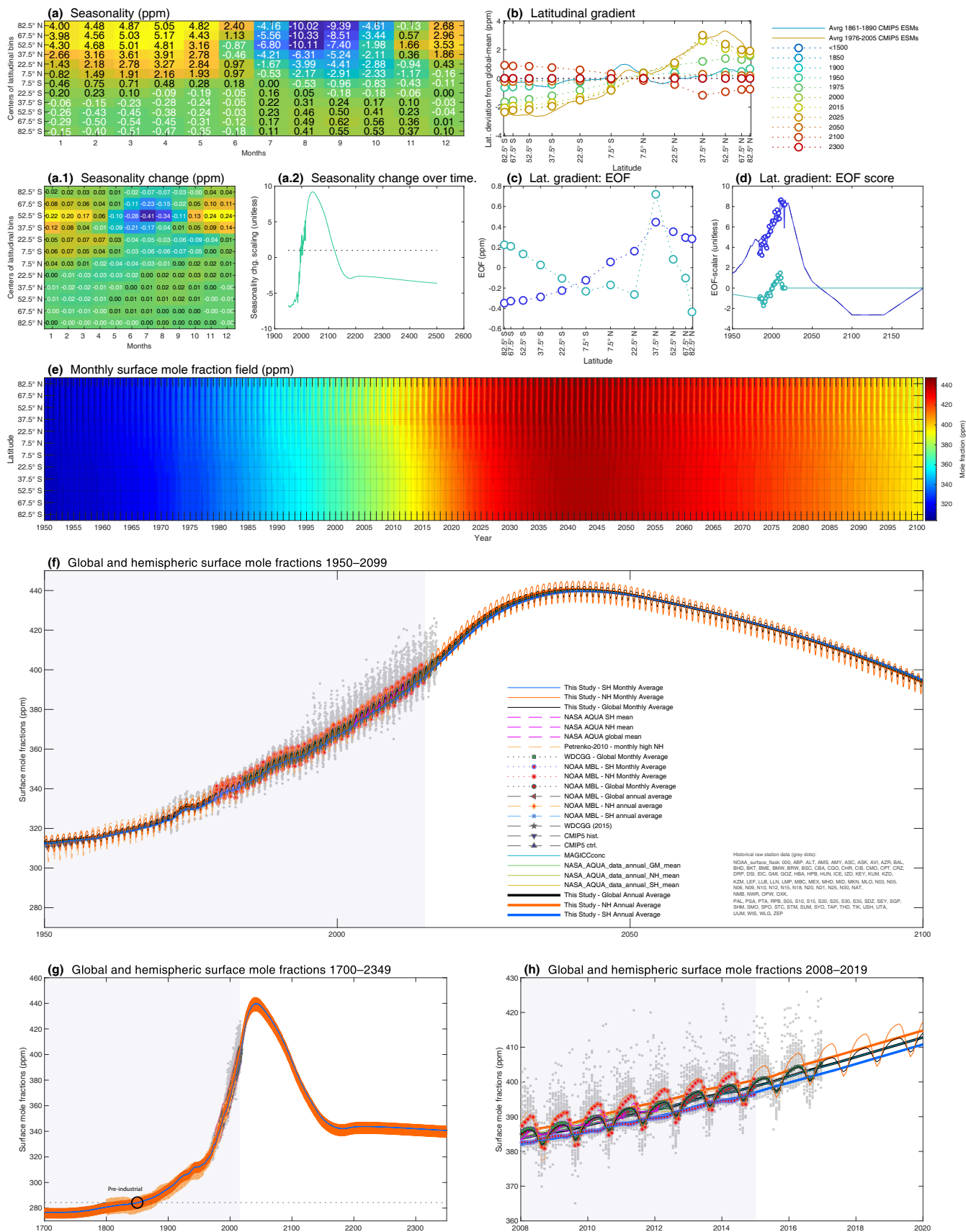


Figure 5

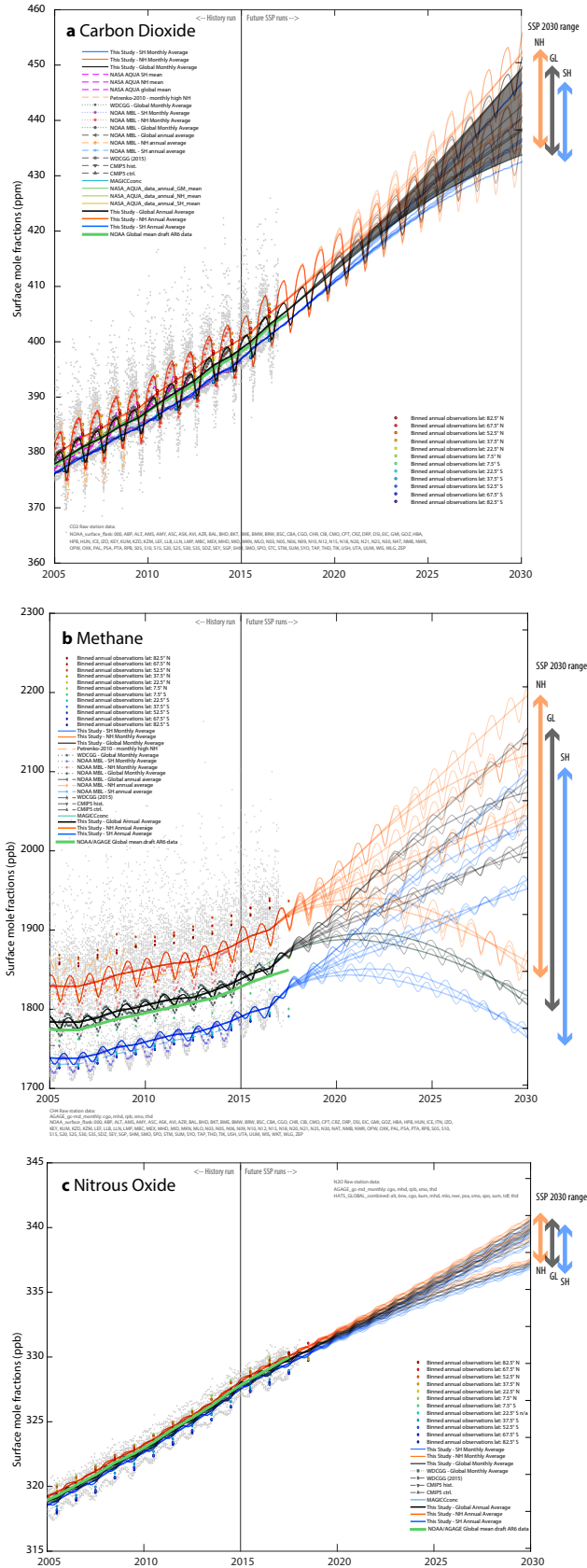


Figure 6



SSP scenarios greenhouse gas radiative forcings

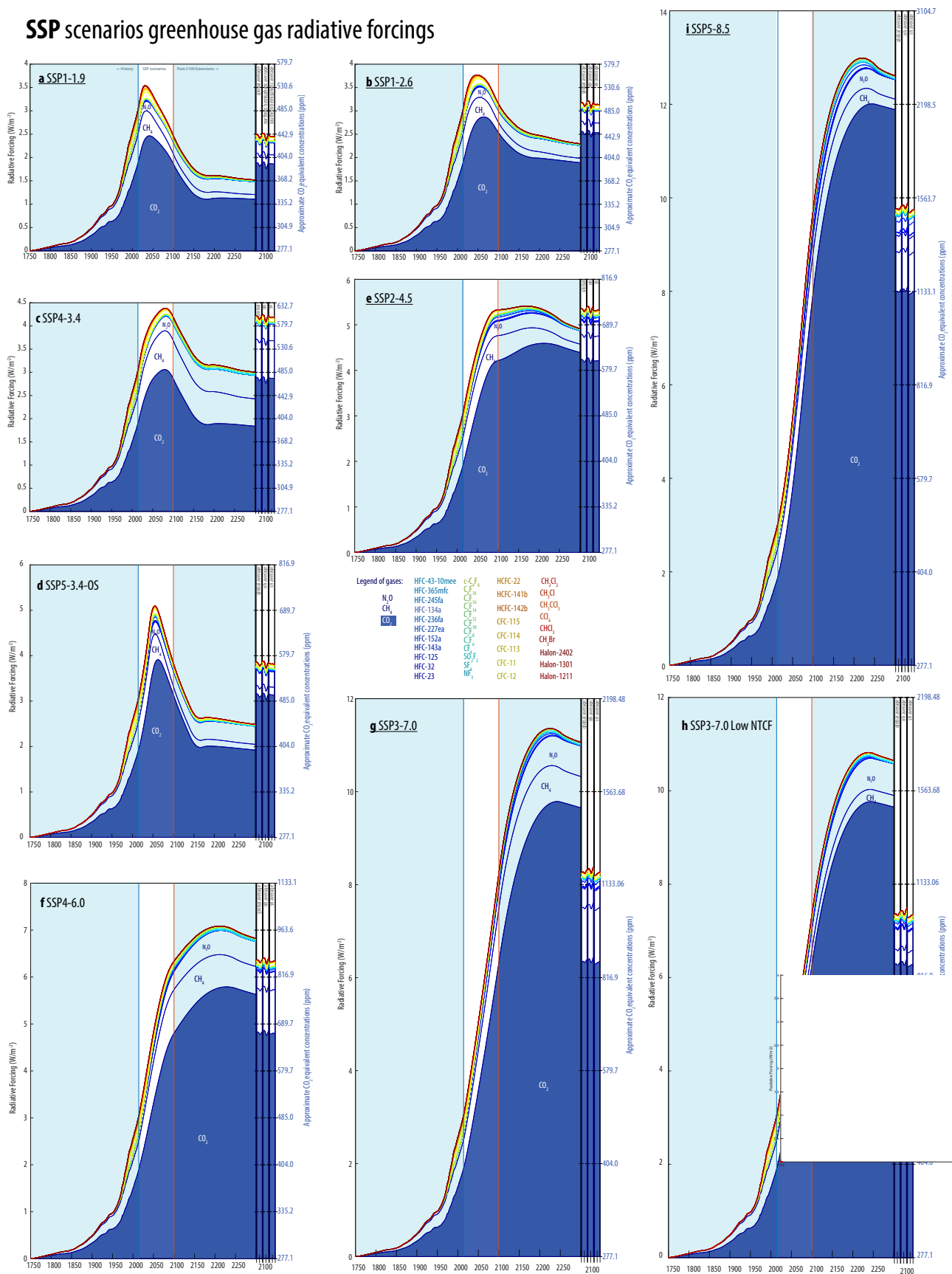


Figure 7

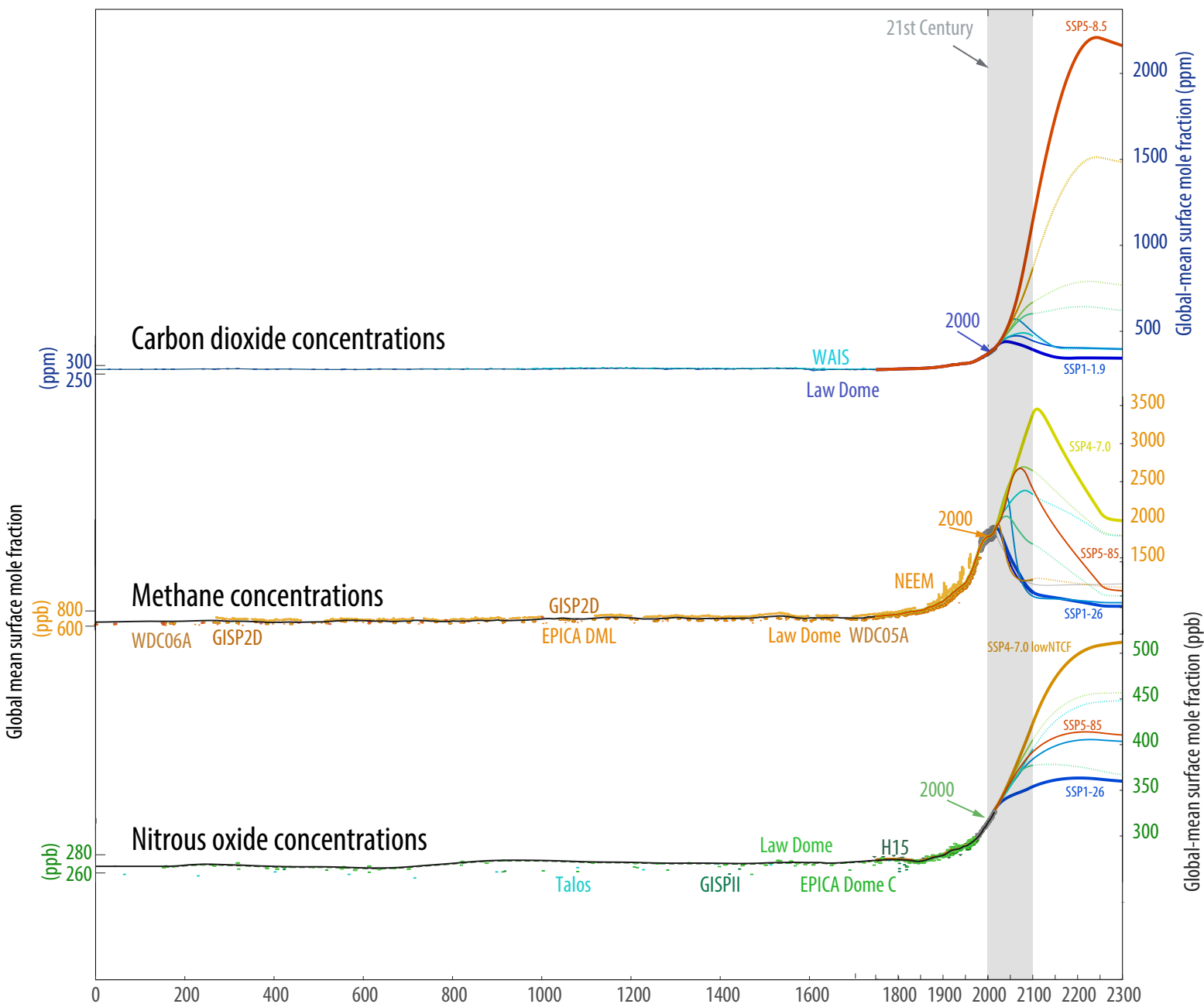


Figure 8

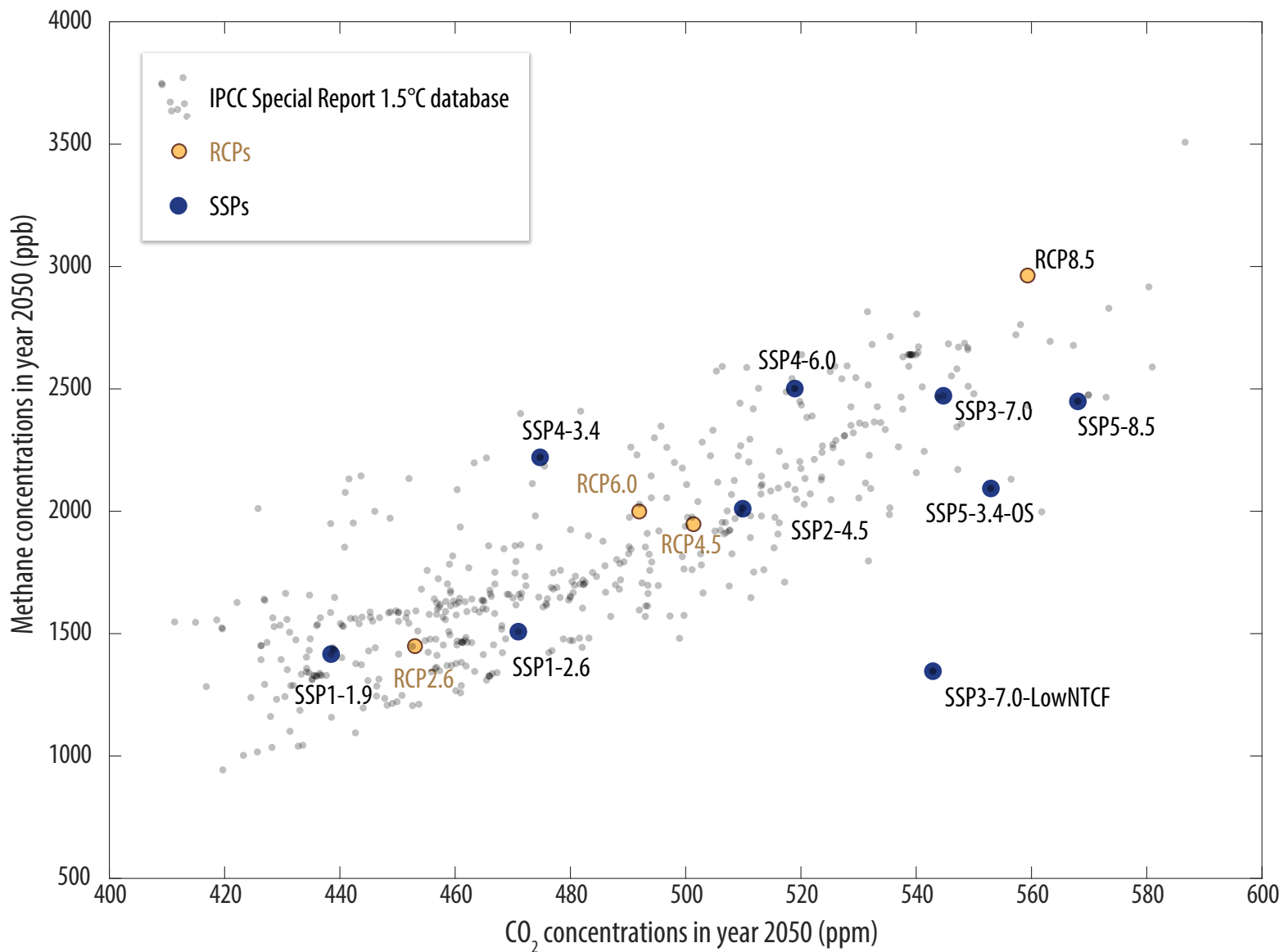


Figure 9

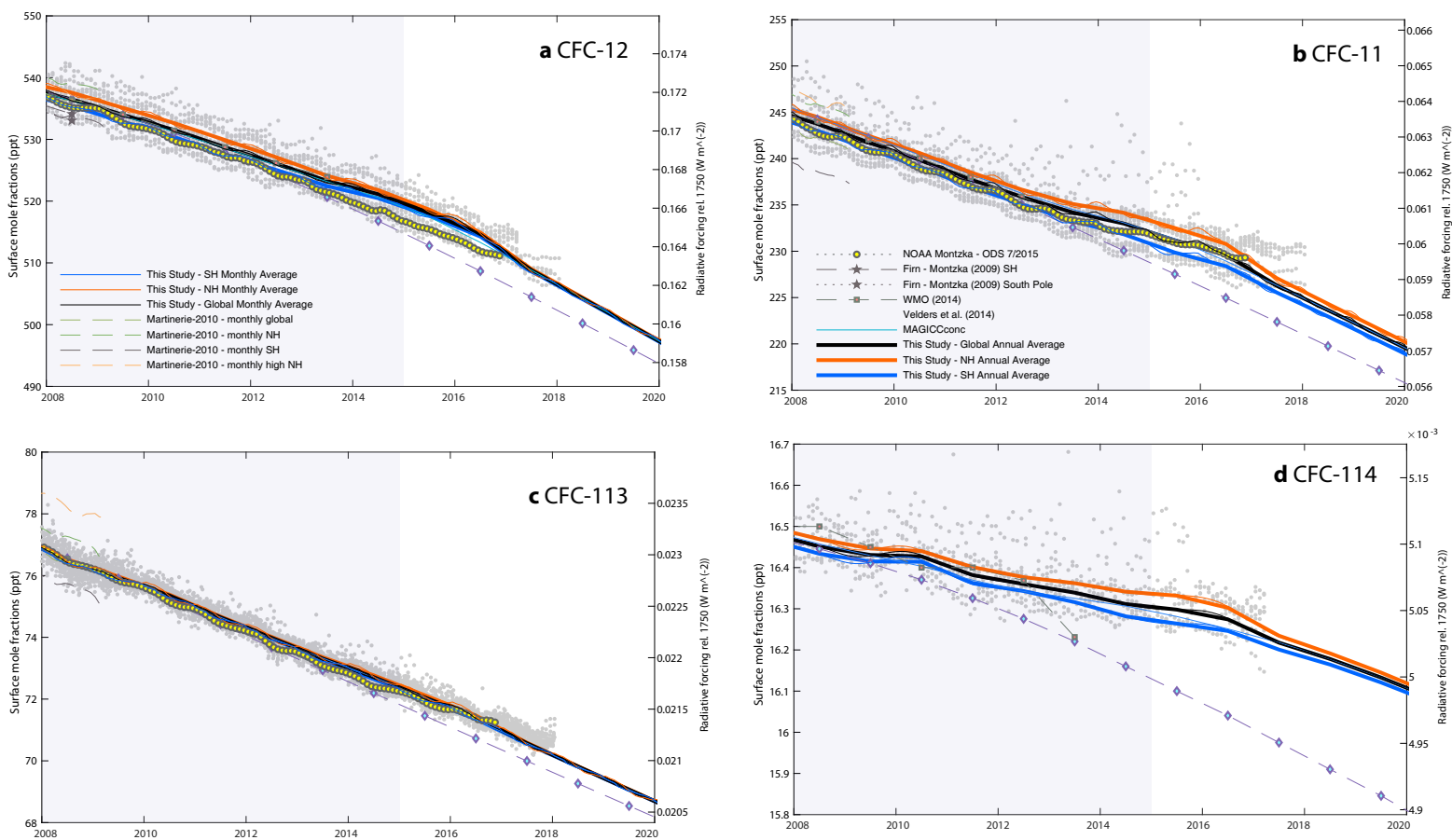


Figure 10

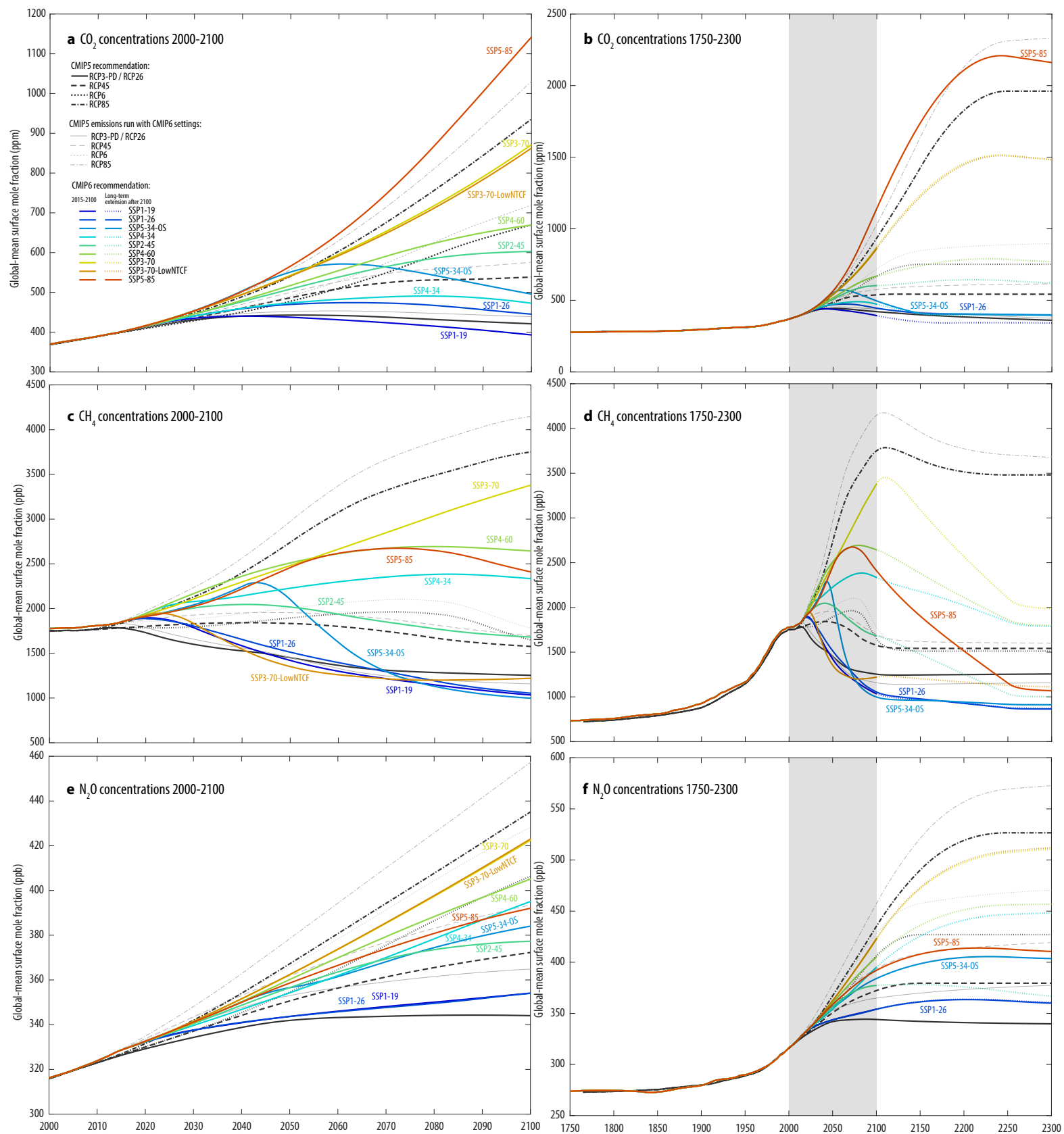


Figure 11

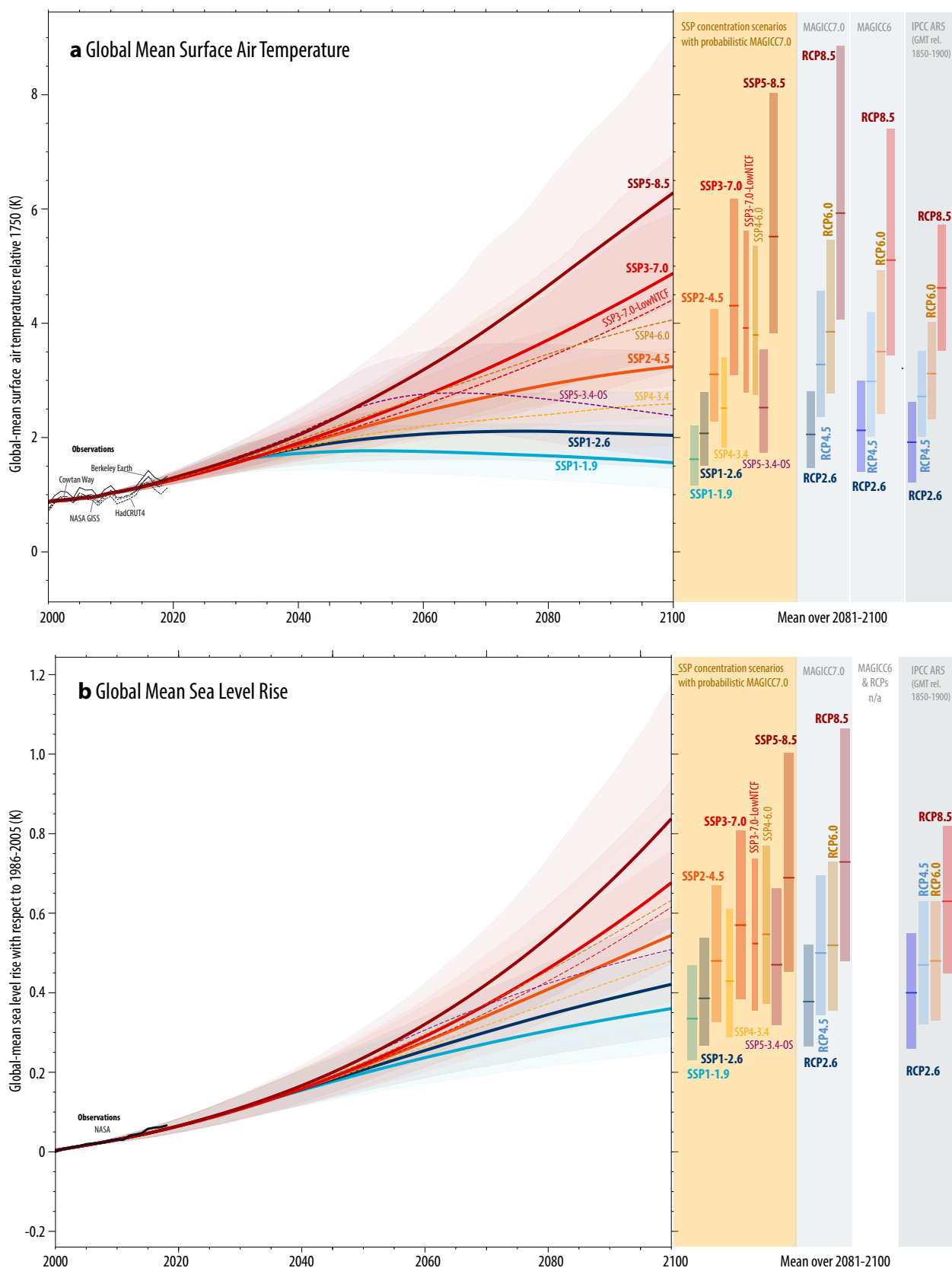


Figure 12

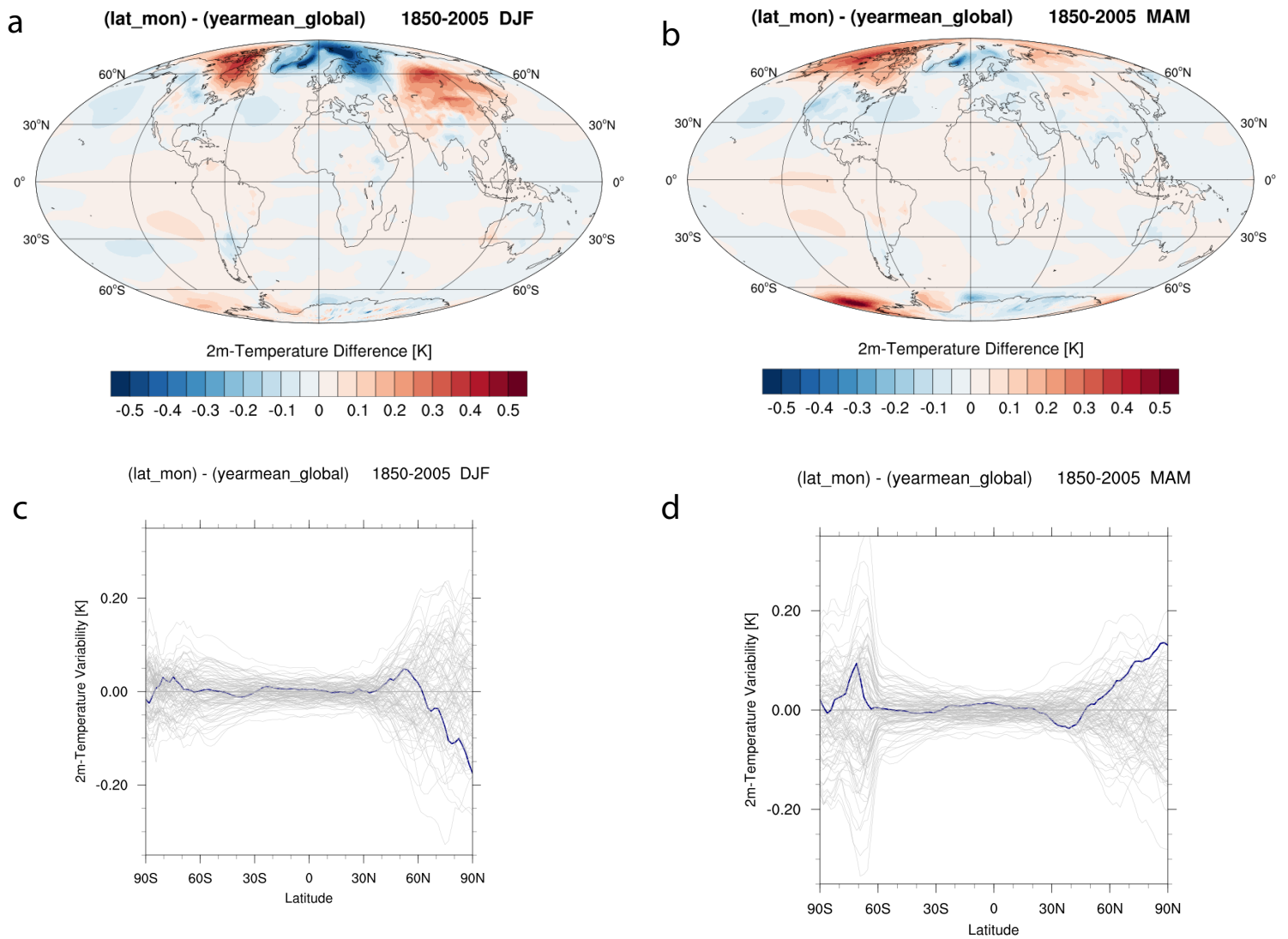


Figure 13